Energetic Materials at Extreme Conditions

David I.A. Millar

A thesis submitted in fulfilment of the requirements for the
degree of Doctor of Philosophy to the School of Chemistry, the
University of Edinburgh.

October 2010

Abstract

In order to effectively model the behaviour of energetic materials under operational conditions it is essential to obtain detailed structural information for these compounds at elevated temperature and/or pressures. The structural characterisation of the high explosives RDX and CL-20 and a series of inorganic azides $[M^{n+}(N_3)_n]$ at extreme conditions is described herein.

In addition to the characterisation of a highly metastable β-form of RDX (1,3,5-trinitrohexahydro-1,3,5-triazine) at atmospheric pressure, the structure solution of a high-pressure/high-temperature polymorph is described. This form, obtained above 4.3 GPa and 450 K, has been shown to be distinct from the β-form and has therefore been denoted ε-RDX. Furthermore, ε-RDX is sufficiently metastable to allow its recovery to ambient pressure at 150 K; it only transforms to the α-form upon warming to 230 K. Finally, the ambient-temperature compression of RDX has been investigated to a maximum pressure of 23.0 GPa, using methanol:ethanol (4:1) as the pressure-transmitting medium; no phase transition was observed under these conditions, other than the $\alpha \rightarrow \gamma$ transition at 3.9 GPa.

The structure of a high-pressure polymorph of CL-20 (2,4,6,8,10,12-hexanitrohexaazaisowurtzitane) has also been determined by a combination of powder and single-crystal X-ray diffraction. Compression of γ-CL-20 to above 0.7 GPa using Fluorinert (FC-77) as the pressure-transmitting medium results in a phase transition to the ζ-form, which has been found to display structural similarities with both the γ- and ε-forms. The high-pressure behaviour of CL-20, however, depends markedly on the starting polymorph and the pressure-transmitting medium selected. Compression of γ-CL-20 in MeOH:EtOH (4:1) results in the formation of a 2:1 CL-20:MeOH solvate at 0.5 GPa. This solvate is stable upon compression to $P > 5.0$ GPa. It may also be recovered to ambient pressure at 293 K. Meanwhile, no phase transition is observed during the compression of ε-CL-20 to a maximum pressure of 7.2 GPa.

Finally, a series of inorganic azides [NaN_3, CsN_3, TlN_3, NH_4N_3, AgN_3 and $Pb(N_3)_2$] has been characterised under a range of pressure and temperature conditions. Of the six compounds studied, all displayed at least one polymorphic transition – 5 new forms have been structurally characterised in this work and evidence of another 5 is presented. The combined effect of pressure and temperature results in sodium azide adopting a tetragonal structure common to larger alkali metal azides. Caesium azide has been shown to undergo three phase transitions during compression to 6.0 GPa – the structure of the first high-pressure form is

reported. A variable temperature X-ray powder diffraction study of TlN_3 has allowed the structural characterisation of the low-temperature TlN_3-IV (at 230 K) as well as providing evidence for a phase transition to a high-temperature form above 550 K. The high-pressure form III (obtained above 0.76 GPa) has also been determined by neutron powder diffraction.

Silver, ammonium and lead(II) azides have all been shown to undergo a phase transition at high pressures. Compression of silver azide ($P > 0.80$ GPa) removes an orthorhombic distortion observed at atmospheric pressure, resulting in the tetragonal structure adopted by CsN_3 and TlN_3 under ambient conditions. Moreover, NH_4N_3 and $Pb(N_3)_2$ have been found to undergo phase transitions at 2.6 GPa, although their high-pressure structures have still to be determined.

Declaration

I declare that this thesis was written by myself and that the work detailed herein is my own, or I have contributed substantially to such work, except where proper reference is made to the work of another author.

David I.A. Millar

Acknowledgements

There are numerous people that I would like to thank for their contributions and advice, without which the last three years would not have been quite so successful or enjoyable. I am greatly indebted to my supervisor, Professor Colin Pulham, for his knowledge and enthusiasm (both apparently unending, even at 4 a.m. at the synchrotron). Two other former 'Pulhamites' who have been immense sources of wisdom and humour (and quite often drinking partners) are Drs Iain Oswald and Helen Maynard-Casely. Thank you as well to all members of the Pulham group, past and present.

Dr Bill Marshall has also been instrumental in this research, not only providing guidance on everything related to neutron diffraction and Rietveld refinement, but also coming up with various new avenues to explore. Naturally, the success of the experiments reported herein is a reflection of the quality of the instrument scientists and technicians, with whom we have collaborated. Many thanks to Messrs Chris Barry and Duncan Francis (PEARL-HiPr, ISIS), Drs Alistair Lennie and Chiu Tang (I11, Diamond Light Source), Dr Annette Kleppe (I15, DLS) and Dr Dave Allan (I19, DLS).

In addition, I would like to thank Dr Adam Cumming (Defence Science and Technology Laboratory) for his insights into the energetics community and his keenness for a wide-ranging project. Moreover, I am gratefully indebted to Dstl for their joint studentship with EPSRC. I would also like to acknowledge STFC for provision of beamtime at ISIS and Diamond that has been vital to the success of this work.

Finally, I am hugely grateful for the love and support of my family and friends.

Contents

Chapter 1

Introduction

1 Introduction

1.1 Energetic Materials

1.1.1 Definition

Energetic materials are regarded as those with high enthalpies of formation, which can release the chemical energy stored within their molecular structures in a reproducible manner upon stimulus by heat, impact, shock, spark, *etc*, generally with the release of large quantities of hot gaseous products. A chemical explosion arises when an exothermic transformation occurs over an extremely short timescale (typically < 0.01 s). Due to the speed of the reaction, the product gases do not instantaneously expand but remain inside the chamber that held the explosive charge. The temperature in the moments succeeding explosion is commonly of the order of several thousand Kelvin – the pressure resulting from the confinement of these extremely hot combustion products in the small volume of the blast chamber can reach several thousand atmospheres.[1] This is sufficient to produce a shock-wave capable of breaking the walls of the chamber and causing damage to the surroundings. One should note, however, that the high-pressure shock-wave that passes through the energetic material itself is many orders of magnitude greater than this.

The majority of compounds classed as energetic materials contain a high proportion of oxygen and nitrogen (often as NO, NO_2 or NO_3 groups) within their structures, along with oxidisable 'fuel' elements such as carbon and hydrogen. Significant exceptions to this rule, however, are energetic compounds that contain no oxygen, for example metal azides ($M^{n+}(N_3)_n$) and nitrogen compounds such as nitrogen triiodide (NI_3). Upon initiation the explosive molecule dissociates into its atomic constituents before recombination to form small, stable molecules as shown in Reaction Scheme 1.1. The net energy of the explosion equates to the difference between the energy required to cause the fragmentation of the molecule and the energy released upon bond formation within the product gases. The nature of the products is largely dependent on the amount of oxygen available during the reaction (either within the molecular structure or from its surroundings); very rarely is an infinite supply of oxygen available during the explosion and mixed oxidation products (*i.e.* $C/CO/CO_2$) are therefore common.

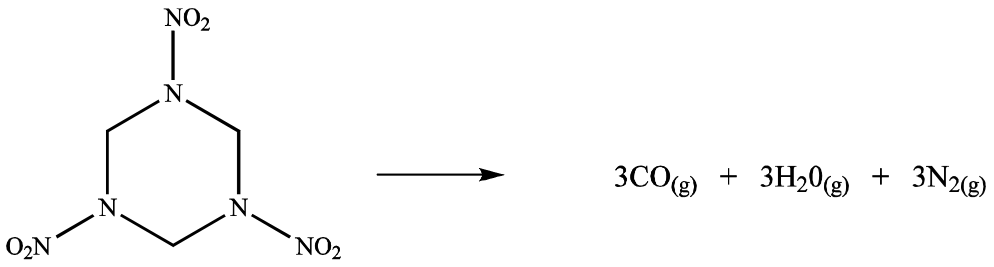

Reaction Scheme 1.1 Explosion of RDX (Section 3.1) to its gaseous products.

1.1.2 Classification

Energetic materials may be broadly classified into three categories: pyrotechnics, propellants (including gas generators) and explosives, which themselves may be further sub-divided into primary and secondary explosives. Pyrotechnic formulations undergo combustion at visibly observable rates, giving rise to coloured smoke, noise and/or brightly-coloured light. Propellants, such as ammonium perchlorate [NH_4ClO_4], contain all the oxygen necessary for their combustion within their structure. They undergo more rapid combustion than pyrotechnics but do not detonate, although burning may be violent and accompanied by sparks or flames and a hissing/crackling sound. The resultant production of large volumes of hot gas can then be utilised for the propulsion of projectiles (ranging from bullets to spacecraft) or to power turbines in torpedoes, for example.[1]

Primary explosives are sensitive to mild stimuli, such as heat or shock, causing a detonation event that gives rise to a short, strong shock-wave. Primary explosives are therefore commonly used to initiate the detonation of the less-sensitive secondary explosives. Despite many compounds displaying explosive decomposition upon initiation by a mild stimulus, very few primary explosives have been incorporated into practical and usable detonators. This is due to the rigorous constraints on thermal stability, hygroscopicity and shelf-life, that are required of a technically viable initiator.[2] The explosive properties of a range of metal azides, fulminates and styphnates (see Figure 1.1) are known, yet the majority of blasting caps utilise either lead styphnate or lead azide. In recent years, however, the toxicological and ecological hazards presented by the dispersion of minute, but cumulative, quantities of lead has motivated research into so-called ‘greener primaries’.[3] These endeavours, while worthy of merit, have so far had limited success due to the stringent quality controls placed on new detonators – lead replacements should display the same (or greater) explosive performance than the current optimum detonator, while also displaying physical and chemical stability *and* being devoid of toxic heavy metals or teratogenic perchlorates.[4]

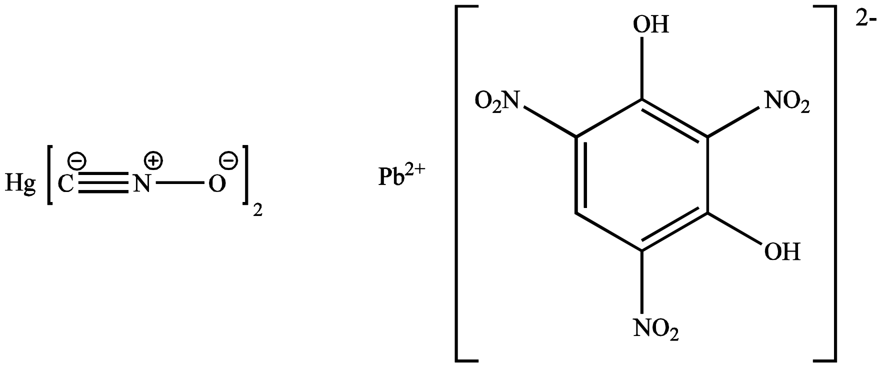

Figure 1.1 Well-known primary explosives: mercury fulminate and lead styphnate.

Secondary explosives (also referred to as high explosives) differ from primary explosives in that they are not easily detonated by heat or shock and instead require initiation by the intense shock-wave produced by a primary explosive. Once detonated however, secondary explosives create a sustained shock-wave over longer distances.

Unlike primary explosives, a raft of high explosives has been developed; many display common features however, such as the prevalence of nitro groups. The most famous explosive molecule is, of course, TNT (trinitrotoluene, see Figure 1.2(a)) which was developed at the turn of the 20th century as a replacement for picric acid, Figure 1.2(b). Picric acid was the most common military explosive of the 19th century, but its sensitivity and hazardous casting process meant that replacements were eagerly sought. After World War I, research programmes were initiated with the aim of synthesising and developing more powerful explosives, the results of which were primarily RDX and HMX. These compounds, depicted in Figure 1.2(c) and (d), remain the most widely-used explosives in current munitions.

Recent developments in explosive formulations have been more adventurous with the design of polycyclic compounds, such as CL-20 and octanitrocubane, shown in Figure 1.3. The explosive performance of CL-20, attributed to the inherent strain and the high energy-density within the molecule, has been shown to exceed that of HMX.[5] However, concerns remain over its sensitivity. Nitrocubanes meanwhile are predicted to be the most powerful explosives ever synthesised. Eaton *et al.* successfully synthesised a range of polynitrocubanes, including octanitrocubane shown in Figure 1.4, although the complicated synthetic procedure and the exorbitant cost of the raw materials ($40 000 per kg in 2000) have hindered full characterisation of its explosive performance and hence its implementation in munitions.[6]

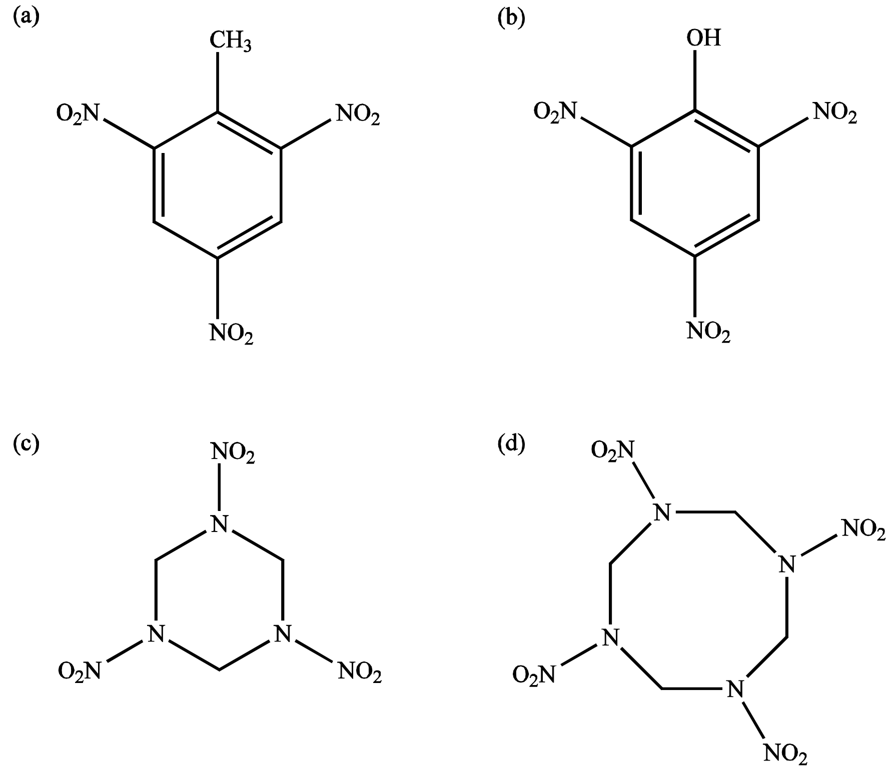

Figure 1.2 (a) the molecular structure of TNT, trinitrotoluene, presented alongside (b) picric acid, the molecule which it would come to supersede; the production of (c) RDX and (d) HMX was developed in the 1940s, but both remain widely used in current munitions.

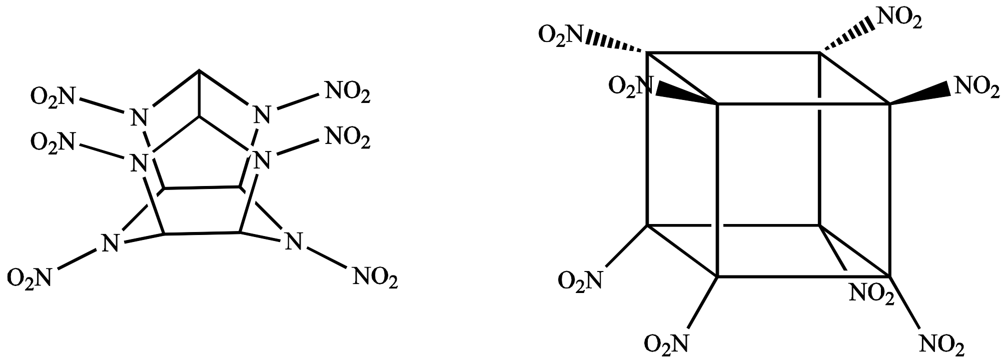

(a)

(b)

Figure 1.3 Molecular structures of the high-energy polycyclic materials (a) CL-20 and (b) octanitrocubane.

While significant research effort has been directed at improving explosive power, recent developments have also been motivated by reducing the sensitivity of energetic materials to accidental detonation. Nitro-1,2,4-triazole-3-one (NTO) is a heterocyclic compound with high energy and low sensitivity; FOX-7 (or 1,1-diamino-2,2-dinitroethene) also displays a detonation velocity comparable to RDX but with dramatically reduced sensitivity, attributed to the high-degree of conjugation and hydrogen bonding within its crystal structure.[7] NTO and FOX-7 are illustrated in Figure 1.4. Finally, the desire for an energetic material that produces no greenhouse gases upon detonation has led to the development of another range of energetic materials, sometimes referred to as ‘environmentally-friendly’ explosives. While this concept may appear initially paradoxical, it has become a priority for current researchers, since the responsible disposal of these materials is now the subject of international regulation.

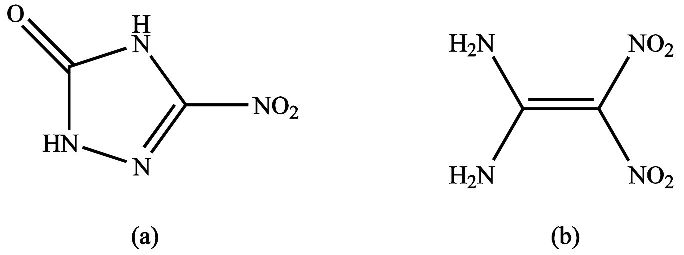

Figure 1.4 Molecular structures of the insensitive munitions, NTO and FOX-7.

Recent advances in the synthesis of novel energetic materials have been thoroughly reviewed by Agrawal [8], Pagoria *et al.* [9] and Badgujar *et al.*[10]

1.1.3 Energetic Performance

It is essential that the performance and reproducibility of energetic materials are fully assessed prior to their application in munitions. Properties that are critical to energetic performance include sensitivity to detonation (by impact, friction, shock or charge); the detonation velocity (defined as the velocity of the shock-wave passing through the detonated material); thermal stability and crystal morphology.[11] The crystal density is also a critical criterion for performance assessment, since it is desirable to obtain the material in as dense a form as possible for applications where volume is limited (such as in explosive charges). Moreover the detonation velocity is, to a first approximation, proportional to the crystal density [1] and it is therefore common to use experimental densities (and calculated densities for novel materials) as an approximate index for explosive power.

The solid-state chemistry of this class of compounds often strongly influences these properties and may therefore have significant consequences for explosive performance and its reproducibility.[12] This is especially true for materials that exhibit the phenomenon of polymorphism.

1.2 Polymorphism

1.2.1 Definition

The term ‘polymorphism’ can have different connotations depending on the field in which it is applied. Most commonly used in genetics and molecular biology, as determined by a recent survey of the Chemical Abstracts [13], it describes the co-existence of two or more discrete phenotypes or genotypes within a sample population. It can also be used to describe the ability of a computer programming code to deal with different input sources. In chemistry and materials science however, the term is generally given to a situation in which “a substance can exist in more than one crystalline state.”[14] These different crystalline states, or polymorphs, are identical in the liquid and vapour states but display different crystal structures in the solid state. Polymorphism can therefore greatly affect a range of properties such as melting/sublimation temperature, heat capacity, conductivity, solubility, density, refractive index and solid-state reactions.[15] Such is the impact of this phenomenon on materials chemistry, it has been the subject of numerous reviews and special issues within the literature, a sample of which can be found in [16-21] and references therein.

A familiar example of polymorphism is elemental carbon. Carbon can exist in numerous allotropic[1] crystalline forms: primarily graphite and diamond, although lonsdaleite (a hexagonal analogue of diamond), fullerenes (three-dimensional cages made solely of carbon atoms, for example C_{60} and C_{70}) and carbon nanotubes either exist naturally, in minute quantities, or have been synthesised by researchers.[22-26] The striking structural variety of these forms is presented in Figure 1.5 alongside a representation of amorphous carbon (displaying no long-range crystalline order) for completeness. These structural differences imbue each allotrope with dramatic differences in their chemical, physical and electrical properties. Diamond is the hardest material known and is electrically insulating, optically transparent and chemically inert. In contrast, graphite is black, soft, electrically conducting and chemically reactive.

---

[1] In this case, the term allotropy is more often used as the substance in question is an element.

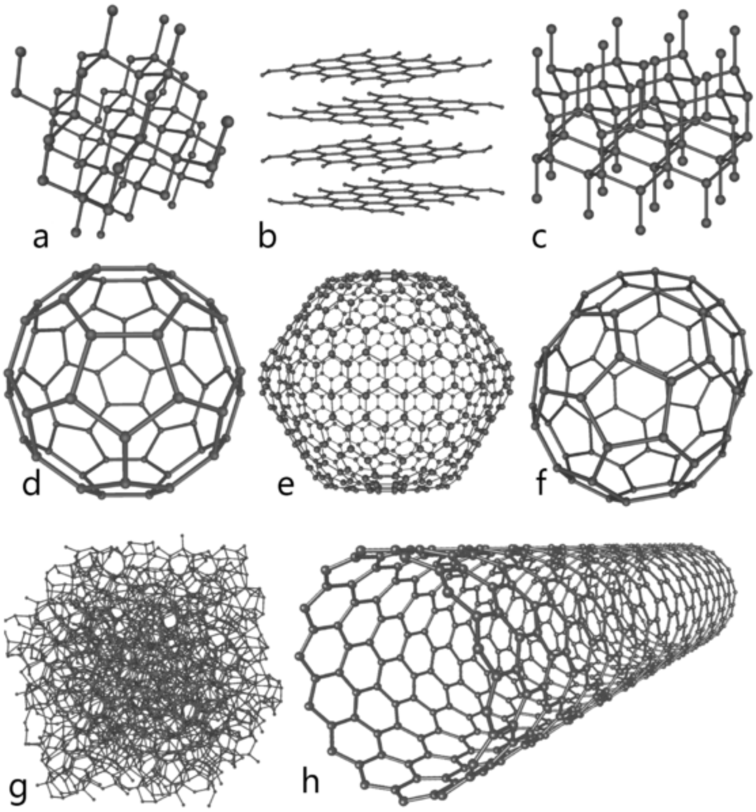

Figure 1.5 Allotropes of carbon: (a) diamond, (b) graphite, (c) lonsdaleite, (d) buckminsterfullerene, C_{60}, (e) C_{540}, an icosahedral fullerene, (f) C_{70}, fullerene, (g) amorphous carbon, and (h) single-walled carbon nanotube.

This example not only highlights the structural diversity of different polymorphs but also underscores the delicate balance between thermodynamics and kinetics during crystallisation. While thermodynamics governs the stability of a particular crystalline form, the crystallisation process itself is often dictated by kinetics. This may result in the appearance of metastable polymorphs, some of which may exhibit sufficient stability to exist for years. Under ambient conditions the most thermodynamically stable allotrope of carbon is graphite. However, due to the high energy barrier to conversion of diamond to graphite, this process is extremely slow (in effect impossible) at ambient conditions. The crystallisation of metastable polymorphs has been 'formalised' in Ostwald's Rule of Stages, which states that the metastable form will often crystallise first (a reflection of the initial kinetic control) but over time this form will transform to a more stable form (due to thermodynamics).[27]

The sometimes competing influences of kinetics and thermodynamics mean that a wide range of materials have been documented to display polymorphism. Indeed comments like McCrone's "*in general, the number of forms known for a given compound is proportional to* *the time and money spent in research on that compound*" [28] suggest that polymorphism is the rule, rather than the exception. While it is no doubt the case that the *possibility* of polymorphism always exists for a given compound, the exact conditions for the crystallisation of other forms are not necessarily obvious, nor achievable. Of the *ca* 500 000 crystal structures deposited in the Cambridge Structural Database as of November 2009, 16 014 bear the tag 'polymorph'.[29] This clearly demonstrates that compounds displaying proven polymorphism are in the minority (3.3%), especially when one considers that this is a measure of the number of individual polymorphs in the database, not the number of polymorphic molecules. Despite this, the implications of polymorphism on myriad physicochemical properties underline the importance of the characterisation of all possible polymorphic modifications, particularly in an industrial setting.

1.2.2 Implications of polymorphism

Materials Science

The dramatic consequences that may arise from a polymorphic transition can be best exemplified by reference to the catastrophic deterioration of tin objects upon exposure to long durations of sub-ambient temperatures. Tin undergoes an allotropic conversion from white tin (β-Sn) to grey tin (α-Sn) at 286 K.[30] In the β-form, tin is a ductile metal that adopts a body-centred tetragonal structure ($I4_1/amd$), with a density of 7.28 Mg m^{-3}; below the transition, α-Sn is a brittle semi-conductor with a considerably less-dense, cubic structure (5.75 Mg m^{-3}, $Fd3m$).[31] The $\beta \rightarrow \alpha$ transition therefore results in a catastrophic volumetric expansion of ~ 27%, characterised by the appearance of discrete powdery efflorescences of grey tin that gradually spread and coalesce, eventually reducing the tin to powder (see Figure 1.6).[32] The defeat of the Napoleonic army in the Russian steppes and the ill-fate that befell Captain Scott and his crew on their expedition to the South Pole have both, perhaps erroneously, been attributed to this phase transition.[32]

Observations of this 'tin pest' or 'tin disease' were first reported by German and Russian scientists who noted the marked deterioration in large portions of tin organ pipes and other tin artefacts in the mid 19th century.[33, 34] This curious behaviour was only rationalised in the early 20th century as a result of Cohen's rigorous investigation of the transition temperature, its kinetics and its reversibility (the results of which were published in a series of articles in *Zeitschrift für physikalische Chemie*, for example [35, 36]). He found that the transition occurred most quickly at ~ 225 K, that it was reversible but also that samples that had previously undergone temperature-cycling underwent the $\beta \rightarrow \alpha$ much more swiftly.

This observation was rationalised by the presence of grey-tin nuclei providing nucleation sites for subsequent transitions.

Figure 1.6 Total disintegration of a tin test piece after prolonged exposure to temperatures *ca* 255 K.[37]

Commercial grades of tin were shown not to undergo this disintegration however – trace impurities commonly found in such samples have been credited with retarding the β → α transition or even stopping it altogether.[37] One may therefore assume that tin pest may be consigned to the history books and, quite literally, to museum pieces (and their conservation). However, recent European regulations restricting the use of hazardous substances have meant that lead-free solders containing 95 – 99% Sn have had to be developed.[38] This had led to a recent resurgence in research into this polymorphic transition, particularly since circuitry in cold environments (*e.g.* aerospace) risk failure in this way. Small quantities of elements that are soluble in tin (Sb and Bi, for example) have been shown to decelerate the rate of transition; insoluble elements such as Zn, Al and Mg actually promote it.[39]

Food Science

Polymorphism has also been shown to play an important role in the processing of foods based on fat molecules (triglycerides), such as margarine, ice cream and chocolate. The melting behaviour of such molecules is intrinsically linked with the sensory experience of these products, affecting texture and appearance. This is further complicated for producers of chocolate, since cocoa butter can adopt one of six polymorphs over a very narrow temperature range (289 – 309 K), only one of which has the desired characteristics.[40] If the wrong form is present, or the fat has not been crystallised (tempered) correctly, white powdery deposits form on the surface, known as fat bloom. There has therefore been considerable industrial impetus for the structural characterisation of a range of triglycerides as well as the determination of their physical properties and the optimum conditions for their crystallisation.[41-43]

Pharmaceuticals

Despite these illustrative examples of the implications of polymorphism in materials science and food technology, polymorph screening experiments are still primarily carried out on pharmaceuticals. This is because polymorphism can lead to profound effects during processing, serious implications for patient risk and costly challenges to intellectual property.

Throughout the manufacturing process drug molecules are exposed to a range of pressure and temperature conditions, during grinding, freeze-drying and tabletting for example. It is therefore crucial to determine whether any polymorphic transitions are likely to occur under such conditions if one is to ensure the consistent and selective production of the desired form.[44] Furthermore, throughout its shelf-life a pharmaceutical product will experience fluctuations in environmental factors such as temperature and relative humidity which may also promote phase transitions. This is best illustrated by the case of Ritonavir, a protease inhibitor used in HIV treatments: the crystallisation of a thermodynamically more stable (and therefore less soluble) form of the drug two years after its introduction to the market resulted in substantial costs for its producers.[45]

Since the majority of drug molecules rely on their dissolution in the gastro-intestinal tract to allow their function within the body, it is reasonable to conclude that the bio-availability of a given polymorph is related to its solubility.[46] Two polymorphs will therefore have significantly different activities, and thus dosages must be adapted to reflect this. It is essential therefore that solubility and bio-availability are ascertained before the drug is administered.

As a result of the significant impact of these properties on the effectiveness and safety of pharmaceuticals, it has now become a legal requirement for companies to provide detailed information regarding drug polymorphs to licensing bodies such as the United States Food and Drug Administration (USFDA).

Finally, pharmaceutical companies are motivated to carry out extensive polymorph screening operations in order to protect their own intellectual property and patents. Although international patent legislation varies, challenges to patents have been successful on the basis of the discovery of new polymorphs. As demonstrated above, a new crystalline form may be expected to exhibit very different physical, chemical or biological properties thus subverting patent protection. Therefore in order to maintain, or in certain cases lengthen, the exclusivity of the patent, it is necessary to characterise all polymorphs prior to its issuance. Bernstein's monograph contains various case studies illustrating this subject.[11]

Energetic Materials

As outlined in Section 1.1.3, the performance of an energetic material depends on a number of factors, such as sensitivity, detonation velocity and thermal stability. Since these factors are inextricably linked with the material's solid-state chemistry, polymorphism can have significant implications for explosive performance and reproducibility. Much like in the pharmaceutical industry, it is therefore essential that all polymorphs are identified, their stability (or metastability) is assessed critically, and the conditions under which they are formed are characterised. Furthermore any polymorphic transitions which may be reasonably expected to occur during storage or application should be studied – structural investigations at variable temperature and pressure have therefore been pursued more extensively in this industry than in any other. The occurrence of polymorphism in nitroglycerine, TNT, RDX and HMX, for example, is well documented (such as in [11] and references therein).

HMX (Figure 1.2(d)) is an excellent illustrative example of the role played by polymorphism in energetic materials. Four forms of HMX have been identified and structurally characterised (α, β, γ, δ), although the γ-form has been shown to be a hemihydrate, and not a true polymorph.[47-49] Investigations have shown that the sensitivities to impact follow the order $\delta > \gamma > \alpha > \beta$.[50] The risk of accidental detonation of the δ-, γ-, and α-forms means that only β-HMX is permitted in munitions used by the British armed forces.

Of particular note in recent years, mainly due to concerns over sensitivity, is the polymorphism of triacetone triperoxide (TATP, see Figure 1.7). TATP is an improvised explosive that can be synthesised from readily-accessible raw materials and has gained notoriety due to its alleged use in terrorist attacks. TATP is extremely sensitive to detonation, making it impractical for military and civilian munitions. This situation is exacerbated by the recent identification of six polymorphs of this material - the sensitivity and explosive characteristics of each is currently being investigated.[51]

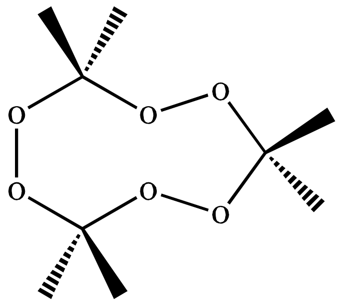

Figure 1.7 Molecular structure of triacteone triperoxide (TATP).

In many cases, the conditions experienced by energetic materials during manufacturing and storage are similar to those applied to pharmaceuticals – it is therefore essential to determine if the material is at risk of undergoing polymorphic conditions under these conditions. A catastrophic example of the sensitisation of an explosive during its shelf-life is that of ammonium nitrate. Ammonium nitrate is primarily used as a fertiliser, although it is a strong oxidiser and can therefore be incorporated into energetic formulations with hydrocarbons such as diesel or kerosene. Accounts of polymorphism of NH_4NO_3 are among the oldest of any energetic material, dating to 1903.[52] It has been shown to adopt four different polymorphic structures at atmospheric pressure, depending on temperature.[53]

Of critical importance for handling and storage of NH_4NO_3 is the phase transition between the forms IV (*Pmmn*) and III (*Pnma*) at 305 K, which is accompanied by a significant (~ 4%) volume change and the formation of dislocations in the crystal structure. Temperature-cycling through this transition, due to diurnal temperature fluctuations, resulted in large quantities of stored material caking together. Attempts to break up caked masses (using blasting explosives!) resulted in the detonation of the ammonium nitrate stockpile, causing widespread destruction and a number of deaths and injuries in the first half of the 20th century.[54] It has subsequently been shown that the IV → III transition can be retarded, and even halted, by the addition of small quantities of additives such as KNO_3, $Mg(NO_3)_2$ and NiO, and thus doped ammonium nitrate is insensitive enough for use in current armaments.

Finally, crystal density has become an index for explosive power, since density is directly proportional to the detonation velocity. Polymorphs adopt different crystal packing and will therefore exhibit a range of crystal densities. It is therefore desirable to obtain the material in as dense a form as is practicable. An interesting example is provided by octanitrocubane (ONC), depicted in Figure 1.3. Only one polymorph of ONC has been reported in the literature since its successful synthesis.[6] The experimental crystal density, as determined by X-ray single-crystal diffraction, was found to 1.979 Mg m^{-3}. While comparable to other high explosives, such as HMX and CL-20, this is lower than the theoretically predicted density of 2.06 Mg m^{-3}.[6] This is perhaps a tantalising inference to a denser polymorph that may be crystallised, providing the conditions are right. However, in the decade since ONC was first synthesised, no experimental reports on this denser form have been published.

All of the energetic materials included in this discussion so far display polymorphism under ambient conditions – although only one crystal form represents the thermodynamic minimum under these conditions, one (or various) other form is sufficiently metastable to be observed. Polymorphism, however, is not constrained to ambient conditions. As has already been intimated, particularly by the case of ammonium nitrate, different polymorphs may be adopted at different temperatures. A further thermodynamic variable which can drastically alter the relative stabilities of known polymorphs, and indeed can result in the formation of entirely new polymorphs, is pressure. This is particularly pertinent to a discussion of the polymorphism of energetic materials, which often experience pressures of several thousand times greater than atmospheric pressure during a detonation event. High-pressure polymorphism in these materials can have equally dramatic consequences for their performance and should therefore be explored equally as fully as ambient pressure studies.

In the sections that follow, a general introduction to high-pressure science is given, outlining the general concept and the motivation for the wealth of science that has been carried out at extreme conditions. This will be illustrated by examples from a range of fields, such as biotechnology and materials science. Finally, the importance of obtaining high-quality structural data on energetic materials at elevated pressures will be underscored with a discussion of previous high-pressure studies and an outline of the research presented in this work.

1.3 High Pressure

1.3.1 General Concept

The free energy of a particular system can be related to the pressure (P) and temperature (T) conditions by the following equation:

$$G = U - TS + PV$$

where G represents the Gibbs' free energy, U is the internal energy of the system, S is entropy and V is volume. Pressure therefore is a fundamental thermodynamic variable. While it is common practice to vary the temperature of a system, we are limited to a range of a few thousand degrees. This range is narrowed further if the system of interest is based on small organic molecules that decompose at temperatures of a few hundred Kelvin. In stark contrast, high-pressure studies in the terapascal (1 000 GPa) regime have been reported recently.[55, 56] This represents a pressure range from atmospheric pressure to 1.0 TPa of the order of 10^7. Although terapascal experiments are by no means routine (they utilise high-pressure shock-waves), pressures of 0.1 – 10 GPa are regularly attained in laboratory studies and are sufficient to induce an exciting array of structural changes.

By altering the pressure of the system, we are readily able to alter its free energy. In so doing, it is possible to induce polymorphism or to divert a reaction pathway. Moreover by undertaking structural investigations at a range of pressures, we gain information on the relative contributions that inter- and intramolecular interactions make to the total free energy of a crystalline system. High-pressure structural studies also present a very rigorous test of intermolecular potentials used in molecular modelling.[57]

Descriptions of the apparatus used to generate high pressures in this study will be detailed in later sections. It is instructive, however, to include a short review of the development of this field and acknowledge the achievements that have propelled the field to the forefront of structural science.

The pioneering work by Bridgman pushed the boundaries of controlled high-pressure experiments, firstly to 7000 atmospheres (0.7 GPa) in the 1930s, then to pressures in the region of 2 GPa.[58] In this pressure regime, well-known substances began to display intriguing properties – solid H_2O transformed into its ice-VI form, which was observed to begin melting about 373 K.[59] Further technical innovation and development led to the introduction of opposed-anvil devices that had the capability of reaching pressure between 5 and 10 GPa.[60, 61]

The most important breakthrough since Bridgman's work has been the invention of the diamond-anvil cell (DAC). This elegant device, which will be discussed in detail in Section 2.2, has facilitated the generation of pressures greater than 100 GPa and has allowed the characterisation of materials *in situ* by diffraction and spectroscopy. A summary of the advances in high-pressure technology, as well as those in experimental techniques, can be found in Katrusiak's excellent review.[62] Moreover, an edition of *Reviews in Mineralogy and Geochemistry* is devoted entirely to the crystallographic characterisation of a range of materials (from small molecules to minerals) at extreme conditions.[63]

In high-pressure research, it is common to find various units used, sometimes interchangeably, as a measure of pressure. All pressures in this study will be reported in gigapascals (GPa), which may be related to other units as follows:

1 GPa = 10 kbar = 9869.2 atm.

1.3.2 Previous High-Pressure Research

The impact of high-pressure research not only in the areas of physics, chemistry and materials science, but also biotechnology and food science, has been profound. A review of the recent applications of high-pressure science, which is by no means exhaustive, is given below.

Simple Elements and their Exotic Structures

The application of high pressure to simple (or *sp-*) elements has proven to be a particularly fertile research area, with many elements displaying complex crystal structures and anomalous physical properties at elevated pressures. The high-pressure behaviour of elements has been the subject of numerous reviews and for more in-depth discussion, the reader should consult [64-66] and references therein. Two examples have been selected to illustrate the structural diversity of supposedly simple elements under pressure however: sodium and oxygen.

Sodium displays a rather complex phase diagram with respect to pressure and temperature. Throughout compression at ambient temperature, the body-centred cubic (bcc) form remains stable to a maximum pressure of *ca* 65 GPa, at which point it undergoes a phase transition to a face-centred cubic (fcc) structure.[65] Compression studies carried out at elevated pressures and temperatures, however, presented evidence for the anomalous melting behaviour of sodium in the high-pressure regime. Gregoryanz *et al.* showed that the melting line reaches a maximum at *ca* 31 GPa and 1000 K and decreases steeply in its fcc phase.[67] Furthermore, this reaches a minimum at *ca* 118 GPa and 300 K, meaning it is possible to melt a sample of sodium solely by one’s body heat (!), provided the sample is at sufficient pressure.[68] Using single-crystal X-ray diffraction, the authors were able to characterise seven different crystalline phases located around this minimum. Finally, above 180 GPa sodium has been shown to become optically transparent and insulating – a truly remarkable observation.[69]

To date six distinct crystalline forms of oxygen have been identified, at variable temperature and pressure. The α-, β- and γ-forms can be adopted at temperatures below 100 K at ambient pressure. Under compression at 295 K, liquid oxygen solidifies into the β-form at 5.4 GPa before transforming to the 'orange' δ-form (9.6 GPa), which itself undergoes a phase transition to the 'red' ε-form at 10 GPa.[70] Single-crystal X-ray diffraction has shown that in the ε-form the oxygen atoms organise themselves into rhombohedral O_8 molecular units, rather than maintaining the diatomic nature of the lower pressure phases.[71] Finally, at very high pressures (*i.e.* $P > 96$ GPa) oxygen becomes metallic; this high-pressure metallic ζ-form even becomes superconducting at very low temperatures ($T_c = 0.6$ K).[72, 73] The exotic behaviour of an element that we are all familiar with in the gaseous state underscores the power that pressure has in dramatically changing not only the crystal structure of materials, but also their chemical, physical and electronic properties.

Molecular Systems

While the exotic structural behaviour displayed by elemental samples often requires pressures in the range of 10 – 100 GPa, a considerable amount of information can be gleaned by compression of organic materials to modest pressure (0.1 – 10 GPa). The development of high-pressure apparatus and the increasing brightness of X-ray sources, for example synchrotron sources (see Section 2.3.5), has facilitated the structural characterisation of weakly-scattering samples at high pressure. This is an immense accomplishment, especially when one considers the low symmetry (monoclinic or even triclinic) crystal systems that organic molecules often adopt.

The driving force behind the considerable body of work in this field is the identification, characterisation, and, ultimately, prediction of polymorphism in molecular systems. Moreover, high-pressure studies can afford detailed knowledge of intra- and intermolecular interactions and allow an appraisal of the relative contributions these interactions make to the free energy of a crystalline system. Rather than attempting to summarise the prodigious high-pressure research carried out on molecular systems, this section will instead feature illustrative examples. For a broader introduction, the reader should consult Bernstein's monograph [11], or one of the numerous review articles, such as [57, 74-76].

The high-pressure study of molecular materials can be largely partitioned into: (i) the direct compression of solid materials, generally under hydrostatic conditions; and (ii) their crystallisation at pressure, from either the liquid or solution phases. Direct compression is often a fundamental objective of high-pressure analyses, whether to obtain a measure of the compressibility of the material, to initiate polymorphic transitions, or to induce or affect chemical reactions. High-pressure crystallisations meanwhile exploit pressure as a thermodynamic variable to cause the precipitation of high-pressure polymorphs, some of which may not be accessible by direct compression.

At the relatively modest pressure utilised in these studies (< 10 GPa), covalent bonds do not deviate significantly from their ambient pressure values. However, intermolecular interactions, such as van der Waals interactions and hydrogen bonds, are sensitive to compression. Furthermore, molecular conformations can be readily modified by the application of pressure, particularly if this results in a more efficient crystal packing at elevated pressures. By monitoring compression mechanisms and by structurally characterising high-pressure forms, it is possible to gain an understanding of how molecular crystals adapt to pressure.

Comprehensive studies of the compressibility of small molecules bearing particular functional groups or packing motifs have allowed some generalisations to be made about the effect of pressures on these materials. For example, the high-pressure polymorphism of amino acids has been extensively studied by various groups.[57, 75, 77] Phenomenological evidence from studies such as these suggests that compression is often accompanied by: the collapse of voids within the ambient pressure crystal structure; the particular sensitivity of interplanar distances to compression; a marked rigidity of hydrogen-bonded chains or layers; or the strengthening of favourable intermolecular interactions. For example, the α-form of the amino acid glycine is reported to be 20% more compressible along the direction parallel to interplanar C-H…O hydrogen bonds, when compared to intraplanar N-H…O interactions. This observation has been rationalised in terms of the minimisation of the stacking distance between layers.[78,79]

Nevertheless, significant exceptions to these rules have been reported. For example, Moggach *et al.* actually observed an *increase* in pore size upon compression of a metal-organic framework, although this has been attributed to dynamic interactions between the sample and the pressure-transmitting medium.[80]

In order to rationalise the effects of pressure, a method for the calculation of intermolecular packing energies has been developed in recent years.[81] The PIXEL method has been shown to be valid for the high-pressure phase transitions observed in salicylaldoxime [82] and serine.[83] However, the application of PIXEL calculations to the phase transition in L-serine monohydrate had unexpected results. Although a strengthening of interplanar Coulombic interactions between serine molecules was observed and the water molecules become co-ordinatively saturated with respect to hydrogen bonding, the intermolecular interactions are reported to be weaker in the high-pressure form II.[84] In this case, the more efficient crystal packing in form II is more dominant than favourable intermolecular interactions. The maximisation of packing efficiency has also been found to be dominant in the high-pressure behaviour of a rather unusual crystal structure. Methyl 2-(carbaxol-9-yl)benzoate adopts a monoclinic structure with eight molecules in the asymmetric unit (*Z'* = 8), represented in Figure 1.8. Compression to 5.3 GPa, however, results in a phase transition to an orthorhombic structure with *Z'* = 2.[85] The stabilisation due to the dominance of the *PV* term at high pressures is sufficient, in fact, to outweigh the unfavourable molecular conformations adopted in the *Z'* = 2 structure (as determined by *ab initio* methods).

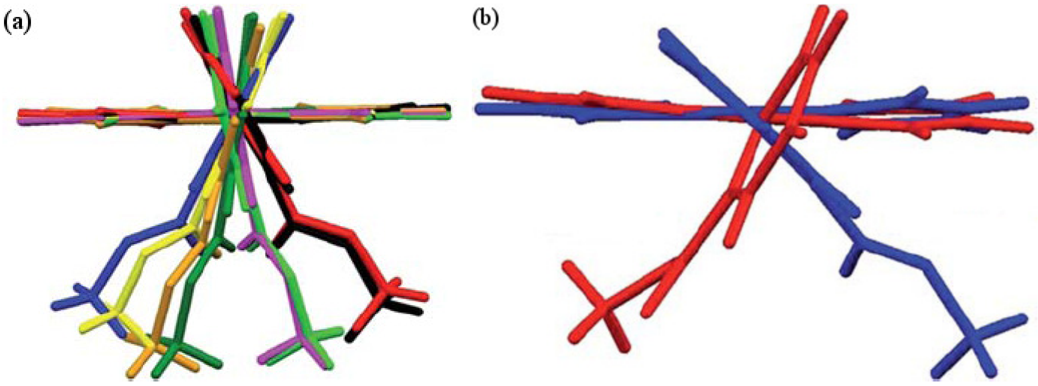

Figure 1.8 Representation of (a) the 8 molecular conformations in methyl 2-(carbaxol-9-yl)benzoate at ambient pressure and (b) the 2 conformations at 5.3 GPa.[85]

As an alternative to the direct compression of solid materials (in which pressure is applied to the ambient-pressure form), pressurisation of liquids or solutions may allow the crystallisation of high-pressure forms to be accomplished directly. In the simplest cases, crystallisation by the application of pressure to pure liquids is analogous to the crystallisation observed upon cooling. For example, the high-pressure and low-temperature forms of 1,2-dichloromethane have been shown to be isostructural.[86] It is more often the case, however, that the high-pressure and low-temperature forms are quite distinct. A variety of molecules, including benzene [87], water [59], phenols [88-90] and, most recently, nitric acid [91] have been shown to adopt different crystal structures in the high-pressure and the low-temperature regimes.

The pressure-induced crystallisation from the liquid phase is only achievable for samples that are liquid at ambient temperature or those with sufficiently low melting points (*i.e.* < 323 K) such that they may be loaded into a diamond-anvil cell in the molten state. This approach is simply not practical for samples with high melting points (such as large pharmaceutical molecules). This is further exacerbated by the general increase in melting point at elevated pressures. An alternative to this approach is to utilise the decrease in solubility at pressure in order to crystallise high-pressure forms from saturated solutions.

Fabbiani *et al.* have exploited this phenomenon in their 'high-pressure recrystallisations' to obtain a range of novel forms (including polymorphs and solvates) of materials such as paracetamol, parabanic acid and acetamide.[92-94] This technique is perhaps still in its infancy however, since its systematic application in the search of new polymorphs is limited. For example, by simply varying the solvent or the crystallisation pressure, one may dramatically affect the kinetics and/or thermodynamics during crystallisation and hence it may be possible to obtain an array of different forms. Results of such investigations would be invaluable, not only in the identification of new polymorphs, but also in understanding the effects of temperature, pressure *and* solvent on the crystallisation process.

Biotechnology

While the high-pressure polymorphism of the amino acids has been explored extensively, the structural complexity of proteins and other biomolecules makes their high-pressure characterisation far more complicated. Despite this, the desire to understand the effect of pressure on biological systems has driven recent instrumental and methodological advances.[95, 96] For example, Girard *et al.* have developed a pneumatic diamond-anvil cell specifically for macromolecular crystallography [97], although dedicated short-wavelength synchrotron radiation still remains a pre-requisite for crystallographic studies of these complex systems.

Although the pressures in these studies are meagre in comparison to those attained in the investigation of elements, for example, biological systems are observed to exist over a pressure range spanning almost four orders of magnitude. Natural ecosystems alone are observed between atmospheric pressure (0.1 MPa) and 0.1 GPa at the deepest point of the Mariana Trench.[98] Meanwhile pressures of *ca* 1.0 GPa are routinely attained in high-pressure processing techniques, in the food industry for example (*vide infra*). Characterisation of proteins in this pressure regime therefore provides invaluable information, not only on the piezophilic (*i.e.* pressure loving) bacteria that thrive at these extreme conditions, but also on the origins of life under high pressure.[99]

More recent high-pressure experiments, however, have utilised pressure as a thermodynamic variable to artificially alter the bio-systems under investigation. Although exposure to pressures > 0.4 GPa can result in complete denaturation of proteins, intermediate pressures (*ca* 0.2 GPa) can cause subtle changes in the quaternary structure[2], which may or may not be reversible. In a particularly exciting application, moderate high-pressure treatment is being proposed in the context of vaccine development.[100] The infectivity of the HIV-1 virus was observed to be removed completely at 0.2 GPa, for example.[101]

In addition to the modification of proteins and enzymes, high-pressure treatments have also been applied to mammalian and plant cells. Pressure-induced cellular changes have been shown to protect mammalian cells from damage occurring during cryopreservation.[98] Exposure of fresh bull semen to very gentle pressures (20 – 40 MPa, 90 – 120 mins) prior to its cryostorage was shown to preserve its viability, motility and fertility after thawing.[102] Finally, high-pressure treatment has been shown to increase biomass and grain yield in rice.[103]

Food Science

The modification of biomolecules by high-pressure treatment has also been exploited in the food processing industry to prolong shelf-life without compromising sensory or nutritional properties. Pressure (in these cases up to 1.0 GPa) has been found to influence enzymatic reaction rates and can inactivate micro-organisms, which have the potential to cause the food to spoil and can affect food safety. However, pressure-treatment does not lead to the detrimental effects on the taste or appearance associated with other preservation methods (such as heat), since pressure has limited effects on the covalent bonds within the foodstuff.

The effect of high-pressure (HP) and high-pressure/high-temperature (HPHT) processing on the colour, texture and flavour of fruit- and vegetable-based products has been reviewed in detail by Oey *et al.*[104] They highlighted the benefits of pressure treatment of a selection of foods; the firmness of fruits subjected to high pressures and temperatures, the colour of pressure-treated green vegetables, and the flavour HP fruit juices were all superior to those subjected solely to high-temperature processing. However, since HP-treatment can enhance or retard chemical and biochemical reactions, it can give rise to both desirable and undesirable products. For example, strawberry jam was reported to smell more chemical, rancid and less fruity than traditionally-processed jam.[105]

The sector of the food industry where high-pressure treatments have made a significant impact, and have already been commercialised, is in the processing of shellfish. HP treatment is particularly apposite in this case, since it is necessary to protect against shellfish-

---

[2] The quaternary structure arises from the combination of two or more chains, resulting in a complete unit. Quaternary interactions are simply characterised as being inter- rather than intra-chain.

borne pathogens while maintaining the appearance, flavour and texture of the raw products. The inactivation of bacterial spores in bivalve shellfish (oysters and clams, for example) can be accomplished by mild pressurisation (*ca* 0.1 GPa). Such treatment has the added benefit of shucking or opening shellfish, making this technology particularly beneficial to industry and consumers alike.[106]

Finally, in a very recent development, high-pressure treatment has been shown to eliminate the allergenicity of wheat products. Yamamoto *et al.* have presented UV and fluorescence spectra, which suggested that pressure-treatment results in a structural adaptation in alpha amylase inhibitor (α-AI), thus reducing its allergenicity.[107]

Pharmaceuticals

Throughout their manufacture, pharmaceuticals can be subjected to elevated pressures, in the milling (*i.e.* mechanical grinding) and tabletting processes. These pressures (typically less than 0.1 GPa) have been shown to be sufficient to induce either complete or partial phase transitions in pharmaceuticals.[108, 109] It is therefore critical to add pressure as a variable to the battery of screening tests in order to assess the polymorphism of these important materials fully. For a more illustrative review of the effects of pressure during the manufacture of pharmaceuticals, the reader should consult [110, 111] and references therein.

However, rather than merely playing a reactive role, by characterising undesirable polymorphic transitions during processing, high-pressure studies have recently been employed to enhance the properties of the active pharmaceutical ingredient (API). Compression studies using the diamond-anvil cell (DAC) have extended the pressure range, for which pharmaceuticals can be structurally characterised and have thus broadened the potential for the identification of new polymorphs. In select cases, these high-pressure polymorphs may display sufficient metastability to allow their recovery to ambient pressure and subsequent use as seed crystals to direct large-scale crystallisation processes. Furthermore high-pressure recrystallisation experiments developed by Fabbiani *et al.* [92-94] have been shown to be particularly successful in the production of a range of solvates as well as novel unsolvated polymorphs.

An excellent example of the different possible forms that can be obtained depending on the crystallisation technique, including direct compression and high-pressure recrystallisation, is paracetamol (Figure 1.9). Under ambient conditions, the thermodynamically most stable form is the monoclinic form I [112-114] but a metastable orthorhombic form II has also been identified.[115] In addition, an orthorhombic form III, which has proven to be an elusive polymorph has only recently been structurally characterised by X-ray powder diffraction.[116-119]

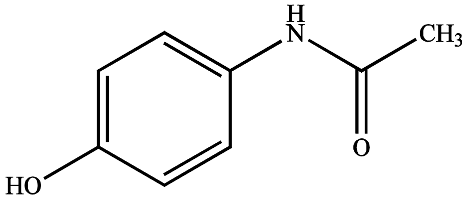

Figure 1.9 Molecular structure of paracetamol (acetaminophen).

The relatively poor compaction properties of the monoclinic form are well known – it is often necessary to include binding agents such as gelatine or starch derivatives during tabletting, thus complicating the manufacturing process.[120] In contrast, form II exhibits much more isotropic compression, thereby presenting a much more facile production.[121] There is therefore considerable interest in selectively and reproducibly obtaining form II.

Numerous methods have been shown to be successful for the crystallisation of this metastable polymorph, although techniques are often involved and not sufficiently discriminating.[122-125] In addition to these ambient pressure techniques, Boldyreva *et al.* showed that polycrystalline samples of form I could be converted to form II by compression to above 4.0 GPa.[121] However, this did not result in complete conversion and it was noted that single crystals did not undergo a phase transition in a similar pressure regime. It is clear from these observations that direct compression alone is not sufficient to obtain the desired pure form II.

High-pressure recrystallisation (DAC) experiments on paracetamol meanwhile have produced small quantities of a range of co-crystals [92, 93] and, indeed, a pure sample of form II at 1.1 GPa.[93] These observations stimulated an investigation into the possibility of the reproducible production of larger quantities of form II by the pressure-induced precipitation from concentrated solutions. Oswald *et al.* have reported the successful recovery of *ca* 0.3 g paracetamol form-II and noted that control over which form is obtained can be exercised by simple modification of the solution concentration and/or crystallisation pressure.[126]

Energetic Materials

As discussed in Section 1.1.1 a high velocity shock-wave passes through an energetic material during its detonation generating pressures of up to 50 GPa and temperatures up to 5500 K.[127] It is essential that one can model and understand the behaviour of energetic materials under these extreme conditions. There has therefore been significant research studying the structural and physical properties of these materials at elevated temperatures and/or pressures, which has been extensively reviewed.[128-130]

Computational methods are currently employed to explore the response of energetic materials to extreme temperature and pressure conditions. These methods may provide valuable information on reaction mechanisms and rate during high energy processes such as explosive decomposition. The aim of such studies is to accurately predict and model the behaviour of current and novel energetic materials, without the need for expensive and hazardous field experiments.[131, 132] However, in order to provide detailed structural information to complement and validate these computational models, it is imperative that empirical high-pressure studies are performed. This information may be obtained by the application of either dynamic or static pressure.

Dynamic compression experiments utilise shock-waves created by firing a high-velocity projectile at the material in question. Velocities of up to 8000 ms^{-1} can be achieved by firing the projectile from either a gas gun or from an explosive charge. Pressures of up to 100 GPa can be attained upon impact. Similar results may be achieved using high-pressure plasmas (generated by the action of high-power lasers on substrates). The equation of state (see Section 2.6) of the material can be determined by the measurement of the propagation speed of the shock-wave through the material and the change of the velocity across the front (*i.e.* the velocity of the material behind the front if the material ahead of the front is at rest). In addition, recent advances in extremely ultra-fast spectroscopy have allowed the response of molecular materials to shock-wave compression to be analysed *in situ*, thus allowing any high-pressure/high-temperature phase transitions to be identified.[133] In contrast, diffraction experiments have been limited to recovered materials.

In order to ascertain the crystal structure of energetic materials at extreme conditions, it is necessary to conduct direct static compression. In these studies it is possible to generate pressures up to ~ 30 GPa and temperatures *ca* 650 K using mechanical apparatus, such as the diamond-anvil cell. The sample may then be studied *in situ* by both spectroscopic and diffraction techniques, allowing an unambiguous assessment of its compression behaviour. Thus it is possible to characterise directly any anisotropy in the compression mechanism, the development of intra- and intermolecular interactions, and the structure of any high-pressure polymorphs.

Previous high-pressure research on RDX (Figure 1.2), CL-20 (Figure 1.3) and a series of inorganic azides will be reviewed in more detail in subsequent chapters. In addition to these compounds, however, there has been a substantial body of work pertaining to the high-pressure behaviour of HMX, FOX-7 and a series of energetic ammonium compounds. This selection, while not exhaustive, illustrates not only the difficulties of performing high-pressure studies, but also the accomplishments that have been made in this field.

HMX (Figure 1.2) displays rich polymorphic behaviour at ambient temperature and pressure – three polymorphs (α, β and δ) and a hemihydrate (γ-HMX) have been structurally characterised by a combination of single-crystal X-ray and neutron diffraction.[47-49] The stability of the β-form with respect to pressure has been studied by a combination of spectroscopic [134], diffraction [135, 136] and computational methods.[137, 138] X-ray powder diffraction experiments to 45 GPa under quasihydrostatic conditions[3] identified (i) a conformational transition at 12 GPa to ε-HMX, with no abrupt volume change, and (ii) a first-order transition at 27 GPa to a further high-pressure form.[139] However, the phase transition at 27 GPa was not observed during the isentropic compression of single crystals of β-HMX.[140] Recent computational studies, which have extended the pressure range for theoretical calculations on HMX to 40 GPa, have produced conflicting accounts of the compression behaviour *ca* 27 GPa. Lu *et al.* do detect an abrupt volume change in their molecular dynamics calculations [141], but not in their DFT (density functional theory) study.[142] Similar DFT studies by Zhu *et al.* and Cui *et al.* did not show any evidence of a phase transition up to 40 GPa.[143-145]

While the majority of experimental and theoretical studies have focussed on the β-form, the stability ranges of the other forms have also been determined. Goetz *et al.* used Raman spectroscopy to show that α-HMX remains stable upon compression to 4.2 GPa, the maximum pressure studied; the γ-form transforms to the β-form at 0.55 GPa; and that δ-HMX converts to a mixture of the α- and β-forms below 0.05 GPa.[134] Finally, Gump and Peiris presented X-ray powder diffraction data suggestive of a β → δ transition upon decompression of the former from *ca* 5 GPa, highlighting the importance of conducting thorough examinations of the decompression behaviour.[135]

FOX-7 has been shown to display rich polymorphic behaviour with temperature (at ambient pressure). In addition to the ambient temperature α-form, two high-temperature forms have already been structurally characterised: β-FOX-7 results from a reversible transition from the

---

[3] Argon was used as the pressure-transmitting medium; Ar has an approximate hydrostatic limit of 1.9 GPa (Angel *et al.*, ref. [13], Chapter 2).

α-form at 389 K [146]; γ-FOX-7 meanwhile is obtained above 435 K and subsequently can be quenched to ambient temperature.[147] In addition, Peiris *et al.* have performed a thorough investigation of the compression behaviour of the α-form to 8.2 GPa, although the significant reduction in intensity of their X-ray powder diffraction patterns at 4.5 GPa during the non-hydrostatic compression led them to suggest that the sample becomes amorphous under these conditions.[148] Neutron powder diffraction studies on FOX-7-d_4 showed the same loss of intensity.[149] No high-pressure investigation has been carried out on a recovered sample of γ-FOX-7. However, decompression of the 'amorphous' high-pressure sample results in a phase transition to the γ-form when this is conducted at elevated temperatures.[149]

Finally, Davidson *et al.* have recently characterised the high-pressure polymorphism of a series of energetic ammonium compounds (ammonium nitrate [NH_4NO_3], ammonium perchlorate [NH_4ClO_4] and ammonium dinitramide [$NH_4N(NO_2)_2$]).[150] Ammonium nitrate was found to be stable upon hydrostatic compression to the highest pressure studied (7.85 GPa). The authors note, however, that previous observations of a phase transition at *ca* 3.0 GPa were made in studies using either a non-gasketed diamond-anvil cell [151] or shock compression.[152] These results therefore highlight the effect of non-hydrostatic conditions on the occurrence of phase transitions.

Ammonium perchlorate, an energetic oxidiser used in solid rocket motors, was observed to undergo a first-order transition between 3.49 and 3.98 GPa, with a 1.8% decrease in volume. By a combination of neutron powder and X-ray single-crystal diffraction, the authors were able to determine the structure of the high-pressure form unequivocally.[150] These observations are broadly in line with previous spectroscopic and power diffraction experiments, although there is a marked variation in the transition pressure. On the basis of their Raman measurements, Brill *et al.* tentatively proposed a phase transition at *ca* 2.4 GPa [153]; shock compression resulted in significant changes in the X-ray powder diffraction pattern reported by Sandstrom *et al.* at 4.7 GPa [152]; and, Peiris *et al.* used vibrational spectroscopy and X-ray powder diffraction to characterise a sluggish phase transition, commencing at 0.9 GPa but only reaching completion at 3.0 GPa.[154] It should be stressed, however, that experimental factors such as hydrostaticity and sample purity may affect phase behaviour dramatically.

Ammonium dinitramide (ADN) is currently being developed as a rocket propellant, since it displays minimum signature characteristics and minimal environmental contaminants. A phase transition has been reported to occur during compression of ADN at 2.0 GPa, as measured by vibrational spectroscopy and X-ray powder diffraction under non-hydrostatic conditions.[155] No such phase transition was observed (up to 4.03 GPa) in the neutron powder diffraction study by Davidson *et al.* [150], nor in recent complementary X-ray single-crystal diffraction experiments.[156]

In their comprehensive review of these energetic ammonium compounds, Davidson *et al.* have not only characterised their high-pressure behaviour but have also drawn attention to the effect of the sample conditions on the occurrence or suppression of phase transitions.

1.4 General Aims and Outline of Research

Pressure has been shown to be an extremely powerful thermodynamic variable, resulting in innumerable phase transitions. This is compounded further by the combined effects of pressure *and* temperature. Such pressure- or temperature-induced phase transitions may therefore dramatically affect the performance of an energetic material. For this reason, it is essential to characterise fully the structural response of energetic materials to extreme conditions. This study therefore aims:

- to investigate the effect of pressure, and in some cases pressure *and* temperature, on the polymorphism of a range of energetic materials;
- to identify and structurally characterise new phases *in situ*;
- to explore whether high-pressure forms can be recovered to ambient pressure, with a view to obtaining energetic materials with enhanced properties at ambient conditions.

Chapter 3 describes the characterisation of the high-pressure/high-temperature polymorphism of RDX using a combination of neutron powder and X-ray single-crystal diffraction. In addition, the structure of the highly metastable polymorph at ambient pressure is reported. Chapter 4 explores the high-pressure behaviour of CL-20 in different pressure media. In Chapters 5 and 6, a series of inorganic azides has been structurally characterised under a range of pressure and temperature conditions. Suggestions of future work pertinent to each study are made in the relevant chapters. However, general conclusions and an outlook for the study of energetic materials at extreme conditions can be found in Chapter 7.

1.5 References

1. J. Akhavan, *The Chemistry of Explosives*, Royal Society of Chemistry, Cambridge, UK, 2004, 2nd edn.
2. J. Bottaro, *Ideas to Expand Thinking About New Energetic Materials*, in *Overviews of Recent Research on Energetic Materials*, R.W. Shaw, T.B. Brill, and D.L. Thompson, Editors, 2005, World Scientific Publishing Co., Singapore.

3. M.H.V. Huynh, M.A. Hiskey, T.J. Meyer, and M. Wetzler, *Proc. Nat. Acad. Sci. USA*, 2006, **103**, 5409.
4. M.H.V. Huynh, M.D. Coburn, T.J. Meyer, and M. Wetzler, *Proc. Nat. Acad. Sci. USA*, 2006, **103**, 10322.
5. R.L. Simpson, P.A. Urtiew, D.L. Ornellas, G.L. Moody, K.J. Scribner, and D.M. Hoffman, *Propellants, Explos., Pyrotech.*, 1997, **22**, 249.
6. P.E. Eaton, R.L. Gilardi, and M.X. Zhang, *Adv. Mater.*, 2000, **12**, 1143.
7. U. Bemm and H. Ostmark, *Acta Cryst.*, 1998, **C54**, 1997.
8. J.P. Agrawal, *Prog. Energy Combust. Sci.*, 1998, **24**, 1.
9. P.F. Pagoria, G.S. Lee, A.R. Mitchell, and R.D. Schmidt, *Thermochim. Acta*, 2002, **384**, 187.
10. D.M. Badgujar, M.B. Talawar, S.N. Asthana, and P.P. Mahulikar, *J. Hazard. Mater.*, 2008, **151**, 289.
11. J. Bernstein, *Polymorphism in Molecular Crystals*, Clarendon Press, Oxford, UK, 2002.
12. J.J. Dick, *J. Phys. IV*, 1995, **5**, 103.
13. *SciFinder Scholar*, 2007, American Chemical Society.
14. S. Rosenstein and P.P. Lamy, *Am. J. Hosp. Pharm.*, 1969, **26**, 598.
15. D. Giron, *Pharm. Sci. Technol. Today*, 1998, **1**, 191.
16. T.L. Threlfall, *Analyst*, 1995, **120**, 2435.
17. G.P. Stahly, *Cryst. Growth Des.*, 2007, **7**, 1007.
18. P.R. Unwin, *Faraday Discuss.*, 2007, **136**, 409.
19. A.J. Matzger, *Cryst. Growth Des.*, 2008, **8**, 2.
20. F. Grepioni, *New J. Chem.*, 2008, **32**, 1657.
21. A.D. Bond, *Curr. Opin. Solid State Mater. Sci.*, 2009, **13**, 91.
22. C. Frondel and U.B. Marvin, *Nature*, 1967, **214**, 587.
23. H.W. Kroto, J.R. Heath, S.C. O'Brien, R.F. Curl, and R.E. Smalley, *Nature*, 1985, **318**, 162.
24. P.R. Buseck, J.T. Semeon, and R. Hettich, *Science*, 1992, **257**, 215.
25. S. Iijima, *Nature*, 1991, **354**, 56.
26. M. Monthioux and V.L. Kuznetsov, *Carbon*, 2006, **44**, 1621.
27. W. Ostwald, *Z. Phys. Chem.*, 1897, **22**, 289.
28. W. McCrone, *Polymorphism*, in *Physics and Chemistry of the Organic Solid*, D. Fox, M.M. Labes, and A. Weissberger, Editors, 1965, Wiley Interscience, New York, USA.
29. D. Braga, F. Grepioni, and L. Maini, *Chem. Commun.*, 2010, **46**, 6232.
30. E.S. Hedges and J.Y. Higgs, *Nature*, 1952, **169**, 621.
31. A.D. Styrkas, *Inorg. Mater.*, 2003, **39**, 683.
32. M. Gilberg, *AICCM Bulletin*, 1991, **17**, 3.
33. O.L. Erdmann, *J. Prakt. Chem.*, 1851, **52**, 428.
34. T. von Fritzsche, *Comptes Rendus*, 1868, **67**, 1106.
35. E. Cohen and C. van Eijk, *Z. Phys. Chem.*, 1899, **30**, 601.
36. E. Cohen and K.D. Dekker, *Z. Phys. Chem.*, 1927, **127**, 178.
37. W.J. Plumbridge, *Circuit World*, 2007, **33**, 9.
38. D. Di Maio and C. Hunt, *J. Mater. Sci: Mater. Electron.*, 2009, **20**, 386.
39. D. Di Maio and C. Hunt, *J. Electron. Mater.*, 2009, **38**, 1874.
40. S.T. Beckett, *Science of Chocolate*, Royal Society of Chemistry, Cambridge, UK, 2008, 2nd edn.
41. R.N.M.R. van Gelder, N. Hodgson, K.J. Roberts, A. Rossi, M. Wells, M. Polgreen, and I. Smith, *Crystallization and polymorphism in cocoa butter fat: in-situ studies using synchrotron radiation x-ray diffraction* in *Crystal Growth of Organic Materials*, 1995, Washington, D.C., USA.
42. K. Sato, *Chem. Eng. Sci.*, 2001, **56**, 2255.

43. S.D. MacMillan, K.J. Roberts, A. Rossi, M.A. Wells, M.C. Polgreen, and I.H. Smith, *Cryst. Growth Des.*, 2002, **2**, 221.
44. J.M. Miller, B.M. Collman, L.R. Greene, D.J.W. Grant, and A.C. Blackburn, *Pharm. Dev. Technol.*, 2005, **10**, 291
45. S.R. Chemburkar, J. Bauer, K. Deming, H. Spiwek, K. Patel, J. Morris, R. Henry, S. Spanton, W. Dziki, W. Porter, J. Quick, P. Bauer, J. Donaubauer, B.A. Narayanan, M. Soldani, D. Riley, and K. McFarland, *Org. Process Res. Dev.*, 2000, **4**, 413.
46. S.R. Vippagunta, H.G. Brittain, and D.J.W. Grant, *Adv. Drug Delivery Rev.*, 2001, **48**, 3.
47. H.H. Cady, A.C. Larson, and D.T. Cromer, *Acta Cryst.*, 1963, **16**, 617.
48. R.E. Cobbledick and R.W.H. Small, *Acta Cryst.*, 1974, **B30**, 1918.
49. P. Main, R.E. Cobbledick, and R.W.H. Small, *Acta Cryst.*, 1985, **C41**, 1351.
50. S.J.P. Palmer and J.E. Field, *Proc. R. Soc. London, Ser. A*, 1982, **383**, 399.
51. O. Reany, M. Kapon, M. Botoshansky, and E. Keinan, *Cryst. Growth Des.*, 2009, **9**, 3661.
52. F. Wallerant, *C.R. Hebd. Seances Acad. Sci.*, 1903, **137**, 805.
53. C.S. Choi, H.J. Prask, and E. Prince, *J. Appl. Crystallogr.*, 1980, **13**, 403.
54. C. Boyars, *Ind. Eng. Chem., Prod. Res. Dev.*, 1976, **15**, 308.
55. H. Nagao, K.G. Nakamura, K. Kondo, N. Ozaki, K. Takamatsu, T. Ono, T. Shiota, D. Ichinose, K.A. Tanaka, K. Wakabayashi, K. Okada, M. Yoshida, M. Nakai, K. Nagai, K. Shigemori, T. Sakaiya, and K. Otani, *Phys. Plasmas*, 2006, **13**, 052705.
56. J.H. Eggert, D.G. Hicks, P.M. Celliers, D.K. Bradley, R.S. McWilliams, R. Jeanloz, J.E. Miller, T.R. Boehly, and G.W. Collins, *Nat. Phys.*, 2010, **6**, 40.
57. S.A. Moggach, S. Parsons, and P.A. Wood, *Crystallogr. Rev.*, 2008, **14**, 143.
58. P.W. Bridgman, *The Physics of High Pressure*, Bell and Sons, London, UK, 1931.
59. P.W. Bridgman, *J. Chem. Phys.*, 1937, **5**, 964.
60. P.W. Bridgman, *Proc. R. Soc. London Ser. A*, 1950, **203**, 1.
61. P.W. Bridgman, *Proc. Am. Acad. Arts Sci.*, 1952, **81**, 167.
62. A. Katrusiak, *Acta Cryst.*, 2008, **A64**, 135.
63. R.M. Hazen and R.T. Downs, eds. *Reviews in Mineralogy and Geochemistry*, *Vol. 41*:*High-Temperature and High-Pressure Crystal Chemistry*, 2000, Mineralogical Society of America, Washington, D.C., USA.
64. U. Schwarz, *Z. Kristallogr.*, 2009, **219**, 376.
65. M.I. McMahon and R.J. Nelmes, *Chem. Soc. Rev.*, 2006, **35**, 943.
66. O. Degtyareva, *High Pressure Res.*, 2010, **30**, 343
67. E. Gregoryanz, O. Degtyareva, M. Somayazulu, R.J. Hemley, and H.K. Mao, *Phys. Rev. Lett.*, 2005, **94**, 185502.
68. E. Gregoryanz, L.F. Lundegaard, M.I. McMahon, C. Guillaume, R.J. Nelmes, and M. Mezouar, *Science*, 2008, **320**, 1054.
69. Y. Ma, M. Eremets, A.R. Oganov, Y. Xie, I. Trojan, S. Medvedev, A.O. Lyakhov, M. Valle, and V. Prakapenka, *Nature*, 2009, **458**, 182.
70. Y.A. Freiman and H.J. Jodl, *Phys. Rep.*, 2004, **401**, 1.
71. L.F. Lundegaard, G. Weck, M.I. McMahon, S. Desgreniers, and P. Loubeyre, *Nature*, 2006, **443**, 201.
72. S. Desgreniers, Y.K. Vohra, and A.L. Ruoff, *J. Phys. Chem.*, 1990, **94**, 1117.
73. K. Shimizu, K. Suhara, M. Ikumo, M.I. Eremets, and K. Amaya, *Nature*, 1998, **393**, 767.
74. E. Boldyreva, *Cryst. Growth Des.*, 2007, **7**, 1662.
75. E. Boldyreva, *Acta Cryst.*, 2008, **A64**, 218.
76. S. Moggach and S. Parsons, *CrystEngComm*, 2010, **12**, 2515.
77. P.T.C. Freire, *Pressure-Induced Phase Transitions in Crystalline Amino Acids. Raman Spectroscopy and X-Ray Diffraction*, in *High-Pressure Crystallography*, E. Boldyreva and P. Dera, Editors, 2010, Springer Netherlands.

78. A. Dawson, D.R. Allan, S.A. Belmonte, S.J. Clark, W.I.F. David, P.A. McGregor, S. Parsons, C.R. Pulham, and L. Sawyer, *Cryst. Growth Des.*, 2005, **5**, 1415.
79. E.V. Boldyreva, H. Ahsbahs, and H.P. Weber, *Z. Kristallogr.*, 2003, **218**, 231.
80. S. Moggach, T. Bennett, and A. Cheetham, *Angew. Chem. Int. Ed.*, 2009, **48**, 7087.
81. A. Gavezzotti, *Z. Kristallogr.*, 2005, **220**, 499.
82. P.A. Wood, R.S. Forgan, D. Henderson, S. Parsons, E. Pidcock, P.A. Tasker, and J.E. Warren, *Acta Cryst.*, 2006, **B62**, 1099.
83. P.A. Wood, D. Francis, W.G. Marshall, S.A. Moggach, S. Parsons, E. Pidcock, and A.L. Rohl, *CrystEngComm*, 2008, **10**, 1154.
84. R.D.L. Johnstone, D. Francis, A.R. Lennie, W.G. Marshall, S.A. Moggach, S. Parsons, E. Pidcock, and J.E. Warren, *CrystEngComm*, 2008, **10**, 1758.
85. R.D.L. Johnstone, M. Ieva, A.R. Lennie, H. McNab, E. Pidcock, J.E. Warren, and S. Parsons, *CrystEngComm*, 2010, **12**, 2520.
86. M. Podsiadlo, K. Dziubek, and A. Katrusiak, *Acta Cryst.*, 2005, **B61**, 595.
87. G.J. Piermarini, A.D. Mighell, C.E. Weir, and S. Block, *Science*, 1969, **165**, 1250.
88. D.R. Allan, S.J. Clark, A. Dawson, P.A. McGregor, and S. Parsons, *Acta Cryst.*, 2002, **B58**, 1018.
89. I.D.H. Oswald, D.R. Allan, G.M. Day, W.D.S. Motherwell, and S. Parsons, *Cryst. Growth Des.*, 2005, **5**, 1055.
90. I.D.H. Oswald, D.R. Allan, W.D.S. Motherwell, and S. Parsons, *Acta Cryst.*, 2005, **B61**, 69.
91. D.R. Allan, W.G. Marshall, D.J. Francis, I.D.H. Oswald, C.R. Pulham, and C. Spanswick, *Dalton Trans.*, 2010, **39**, 3736.
92. F.P.A. Fabbiani, D.R. Allan, A. Dawson, W.I.F. David, P.A. McGregor, I.D.H. Oswald, S. Parsons, and C.R. Pulham, *Chem. Commun.*, 2003, **39**, 3004.
93. F.P.A. Fabbiani, D.R. Allan, W.I.F. David, S.A. Moggach, S. Parsons, and C.R. Pulham, *CrystEngComm*, 2004, **6**, 504.
94. F.P.A. Fabbiani, D.R. Allan, W.G. Marshall, S. Parsons, C.R. Pulham, and R.I. Smith, *J. Cryst. Growth*, 2005, **275**, 185.
95. E. Girard, A.C. Dhaussy, B. Couzinet, J.C. Chervin, M. Mezouar, R. Kahn, I. Ascone, and R. Fourme, *J. Appl. Crystallogr.*, 2007, **40**, 912.
96. R. Fourme, E. Girard, R. Kahn, A.C. Dhaussy, and I. Ascone, *Annu. Rev. Biophys.*, 2009, **38**, 153.
97. E. Girard, R. Fourme, R. Ciurko, J. Joly, F. Bouis, P. Legrand, J. Jacobs, A.C. Dhaussy, J.L. Ferrer, M. Mezouar, and R. Kahn, *J. Appl. Crystallogr.*, 2010, **43**, 762.
98. A. Aertsen, F. Meersman, M.E.G. Hendrickx, R.F. Vogel, and C.W. Michiels, *Trends Biotechnol.*, 2009, **27**, 434.
99. I. Daniel, P. Oger, and R. Winter, *Chem. Soc. Rev.*, 2006, **35**, 858.
100. A.C. Oliveira, A.M.O. Gomes, S.M.B. Lima, R.B. Goncalves, W.D. Schwarcz, A.C.B. Silva, J.R. Cortines, and J.L. Silva, *Effects of Hydrostatic Pressure on Viruses*, in *High-Pressure Microbiology*, C.W. Michiels, D.H. Bartlett, and A. Aertsen, Editors, 2008, ASM Press, Herndon, VA, USA.
101. T. Otake, T. Kawahata, H. Mori, Y. Kojima, and K. Hayakawa, *Appl. Microbiol. Biotechnol.*, 2005, **67**, 746.
102. C. Pribenszky, M. Molnar, A. Horvath, G. Kutvolgyi, A. Harnos, O. Szenci, J. Dengg, and J. Lederer, *Reprod. Fertil. Dev.*, 2007, **19**, 181.
103. G.S. Li, C.K. Bai, J. Duan, C.L. Peng, K.N. Weng, and S.D. Liu, *Chin. J. High Press. Phys.*, 2003, **17**, 122.
104. I. Oey, M. Lille, A. Van Loey, and M. Hendrickx, *Trends Food Sci. Technol.*, 2008, **19**, 320.
105. J. Gimenez, P. Kajda, L. Margomenou, J.R. Piggott, and I. Zabetakis, *J. Sci. Food Agric.*, 2001, **81**, 1228.

106. L.W. Murchie, M. Cruz-Romero, J.P. Kerry, M. Linton, M.F. Patterson, M. Smiddy, and A.L. Kelly, *Innovative Food Sci. Emerg. Technol.*, 2005, **6**, 257.
107. S. Yamamoto, K. Takanohashi, T. Hara, S. Odani, A. Suzuki, and T. Nishiumi, *J. Phys. Conf. Ser.*, 2010, **215**, 012170.
108. H.K. Chan and E. Doelker, *Drug Dev. Ind. Pharm.*, 1985, **11**, 315
109. V.V. Boldyrev, *J. Mater. Sci.*, 2004, **39**, 5117.
110. F.P.A. Fabbiani and C.R. Pulham, *Chem. Soc. Rev.*, 2006, **35**, 932.
111. A. Llinàs and J.M. Goodman, *Drug Discovery Today*, 2008, **13**, 198.
112. M. Haisa, S. Kashino, R. Kawai, and H. Maeda, *Acta Cryst.*, 1976, **B32**, 1283.
113. D.Y. Naumov, M.A. Vasilchenko, and J.A.K. Howard, *Acta Cryst.*, 1998, **C54**, 653.
114. G. Nichols and C.S. Frampton, *J. Pharm. Sci.*, 1998, **87**, 684.
115. M. Haisa, S. Kashino, and H. Maeda, *Acta Cryst.*, 1974, **B30**, 2510.
116. P. Di Martino, P. Conflant, M. Drache, J.P. Huvenne, and A.M. Guyot-Hermann, *J. Therm. Anal. Calorim.*, 1997, **48**, 447.
117. J.C. Burley, M.J. Duer, R.S. Stein, and R.M. Vrcelj, *Eur. J. Pharm. Sci.*, 2007, **31**, 271.
118. M.A. Perrin, M.A. Neumann, H. Elmaleh, and L. Zaske, *Chem. Commun.*, 2009, **45**, 3181.
119. S. Gaisford, A.B.M. Buanz, and N. Jethwa, *J. Pharm. Biomed. Anal.*, 2010, **53**, 366.
120. P. Di Martino, A.M. Guyot-Hermann, P. Conflant, M. Drache, and J.C. Guyot, *Int. J. Pharm.*, 1996, **128**, 1.
121. E. Boldyreva, T. Shakhtshneider, H. Ahsbahs, H. Sowa, and H. Uchtmann, *J. Therm. Anal. Calorim.*, 2002, **68**, 437.
122. M. Lang, A.L. Grzesiak, and A.J. Matzger, *J. Am. Chem. Soc.*, 2002, **124**, 14834.
123. J.S. Capes and R.E. Cameron, *Cryst. Growth. Des.*, 2006, **7**, 108.
124. J.R. Mendez del Rio and R.W. Rousseau, *Cryst. Growth Des.*, 2006, **6**, 1407.
125. J.S. Capes and R.E. Cameron, *CrystEngComm*, 2007, **9**, 84.
126. I.D.H. Oswald, I. Chataigner, S. Elphick, F.P.A. Fabbiani, A.R. Lennie, J. Maddaluno, W.G. Marshall, T.J. Prior, C.R. Pulham, and R.I. Smith, *CrystEngComm*, 2009, **11**, 359.
127. Y.B. Zel'dovich and Y.P. Raiser, *Physics of Schockwave and High Temperature Hydrodynamics Phenomena*, Academic Press, New York, USA, 1966.
128. P. Politzer and J.S. Murray, eds. *Theoretical and Computational Chemistry*, *Vol. 13*:*Energetic Materials, Part 2: Detonation, Combustion*, 2003, Elsevier.
129. R.W. Shaw, T.B. Brill, and D.L. Thompson, eds. *Advanced Series in Physical Chemistry*, *Vol. 16*:*Overviews of Recent Research on Energetic Materials*, 2005, World Scientific Publishing Co., Singapore.
130. S.M. Peiris and G.J. Piermarini, eds. *Shock Wave and High Pressure Phenomena*:*Static Compression of Energetic Materials*, 2008, Springer, Berlin-Heidelberg, Germany.
131. L.E. Fried, M.R. Manaa, and J.P. Lewis, *Modeling the Reactions of Energetic Materials in the Condensed Phase*, in *Overviews of Recent Research on Energetic Materials*, R.W. Shaw, T.B. Brill, and D.L. Thompson, Editors, 2005, World Scientific Publishing Co., Singapore.
132. B.M. Rice, *Applications of Theoretical Chemistry in Assessing Energetic Materials for Performance or Sensitivity*, in *Overviews of Recent Research on Energetic Materials*, R.W. Shaw, T.B. Brill, and D.L. Thompson, Editors, 2005, World Scientific Publishing Co., Singapore.
133. D.D. Dlott, *Annu. Rev. Phys. Chem.*, 1999, **50**, 251.
134. F. Goetz, T.B. Brill, and J.R. Ferraro, *J. Phys. Chem.*, 1978, **82**, 1912.
135. J.C. Gump and S.M. Peiris, *J. Appl. Phys.*, 2005, **97**, 053513.
136. A.J. Davidson, I.D.H. Oswald, D.J. Francis, A.R. Lennie, W.G. Marshall, D.I.A. Millar, C.R. Pulham, J.E. Warren, and A.S. Cumming, *unpublished results,* 2008.

137. T.D. Sewell, R. Menikoff, D. Bedrov, and G.D. Smith, *J. Chem. Phys.*, 2003, **119**, 7417.
138. D.C. Sorescu and B.M. Rice, *J. Phys. Chem. C*, 2010, **114**, 6734.
139. C.S. Yoo and H. Cynn, *J. Chem. Phys.*, 1999, **111**, 10229.
140. D.E. Hooks, D.B. Hayes, D.E. Hare, D.B. Reisman, K.S. Vandersall, J.W. Forbes, and C.A. Hall, *J. Appl. Phys.*, 2006, **99**, 124901.
141. L.Y. Lu, D.Q. Wei, X.R. Chen, G.F. Ji, X.J. Wang, J. Chang, Q.M. Zhang, and Z.Z. Gong, *Mol. Phys.*, 2009, **107**, 2373
142. L.Y. Lu, D.Q. Wei, X.R. Chen, D. Lian, G.F. Ji, Q.M. Zhang, and Z.Z. Gong, *Mol. Phys.*, 2008, **106**, 2569
143. W. Zhu, X. Zhang, T. Wei, and H. Xiao, *Theor. Chem. Acc.*, 2009, **124**, 179.
144. H.L. Cui, G.F. Ji, X.R. Chen, W.H. Zhu, F. Zhao, Y. Wen, and D.Q. Wei, *J. Phys. Chem. A*, 2009, **114**, 1082.
145. H.L. Cui, G.F. Ji, X.R. Chen, Q.M. Zhang, D.Q. Wei, and F. Zhao, *J. Chem. Eng. Data*, 2010, **55**, 3121.
146. J. Evers, T.M. Klapötke, P. Mayer, G. Oehlinger, and J. Welch, *Inorg. Chem.*, 2006, **45**, 4996.
147. M.J. Crawford, J. Evers, M. Göbel, T. Klapötke, P. Mayer, G. Oehlinger, and J. Welch, *Propellants, Explos., Pyrotech.*, 2007, **32**, 478.
148. S.M. Peiris, C.P. Wong, and F.J. Zerilli, *J. Chem. Phys.*, 2004, **120**, 8060.
149. D.I.A. Millar, W.G. Marshall, H.E. Maynard-Casely, C.R. Pulham, and A.S. Cumming, *unpublished results,* 2010.
150. A.J. Davidson, D.R. Allan, I.D.H. Oswald, C.R. Pulham, F.P.A. Fabbiani, D.J. Francis, W.G. Marshall, R.I. Smith, A.S. Cumming, A.R. Lennie, and T.J. Prior, *High-pressure structural studies of energetic ammonium compounds* in *38th International Annual Conference of ICT, Energetic Materials: Characterisation and Performance of Advanced Systems*, 2007, Karlsruhe, Germany.
151. D.M. Adams and S.K. Sharma, *J. Chem. Soc., Faraday Trans. 2*, 1976, **72**, 2069.
152. F.W. Sandstrom, P.A. Persson, and B. Olinger, *AIP Conf. Proc.*, 1994, **309**, 1409.
153. T.B. Brill and F. Goetz, in *Papers in Aeronautics and Astronautics*, T.L. Boggs and B.T. Zinn, Editors, 1978, AIAA, Reston, VA, USA.
154. S.M. Peiris, G.I. Pangilinan, and T.P. Russell, *J. Phys. Chem. A*, 2000, **104**, 11188.
155. T.P. Russell, G.J. Piermarini, S. Block, and P.J. Miller, *J. Phys. Chem.*, 1996, **100**, 3248.
156. D.I.A. Millar, C. Barry, D.J. Francis, A.K. Kleppe, W.G. Marshall, H.E. Maynard-Casely, I.D.H. Oswald, C.R. Pulham, P.A. Szilagyi, and A.S. Cumming, *manuscript in preparation,* 2010.

Chapter 2

Experimental Techniques

2 Experimental Techniques

2.1 Complementarity of High-Pressure Techniques

High-pressure structural science is a particularly strong example of an area that relies upon the complementarity of various techniques to achieve the final aim of the structural characterisation of novel materials. Furthermore, the advances in this field are intertwined with the evolution of complex sample environments for experiments at elevated temperatures and/or pressures, as well as the development of techniques for the collection and analysis of spectroscopic and diffraction data under extreme conditions. In this work, a combination of X-ray diffraction (both single-crystal and powder), neutron powder diffraction and Raman spectroscopy has been used to identify and structurally characterise numerous phases at a range of pressure/temperature conditions. High pressures have been generated using either the Merrill-Bassett diamond-anvil cell (DAC) [1] or the Paris-Edinburgh Cell.[2] This chapter will therefore feature a detailed description of each of these instruments, with a subsequent discussion of the experimental techniques in which they have been employed.

2.2 The Merrill-Bassett Diamond-Anvil Cell

2.2.1 DAC Components

High-pressure X-ray diffraction and Raman spectroscopic studies were performed using a gasketed diamond-anvil cell (DAC). The premise for this device is relatively simple; the sample is placed between two diamond faces (culets) and is subjected to high pressures when a force pushes the opposed anvils together. The DAC utilised in this work was based on developments by Merrill and Bassett in 1974.[1] The small size (~5 cm diameter) and relative ease of use make these cells extremely versatile and perfectly suited for high-pressure X-ray diffraction studies. Prior to the development of DAC technology, high-pressure experiments were limited to using massive Bridgman-type hydraulic or piston-cylinder cells that required specialist laboratories and posed considerable safety hazards in the event of failure.[3] A photograph of the Merrill-Bassett diamond-anvil cell is presented in Figure 2.1, along with a representation of the principles of such a device.

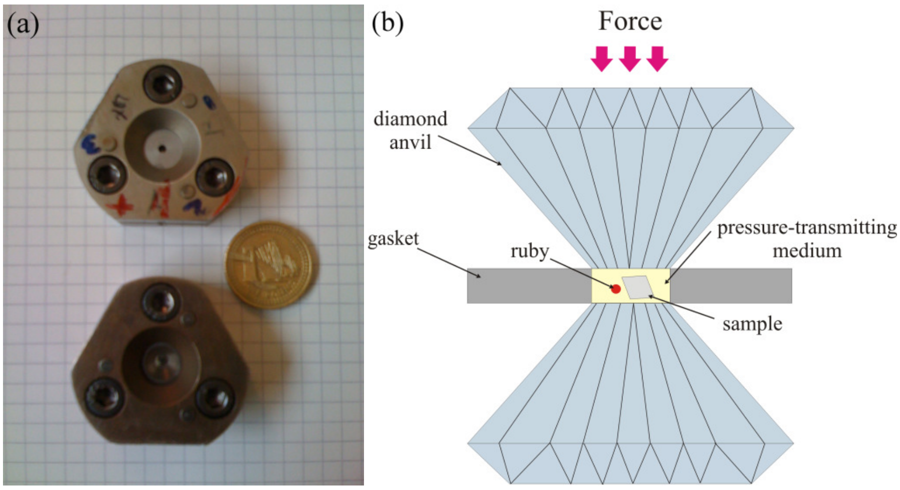

Figure 2.1 (a) photograph of the Merrill-Bassett DAC highlighting its simplicity and size (the top DAC has Be backing plates, while the diamonds are mounted on WC plates in the bottom cell); and, (b) schematic representation of the principles of the diamond-anvil cell.

Although the Merrill-Bassett diamond-anvil cell has garnered widespread recognition in the high-pressure community, the initial inspiration to utilise diamond's compressive strength to generate extreme pressures dates to the late 1940s when Lawson and Tang were able to subject samples to pressures *ca* 2.0 GPa between two halves of a cleaved diamond.[4] A team of scientists at the National Bureau of Standards (Washington, D.C., USA) meanwhile explored a parallel path by modifying Bridgman's opposed-anvil device using two gem-quality diamonds as anvils, instead of steel or tungsten carbide (WC). They were also in the extremely enviable position of being able to acquire bountiful supplies of diamonds as customs officials at the time were willing to entrust other government bodies with confiscated goods, provided that a convincing case for their use was put forward.[5] Thus Van Valkenburg and colleagues were able to construct an opposed-anvil device, in which two gem-quality diamonds were driven together by the turn of a screw, thus facilitating the visual observation of high-pressure phase transitions in a range of materials (such as KNO_3 and AgI).[6]

The ability to see the sample also brought numerous practical boons, primarily the ability to check anvil alignment and the observation of phase transitions and even sample recrystallisations. Indeed the transparency of diamond to large sections of the electromagnetic spectrum allows optical and spectroscopic analysis of the sample *in situ* and makes diamond an ideal anvil material for X-ray diffraction studies. The low atomic number (therefore minimal X-ray absorption) and the high degree of crystal perfection of gem-quality diamonds mean that it is possible to minimise any interference with the sample diffraction. It is important to note, however, that fluorescence from the significant nitrogen impurity in Type I diamonds make them impractical for spectroscopic studies.

The significant achievement of the Merrill-Bassett DAC was its miniaturisation, allowing it to be mounted on a standard goniometer head.[1] In this cell the diamond anvils are mounted on two backing plates (platens), which are encased in a steel body, as shown in Figure 2.2. A force is then applied to the outer faces of the diamonds by tightening three screws in the steel body, which is then multiplied many times at the small inner faces (culets). The culet size is the predominant factor in determining the maximum pressure that can be achieved. In the current study, culet sizes of either 600 or 400 μm were used to reach maximum pressures of *ca* 10.0 and 25.0 GPa, respectively.

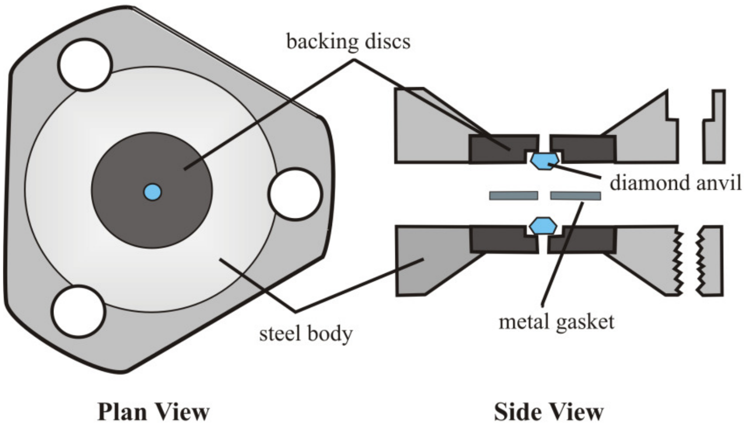

Figure 2.2 Schematic of the Merrill-Bassett diamond-anvil cell.

In their original design Merrill and Bassett exploited the tensile strength of beryllium and its transparency to X-rays for use as the backing-plates, on which to mount the diamond anvils. A major disadvantage of Be backing discs, however, is the presence of powder rings arising from X-ray scattering from the polycrystalline metal, thus contaminating the diffraction image, as shown in Figure 2.3. This is exacerbated when high flux and low divergence synchrotron X-ray beams are necessary since the Be lines become more intense and 'spottier' in appearance.[7] Moreover, the toxicity of beryllium means that great care must be taken when handling these plates.

In response to the shortcomings of Be-backed diamond-anvil cells, the Merrill-Bassett DAC has been modified to incorporate tungsten carbide or steel backing seats, which do not pose a significant safety risk. However, the opacity of these materials to X-rays means that rather than contaminating the sample diffraction pattern, an equally troublesome dilemma presents itself – the absorption of large sections of the diffracted beam, and thus the severe restriction of the reciprocal space accessible in a high-pressure experiment. In order to overcome this, WC backing plates with wider opening angles have been designed into which a conical Böhler-Almax diamond anvil has been embedded (see Figure 2.3).[8, 9] This construction allows the full opening angle of the steel platens (80°) to be utilised, while still ensuring the anvils are adequately supported for applications at very high pressures (> 20 GPa).[7] In both cases (Be and WC), the backing plates are held within the steel body by small screws that allow alignment of the diamond anvils normal to the thrust axis [10]; parallelism can only be accounted for while mounting the anvils on the backing plates. It is essential to ensure the anvils are fully aligned and parallel – neglecting to do so risks (unnecessarily) diamond failure, especially at elevated pressures.

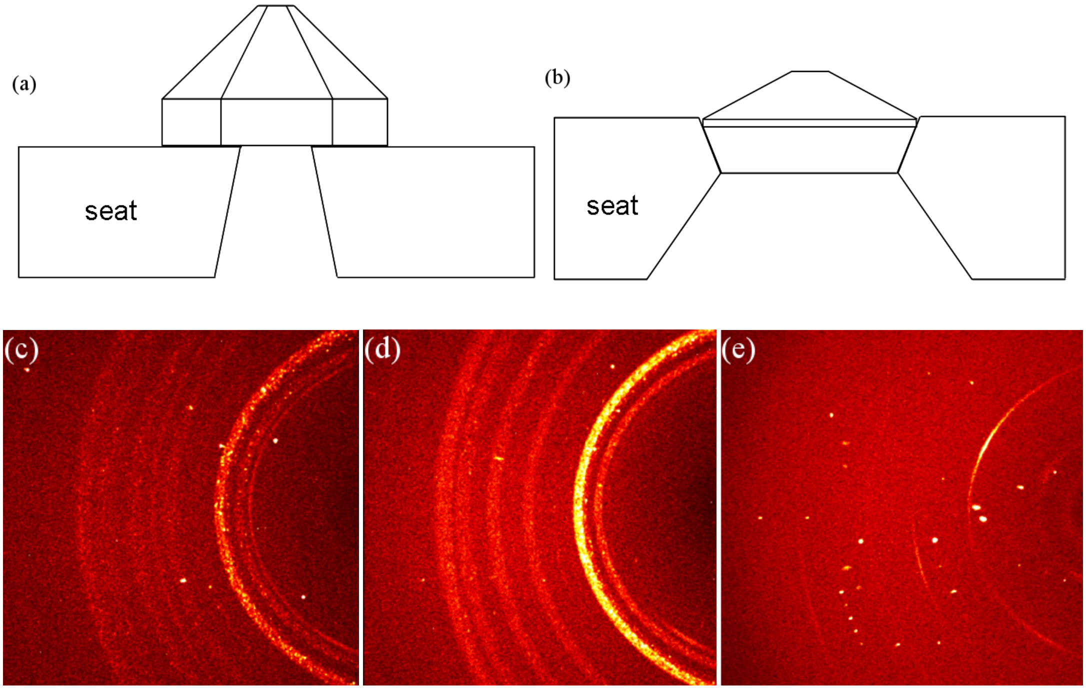

Figure 2.3 Schematic of the different backing plates and the effects each have on the quality of the diffraction data: (a) Be-backed diamond; (b) WC backing plates, with the specially cut diamonds set into the plate; (c) diffraction image collected on a laboratory source using a Be-backed diamond-anvil cell; (d) an analogous image collected using synchrotron radiation; and, (e) diffraction data collected using DAC equipped with WC backing plates. Images kindly provided by Moggach *et al.* [7]

The final constituent of the cell is the metal gasket that is sandwiched between the culets of the diamonds. The pressures attained at the diamond culets are sufficient to cause the gasket to extrude around the anvils, thus sealing the sample chamber while also providing support for the diamonds. A variety of metals, for example Re, steel and inconel (an alloy of Ni, Cr and Fe), may be used, but tungsten has high mechanical strength and thus is often the metal of choice for larger sample volumes. The nature and preparation of the gasket are also of considerable importance. For pressure to increase, the volume of the sample chamber must decrease; normally the reduction in the thickness of the sample chamber as the anvil advances is sufficient. If the gasket is too thick however, the outwards force from the sample will exceed the friction between the anvils and the gasket and the hole will expand. Thus no pressure will be applied to the sample and there is a risk of damage to the diamonds by gasket failure.

A thin gasket will allow higher pressures to be reached and can give better control at low pressure as less force is required to seal the sample chamber initially.[11] It is therefore preferable to pre-indent the gasket by careful extrusion between the diamond anvils prior to drilling a gasket hole. This approach has the added benefits of imbuing the cell with greater stability due to the massive support from the extruded material and improving the gasket's mechanical stability by hardening. However, pre-indentation must be carried out with perfectly aligned diamonds: diamond failure is more likely to occur during pre-indentation than in the high-pressure experiment itself because the radial extrusion of the gasket material puts maximum tensile stress on the anvil tips.[12] In the majority of the work presented herein a 250 μm thick tungsten gasket was pre-indented to a *thickness* of 100 – 150 μm, which was sufficient to allow compression studies up to ~ 6.0 GPa. The compression of RDX to very high pressures (*ca* 25 GPa) necessitated the utilisation of a 150 μm W gasket that was pre-indented to a *pressure* of 30 GPa, as determined by the ruby fluorescence method (see Section 2.2.2).

It is normally desirable to ensure that the pressure applied is homogeneous and is free of any deviatoric stresses or strains because pressure, *i.e.* isotropic stress, is a thermodynamic parameter.[5] Moreover, there are a number of experimental factors which mean that non-hydrostatic conditions should be avoided wherever possible. For example, inhomogeneous strain in the crystal results in broadening of the diffraction peaks; the stresses and strains may promote or suppress phase transitions; irregularities in the relative compression of the unit cell axes may be observed; and, broadening of the ruby fluorescence R_1 line (Section 2.2.2) increases uncertainty in the pressure measurement.

In order to achieve completely hydrostatic compression, the sample must be immersed in a medium that displays hydrostatic behaviour throughout the pressure regime of interest. Furthermore the medium should not dissolve or react with the sample being studied. A range of different media have therefore been developed, the hydrostatic limits of which have been investigated by various groups.[13-16] The pressure-transmitting medium used in the majority of the studies presented in this work (a 4:1 mixture of methanol:ethanol) has been shown to remain hydrostatic to ~9.8 GPa by Angel *et al.*, who measured the X-ray diffraction maxima from quartz single crystals in a range of media.[13] In cases where MeOH:EtOH (4:1) was found to dissolve the sample, alternatives such as a 5:1 mixture of iso:n-pentane or Fluorinert FC77, a mixture of perfluorinated hydrocarbons, were employed although these have been shown to have lower hydrostatic limits (7.4 GPa [14] and 1.0 GPa [15], respectively).

2.2.2 Pressure Measurement

Direct pressure measurement from the applied force is both inaccurate and impractical. Instead, Piermarini *et al.* demonstrated that a small chip or sphere of ruby (Al_2O_3:Cr^{3+}) could serve as a continuous pressure sensor within the DAC by utilising its laser-induced fluorescence.[17] Indeed the simplicity of the ruby fluorescence method for *in situ* pressure calibration is without question a contributing factor to the widespread application of diamond-anvil cell techniques and, as such, was the subject of an extensive review by Syassen in 2008.[18] The spectral lines of ruby undergo a pronounced red-shift with applied pressure; the R_1 electronic transition shows a linear dependence with pressure up to at least 20 GPa at ambient temperature [17] – this pressure scale will be used throughout the present work. At elevated temperatures, however, the fluorescence signal undergoes significant broadening and it becomes difficult to obtain a reliable measure of sample pressure. In this study, all pressure measurements *via* ruby fluorescence have been made at ambient temperature. Unless stated otherwise, spectra were collected using the 632.8 nm line from a He-Ne laser and dispersed and detected by a Jobin-Yvon LabRam 300 spectrometer, with typical precision of ± 0.05 GPa.

Another factor affecting the ruby fluorescence signal is the hydrostaticity within the sample chamber. Under hydrostatic compression the R_1 and R_2 lines remain well resolved and pressure measurement is straightforward. The R_1-R_2 separation has been shown to be strongly dependent on the presence of any deviatoric stresses within the ruby sample (*i.e.* within the sample chamber). In experiments where non-hydrostatic conditions are being investigated it is therefore common to see these spectral lines overlapping, and the uncertainty in the pressure measurement is significantly increased. A comparison of the ruby fluorescence spectra obtained under hydrostatic and non-hydrostatic conditions can be found in Figure 2.4.

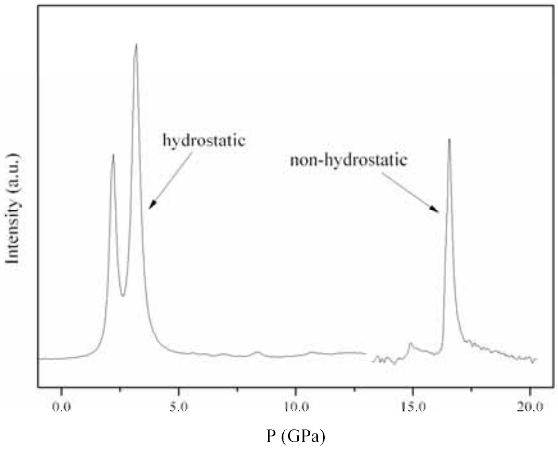

Figure 2.4 Comparison of the hydrostatic and non-hydrostatic ruby fluorescence signals, highlighting the complete reduction of the R_1-R_2 distance under non-hydrostatic conditions. It should be noted that, in this plot, the non-hydrostatic signal has been scaled to have comparable intensity to the hydrostatic signal and so the significant peak broadening observed under non-hydrostatic conditions is not apparent.

2.2.3 Sample loading

The majority of the studies undertaken in this work have been direct compression of either single crystals or polycrystalline powder. In these experiments the sample is initially loaded into the gasket hole along with a small chip or sphere of ruby. Great care must be taken in order to avoid flushing out either the sample or the ruby during the subsequent flooding of the sample chamber with the pressure-transmitting medium. In single-crystal studies it also desirable to ensure that the gasket impinges on neither the sample crystal nor the ruby. This is to avoid additional stresses being applied to either the sample or the ruby upon gasket extrusion, which would result in crystal destruction and/or greater uncertainty in the pressure calibration. Furthermore careful selection of sample crystals is pivotal for the success of a high-pressure diffraction study. Not only should high-quality single crystals be selected, it is essential to ensure that the crystal be small enough to fit inside the gasket – crystals that bridge the separation between the diamond culets will be crushed upon compression. The successful loading of a single crystal is depicted in Figure 2.5.

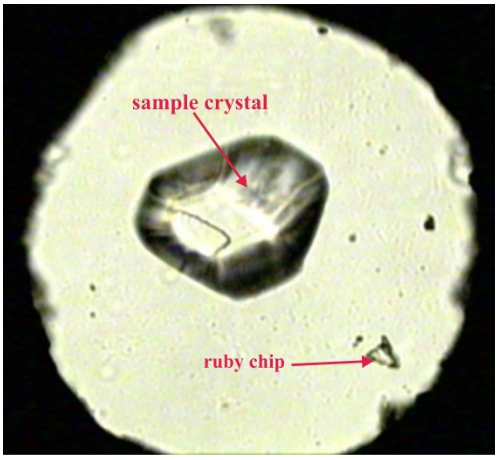

Figure 2.5 Photograph of a single crystal loaded in the DAC with ruby.

2.3 Experimental Techniques using the Diamond-Anvil Cell

2.3.1 X-ray Single-Crystal Diffraction

X-ray single-crystal diffraction is the most definitive method for the determination of atomic positions within a crystalline solid (defined as a three-dimensional array of identical unit cells with long range order and translational symmetry). Diffraction arises from the interference (both constructive and destructive) of scattered photons, which are produced by the elastic scattering of incident electromagnetic radiation by the electron density of atoms within a crystal lattice. The wavelength (or rather range of wavelengths) of X-ray radiation is comparable with interatomic separations, typically of the order of a few Ångstroms. This means that the interference of X-rays scattered by different atomic planes within the lattice will result in the observed diffraction pattern, from which it is possible to determine the relative positions of the atoms within the structure.

The condition for the constructive interference of scattered radiation (wavelength, λ) is satisfied only when the path difference is equal to $n\lambda$, where n is an integer. Bragg demonstrated that the path difference of two scattered X-rays may be expressed in terms of the separation of the lattice planes within the crystal (d) and the angle of incidence (θ).[19] As depicted in Figure 2.6, constructive interference will occur, and thus diffracted beam intensity will be observed, when $n\lambda = 2d\sin\theta$. At other angles of incidence or interplanar distances, the scattered X-rays will be partly or completely out of phase (destructive interference).

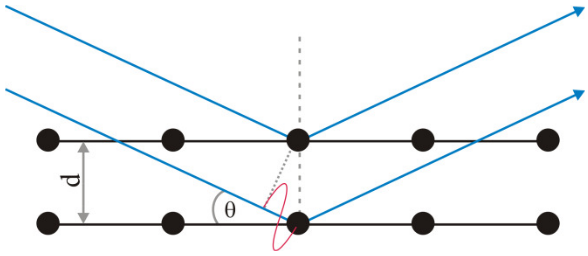

Figure 2.6 The Bragg construction for diffraction by a three-dimensional crystal lattice. In this scheme the incident X-rays (blue) are diffracted by two separate crystal planes (black), separated by a distance, *d*. For constructive interference to occur, the path difference between two diffracted beams should be an integer multiple of their wavelength (red, $n\lambda$). This situation arises only at certain scattering angles (θ); at all other angles the beams will interfere destructively.

A great deal of information (*i.e.* the unit cell indexing and space group) can be extracted directly from an observed diffraction pattern. However, while the observed intensities provide information about the amplitudes of the scattered waves, $|F_o|$, any information about the relative phases (φ) is lost. The so-called 'phase problem' presents a considerable challenge to crystallographers since both the amplitudes and phases of the scattered X-rays are required for an accurate representation of the electron density within the unit cell:

$$\rho(xyz) = \frac{1}{V}\sum_{hkl}|F(hkl)|\exp[i\varphi(hkl)]\exp[-2\pi i(hx+ky+lz)]$$

In chemical crystallography there are two main techniques for overcoming this phase problem: (i) Patterson methods, and (ii) direct methods. Patterson methods rely on either the presence of a few heavy atoms in the structure (such as in a transition metal complex) or a significant portion of the molecule in question having a well-defined and rigid geometry. In the Patterson synthesis the amplitudes of the scattered waves are replaced by their squares, $|F_o|^2$, and the phases (φ) are omitted, such that:

$$P(uvw) = \frac{1}{V}\sum_{hkl}|F(hkl)|^2\cos[2\pi(hu+kv+lw)]$$

Peaks in the resultant Patterson maps do not correspond to the electron density but rather the interatomic vectors. As each peak is proportional to the product of the atomic numbers (Z) of the atoms involved, vectors between two heavy atoms are more easily identified. The task then is to deduce the structure directly from knowledge of the distances between the atoms in the unit cell.

In direct methods, no previous knowledge of the structure is employed in structure solution – the phases of the structure factors and therefore the electron density are derived mathematically from a set of observed X-ray intensities. The method imposes constraints that are valid for the (correct) electron density distribution (such as discrete peaks and non-negative values) to the structure factors. Since the amplitudes $|F_o|$ are known, these constraints restrict the possible phases of the structure factors and, in favourable cases, are sufficient to allow phase determination directly.

In both cases (Patterson and direct methods) the structure may be refined by calculating the residual electron density ($\Delta\rho$) – the difference between the calculated structure factors, F_c, and the observed structure factors, $|F_o|$. Such Fourier syntheses can be used to determine if any electron density has not been accurately modelled by the proposed structure, and therefore represent an effective test of whether a complete model has been reached. Moreover, it may be possible to determine hydrogen positions in high-quality data-sets.

The success of the above methods for structure solution is dependent upon the accurate determination of reflection intensities. However, this can be complicated greatly by peak overlap in X-ray powder diffraction patterns or missing reflection data, which is often the case in high-pressure experiments. In response to the limitations of these reciprocal-space methods, numerous programs such as DASH [20] and FOX [21] have been developed, which aim to generate calculated patterns based on an accurate unit cell indexing and chemical composition. In these direct-space methods, the agreement between the observed and calculated patterns is optimised using a Monte Carlo approach by varying structural parameters (for example, molecular positions and orientations as well as any torsion angles that may be present). The result of this 'simulated annealing' experiment with the lowest goodness-of-fit (χ^2) should therefore correspond to the experimental structure.

Finally, in contrast to the aforementioned methods, the most recent approach to solving the phase problem, the charge flipping algorithm, requires no information on either symmetry or chemical composition and is therefore an extremely powerful tool in structure solution. Although more details may be found in the original manuscript by Oszlányi and Sütó [22], the algorithm may be treated as a subtle adaptation to the simple Fourier cycle between the real-space electron density (ρ) and the reciprocal-space structure factors, F_o. Charge flipping exploits volumes of low electron density in the unit cell by introducing a threshold (δ) into a pixelated electron-density map. Any pixels whose electron density is below this threshold have their signs reversed, such that $\rho(r)$ becomes $-\rho(r)$, where $\rho(r) < \delta$. Temporary structure factors G_c are then calculated based on this modified electron-density map and it is the phases of these temporary structure factors that are subsequently combined with the observed amplitudes F_o to generate the new electron density. This iterative cycle is then repeated several hundred times to obtain an accurate representation of the experimental electron density.

The particular strengths of this method are its simplicity and its truly *ab initio* character. Since the electron density is represented on a grid, no atomicity is acknowledged during structure solution and therefore no prior knowledge of the chemical composition is required. Furthermore, all structures may be solved in the space group *P*1, requiring no knowledge of the crystal symmetry – this can be determined afterwards. Charge flipping therefore represents an attractive alternative to direct-space and reciprocal-space methods, particularly in problematic cases, such as unknown composition, ambiguous space group assignment and the presence of disorder.

For a full discussion of these methodologies, the reader is invited to consult comprehensive texts on X-ray diffraction, such as those of Massa [23] and Giacovazzo *et al.*[24]

2.3.2 High-Pressure Single-Crystal X-ray Diffraction

Although diamond is transparent to X-ray radiation and every effort is made to minimise X-ray diffraction from the atomic planes within the diamonds themselves, it is inevitable that reflections due to the anvils are observed in the course of a high-pressure data collection. Furthermore depending of the orientation of the sample chamber (*i.e.* the DAC) with respect to the incident beam, one can observe powder diffraction rings due to the W gasket and Be backing discs (where used). This is exemplified in Figure 2.7, which clearly shows that in one diffraction image one can observe sample peaks, diamond reflections and W rings, and in Figure 2.8(a).

Another complexity in high-pressure data collections is imposed by shading from the steel body of the cell. While ambient pressure diffraction studies of a crystal mounted on a fibre allow the whole of reciprocal space to be sampled, this is severely restricted in high-pressure studies. A data-collection strategy to optimise completeness of high-pressure diffraction data on a CCD diffractometer was developed by Dawson *et al.*[25] This strategy has been applied in all of the high-pressure single-crystal X-ray diffraction studies presented here. Despite this optimisation, however, one can easily appreciate the severe restriction of the diffraction data accessible in high-pressure studies by comparison of the observed intensities for a high-pressure study, using the strategy outlined in [25], and an ambient-pressure study of a comparable crystal system, in Figure 2.9. In order to increase completeness further, it may be possible to load two single crystals of the same sample into DAC in different orientations (Figure 2.8(b)), although this adds further intricacy to data processing. Finally, another popular method to improve completeness of the data is to follow the same data-collection strategy with the DAC in a different orientation, normally by rotation of the triangular cell by 120°.

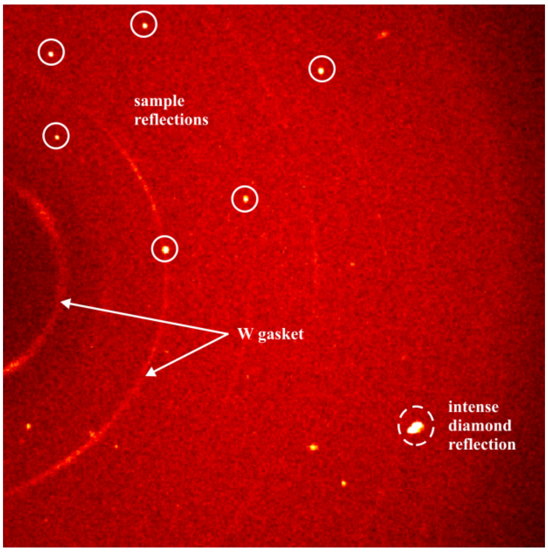

Figure 2.7 Diffraction image collected for an orthorhombic crystal (*Pca*2_1) at 5.5 GPa, showing the juxtaposition of sample reflections, tungsten powder rings and intense diamond reflections.

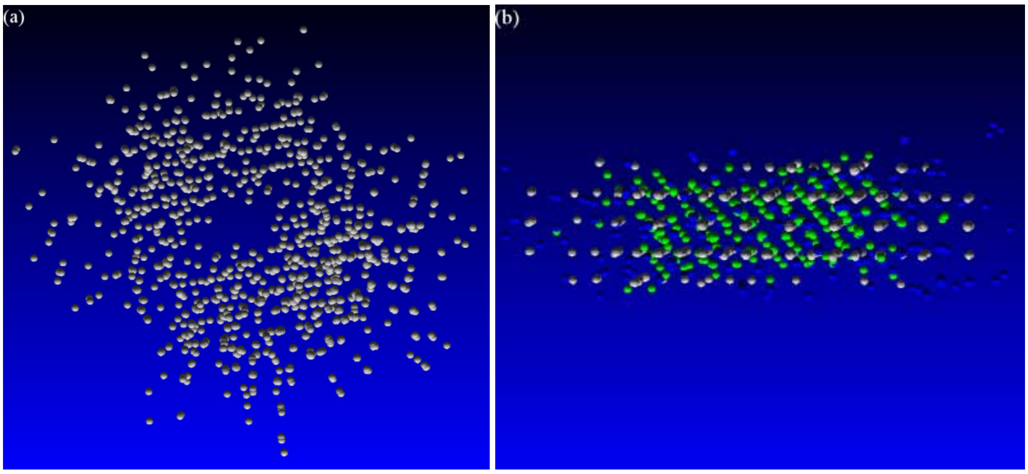

Figure 2.8 Three dimensional renderings of reciprocal lattices, created in RLATT (BrukerNonius) [26]: (a) all of the observed diffraction intensities – indexing of the sample is hampered by scattering from all the other cell components; (b) by judicious selection of the observed reflections, it is possible to separate diffraction from sample crystals (grey and green) from intensities arising from the diamond anvils, ruby and gasket (blue).

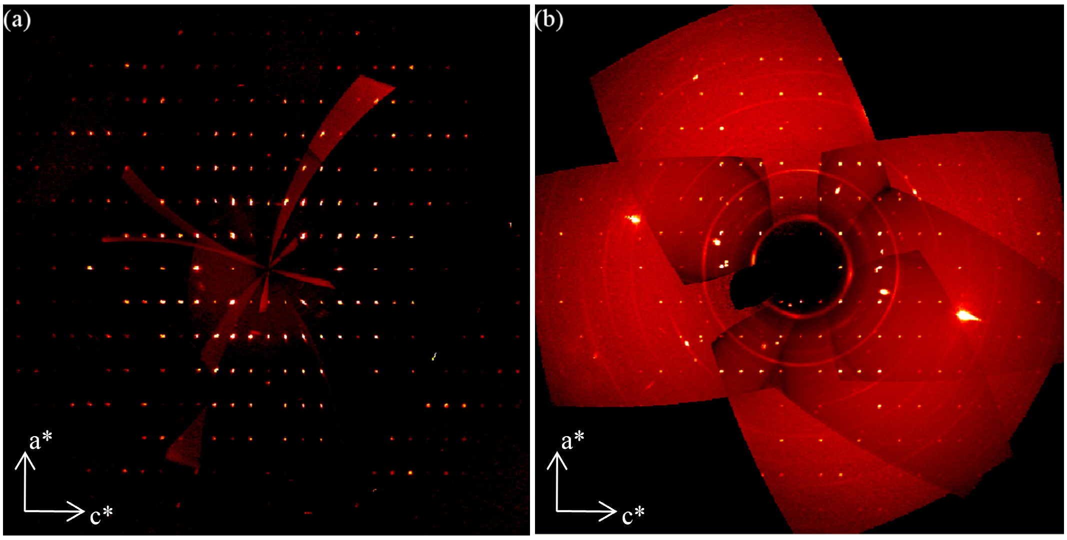

Figure 2.9 Comparison of the completeness of high-pressure data-sets with that of ambient pressure data collections: (a) calculated precession image of the *h*0*l* zone calculated for an ambient pressure data collection for a crystal on a fibre (space group $Pca2_1$); (b) the same image calculated for a high-pressure data-set on an analogous crystal system ($Pca2_1$ at ca 5.0 GPa). Precession images were calculated in the APEX-II program.[26]

In a similar way to the development of data-collection strategies, methods for harvesting the diffraction intensities from CCD images have had to be optimised. Sample reflections were harvested using a threshold algorithm applied within the APEX-II program; orientation matrices and indexing of unit cells were determined using the same program.[26] In order to address the shading of large sections of the detector during data collection, it was necessary to apply a set of dynamic masks (written by Dawson *et al.* [25]) during integration. Integration and global-cell refinement were carried out in SAINT.[27] The avoidance of harvesting data overlapped with reflections from the diamond anvils has also been shown to improve data quality.[28] Other strategies to enhance data-quality include the application of an analytical absorption correction in SHADE [29] (that rejects reflections that lie within 2° of the DAC opening angle (40°) and have poorly-resolved peak profiles); and a multi-scan absorption correction in SADABS [30], which corrects for differences in the X-ray path length arising from the different orientations of the crystal during data-collection. Finally data were merged in SORTAV in the WinGX suite of programs.[31]

In this work, structure solution from single-crystal X-ray diffraction data was carried out using either reciprocal-space methods (Sir92 [32]) or direct-space methods (FOX [21]). Once determined, structures were refined using CRYSTALS.[33] The details for each structure solution and refinement will be expanded upon in the relevant sections. It should be noted, however, that in some cases it was not possible to solve the crystal structure on the basis of the single-crystal data alone due to the low completeness of the high-pressure data-sets. In such cases complementary data provided from X-ray powder diffraction and neutron powder diffraction proved invaluable.

2.3.3 X-ray Powder Diffraction

X-ray powder diffraction may simply be considered an extension of the single-crystal regime discussed in Section 2.3.1, but rather than one crystal being examined, powder samples contain many crystallites oriented at random. This situation results in concentric cones of diffracted intensity emanating from the sample position. These would then appear as a series of concentric rings on an area detector (such as a Mar345 Image Plate) placed normal to the X-ray beam. The development of powder diffraction rings from single-crystal diffraction spots is represented in Figure 2.10. The diffraction images may then be integrated (using calibration values individual to each instrument, such as wavelength and sample-to-detector distance) to produce a 1-dimensional plot of intensity against diffraction angle (2θ).

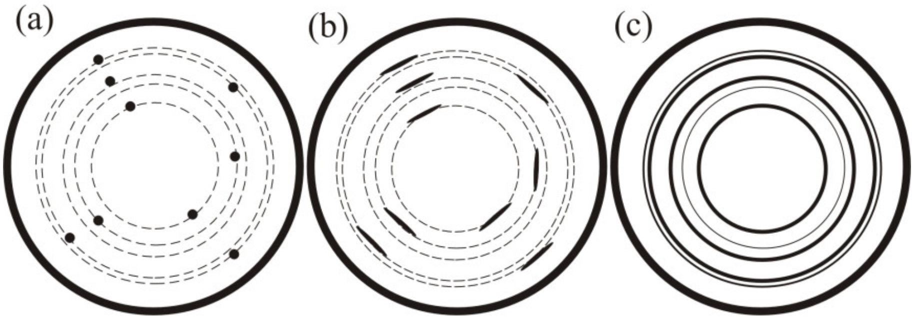

Figure 2.10 Schematic representing the development of a powder diffraction pattern, arising from the spatial averaging of numerous single crystals: (a) diffraction from a single crystal resulting in discrete spots on the image plate detector; (b) poor-quality single-crystal diffraction pattern, in which the diffracted intensities are smeared out along the Debye-Scherrer rings; and (c) ‘ideal’ powder pattern, in which the rings are well-resolved and each is of uniform intensity.[34]

In addition to image plate detectors, ambient-pressure X-ray powder diffraction data in this work were collected using position-sensitive devices (PSD) which measure diffracted intensity at variable angle, thus negating the need for integrating the diffraction image. Diffraction may also be carried out in either of two modes: transmission or reflection. In powder samples of sufficient volume to allow complete powder-averaging, the diffraction patterns observed in these modes should be identical. Reflection mode is often preferred for samples containing heavy atoms as this minimises the effect of X-ray absorption. This may be accounted for by the inclusion of an absorption parameter during refinement or by using thin sample capillaries. One should therefore not be discouraged from attempting to conduct a diffraction study on these materials in transmission mode.

Irrespective of the collection procedure, X-ray powder diffraction presents a quick yet definitive representation of the scattering arising from the atomic planes within the sample of interest. It is therefore an invaluable tool for assessing sample purity and for the detection of polymorphism, without the need for the sometimes arduous task of growing single crystals. Furthermore, as long as the correct structural model is used it is possible to carry out full-profile refinements of the powder diffraction patterns, thus providing important crystallographic information on the bulk sample rather than a solitary crystal. Most commonly this refinement is carried out using the Rietveld method, which facilitates the refinement of the structural model against the diffraction data directly.[35]

A powder diffraction pattern may be described as a plot of diffraction intensity (I_{obs}) against scattering angle (2θ). The Rietveld method progresses by a least-squares refinement of the structural parameters so as to minimise the difference between the calculated and observed intensities (I_{obs} vs I_{calc}). These structural parameters comprise: the structural model, a model to describe the variation in peak-widths over the observed 2θ-range, and a background model. The quality of the diffraction fit is usually quantified by two parameters: wR_p and χ^2. The weighted R-factor (wR_p) represents the minimisation of the difference between the calculated and observed patterns, while χ^2 is a comparison of wR_p to the statistically expected value R_{exp}. Throughout the course of a powder refinement, however, these values may yield erroneously low values, especially with data suffering from a high background or broadened diffraction peaks. It is often the case that visual inspection of the diffraction profile and difference curve is the best assessment for the quality of the refinement.

A secondary refinement method that does not necessitate prior knowledge of the structural model is Le Bail refinement.[36] In this method the calculated diffraction intensities (I_{calc}) are set to be equal to the observed intensities (I_{obs}), while the unit cell, background and peak profiles may be refined. Any peaks which cannot by modelled by a given Le Bail refinement routine are clear evidence that either the unit cell indexing or space group assignment (or both) is wrong. This therefore provides an extremely useful test, particularly in the initial forays into structure solution from powder diffraction. In this work, Rietveld and Le Bail refinements of the various powder diffraction patterns were carried out using GSAS.[37] Any special considerations during refinement will be highlighted in the appropriate chapters.

2.3.4 High-Pressure X-ray Powder Diffraction

Compared to high-pressure single-crystal X-ray diffraction, powder diffraction using the diamond-anvil cell does not present quite such a practical or theoretical obstacle, although for reasons discussed below (Section 2.3.5) these experiments have been carried out using synchrotron radiation. The data presented herein were collected at the Extreme Conditions Beamline (I15) and the High-Resolution Powder Diffraction Beamline (I11) at Diamond Light Source, UK. The experimental set-up for a high-pressure X-ray powder diffraction experiment is represented in Figure 2.11. Data are collected on an image plate detector (Mar345) and are processed according to the procedure outlined for ambient pressure powder diffraction, with one exception. In some cases it may be necessary to mask out intense single-crystal reflections arising from the diamond anvils to ensure no anomalies occur in the I_{obs} vs 2θ profile. The image can then be integrated to provide the one-dimensional powder diffraction pattern using programs such as Fit2D.[38] It is also possible to mask intense powder diffraction rings due to the W gasket although should this interfere with sample peaks it is also possible to carry out Rietveld refinements, in which the tungsten diffraction pattern is incorporated. This process is represented in Figure 2.11(b) – (d).

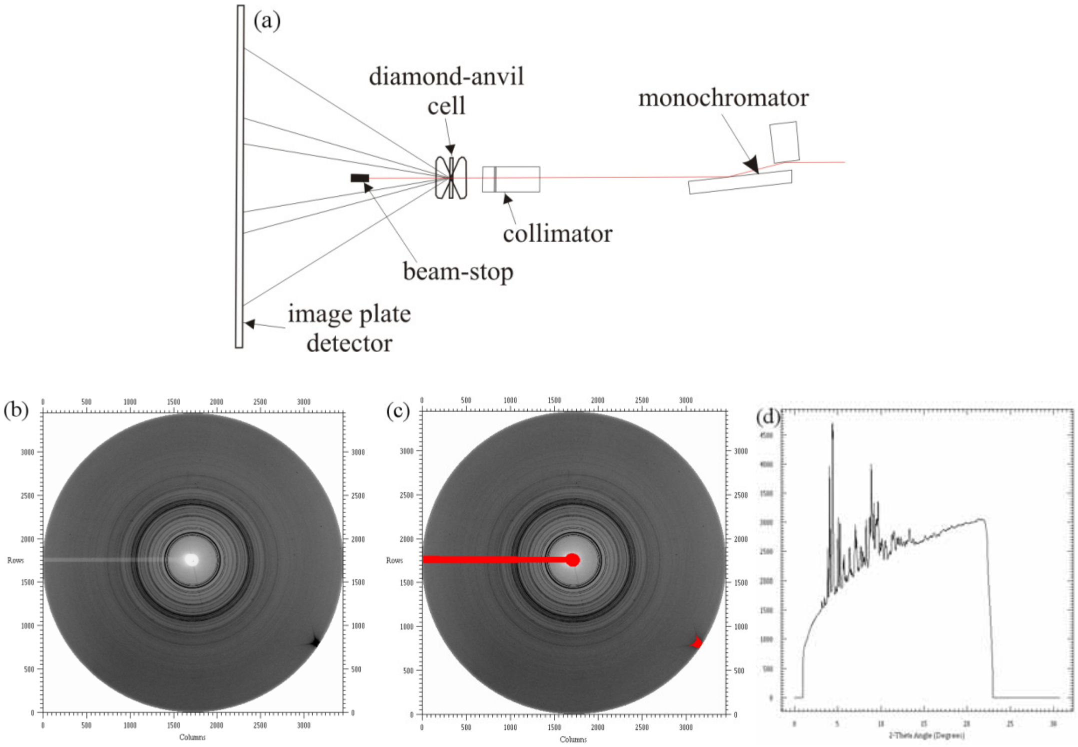

Figure 2.11 (a) schematic illustrating the key components of a high-pressure X-ray powder diffraction experiment; and (b) – (d) the stages of data reduction. The raw image collected on the Mar345 detector is shown in (b). The concentric rings correspond to the diffracted intensities from the sample; the dark spot at the edge of the image is an intense diamond reflection from the DAC. This can be masked to avoid contamination of the sample diffraction pattern - the masking process is shown in (c). It is also necessary to mask the lighter areas of the image that arise due to shading from the beam-stop. Finally the data can be integrated, in programs such as Fit2D [38], thus reducing it to a plot of diffraction intensity against scattering angle (d). The large background common to such data collections is due to Compton (inelastic) scattering from the diamonds and can be subtracted prior to data refinement.

2.3.5 X-ray Sources: Laboratory vs Synchrotron

The ambient pressure X-ray diffraction experiments detailed in this work (both single-crystal and powder) were performed using monochromatic laboratory X-ray sources at the School of Chemistry, University of Edinburgh: both Mo Kα and Cu Kα_1 radiation sources have been utilised (λ = 0.71073 and 1.54056 Å, respectively). High-pressure single-crystal data were collected at ambient temperature using Mo Kα radiation on a modified Bruker SMART APEX-II CCD diffractometer at the Centre for Science at Extreme Conditions (CSEC), University of Edinburgh. In order to allow rotation of the DAC during data collections, a shortened collimator must be used in high-pressure experiments and there was no facility to carry out these studies at sub-ambient temperatures. Details of the data collection procedures will be reserved for discussion in the relevant chapters.

In some cases, however, the restrictions applied to data completeness by the diamond-anvil cell means that it is has been necessary to use X-ray radiation of shorter wavelengths (*i.e.* $\lambda \leq$ 0.5 Å) at synchrotron sources. This improves data completeness relative to laboratory experiments by compressing the characteristic diffraction pattern into a smaller volume of reciprocal space, thus allowing a larger portion to be accessed through the 40° opening angle. Synchrotron radiation has the added benefit of increasing the incident flux that counteracts the weak diffraction from organic samples with restricted volumes and in complex sample environments, *i.e.* the DAC, in which absorption from the diamonds and backing plates reduces the intensity of measured reflections.[37] The results of high-pressure single-crystal diffraction studies conducted at synchrotron sources are not within the scope of this thesis, but the productivity of beamlines with high-pressure capabilities (such as Station 9.8 at the Daresbury Laboratory [40], Beamline I19 at Diamond Light Source [41] and ID09 and ID27 at the European Synchrotron Radiation Facility [42]) is a strong indication of the thriving research in this field.

In the current work synchrotron radiation has been essential in obtaining high-resolution powder diffraction data using the diamond-anvil cell, which is impossible using typical laboratory diffractometers. As outlined above, the short wavelengths and high flux of the synchrotron beam improve data quality significantly. Moreover it is relatively straightforward to change parameters such as the sample-to-detector distance to suit the requirements of the experiment at hand. A further experimental parameter that may be changed (although not so easily) is the wavelength selected for the experiment, thus allowing the optimisation of the data-collection strategy. Finally an important factor in diffraction studies at very high pressures (> 10 GPa) is the high degree of collimation possible, allowing the analysis of very small sample diameters without contamination from the DAC components. In such studies, however, great care must be taken to ensure effective powder averaging of such a small sample volume.

2.3.6 Raman Spectroscopy

Scattering of light by a molecule occurs by the promotion of the molecule from its ground state to a virtual energy state and the subsequent relaxation, which results in emission of a photon (i.e. the scattered light). The vast majority of the scattered light is of the same frequency as the incident radiation (elastic; Rayleigh scattering). Raman spectroscopy, however, relies on inelastic scattering of intense monochromatic light (< 5% of cases). In such cases the molecule relaxes to a different vibrational ground state, resulting in an energy difference between the incident and scattered photons. This is perhaps best explained pictorially. In Figure 2.12 it can be seen that if the molecule relaxes to a vibrational state of lower energy than the starting level, the scattered photon will have a higher energy than the incident radiation (anti-Stokes radiation); if the $E_{virtual}$-E_{final} difference is less than the initial transition, the scattered photon will instead undergo a red-shift (Stokes).

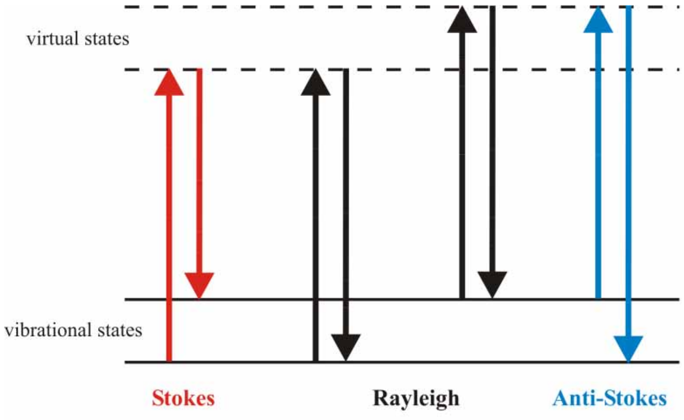

Figure 2.12 A representation of the transitions involved in Raman spectroscopy. Incident photons excite the molecule into a virtual state and the relaxation of the molecule results in emission of a 'scattered' photon. Rayleigh scattering occurs when the incident and emitted photons are of the same frequency. When the molecule relaxes to a vibrational energy level higher than the starting level, the emitted photon will be shifted to a lower frequency (Stokes). Conversely, anti-Stokes radiation has higher frequency than the incident radiation.

Generally Raman spectra are plotted such that the Rayleigh band lies at 0 cm^{-1}. On this scale, the band positions will lie at frequencies that correspond to the energy levels of different functional group vibrations, facilitating comparison with similar (but complementary) results from IR spectroscopy. The selection rule that must be satisfied for a vibrational mode to be Raman active is that there must be change in the polarisability tensor of the vibration. This is best imagined as the ease with which the electron cloud is distorted (*i.e.* polarised) and explains the complementarity between Raman and IR spectroscopy, which relies on changes in dipole moments.

An advantage of Raman spectroscopy, particularly in high-pressure studies, is that since monochromatic light is used, any material that is transparent to visible light may be used as a sample chamber (*e.g.* glass capillaries and diamond-anvil cells). Furthermore Raman spectroscopy is sensitive to changes in the molecular symmetry and changes in the inter- and intramolecular interactions and is therefore an extremely powerful tool in the identification and characterisation of new polymorphs and the observation of phase transitions. Although not conducted in this study, it may also be appropriate to plot the general increase in frequency of a selected vibrational mode with increasing pressure. If the sample remains in the same phase, a linear shift in wavenumber is generally observed but in the event of a new spectral bands may be observed and there may be an abrupt change in the gradient of $\bar{\nu}$ *versus* P plots.

Raman spectra were collected using a LabRam instrument equipped with a 50 mW He-Ne laser (λ = 632.8 nm); typically, objectives of 10x and 20x magnifications were used.

2.4 The Paris-Edinburgh Cell

2.4.1 Construction of the Paris-Edinburgh Cell

Neutron diffraction experiments (see Section 2.5.1) require sample volumes *ca* 10^6 times larger than those required for X-ray powder diffraction, thus precluding the use of diamond-anvil cells. High-pressure neutron diffraction experiments were therefore severely limited until the advent of the Paris-Edinburgh cell (PEC), developed in 1992, which extended the pressure range to 10 – 20 GPa.[2] The popularity of the PEC arose from its (relatively) light-weight design and its portability – the Paris-Edinburgh cell weighs ~ 50 kg, in contrast to other commercial devices of the time with comparable sample volume that weighed close to 1 tonne. This portability, coupled with the fact that load can be applied to the cell by a hydraulic ram while it remains *in situ* on the beamline, greatly simplified high-pressure experiments.

The PEC is also an opposed-anvil device, like the diamond-anvil cell and the Bridgman cell. In this construction, however, the sample is compressed between anvils made of either tungsten carbide (WC) or sintered diamond, see Figure 2.13(a). Early designs utilised null-scattering TiZr toroidal gaskets located into corresponding grooves machined into the anvil faces to confine the sample and, generally, a solid pressure-transmitting medium.

Compression studies using the preferred fluid pressure-transmitting media (methanol:ethanol and iso:n-pentane) were limited to *ca* 2.0 GPa before anvil failure. It was realised that complete encapsulation of the sample and pressure-transmitting medium in two flanged hemispherical caps (TiZr) would prevent the fluid media coming into direct contact with the anvil surface.[43] In this way the anvils were shown to be protected and the available pressure range for hydrostatic studies were extended up to the freezing pressure of methanol:ethanol (*i.e.* > 9.0 GPa). The encapsulated gasket is compared to the 'standard' TiZr toroidal gasket in Figure 2.13(b).

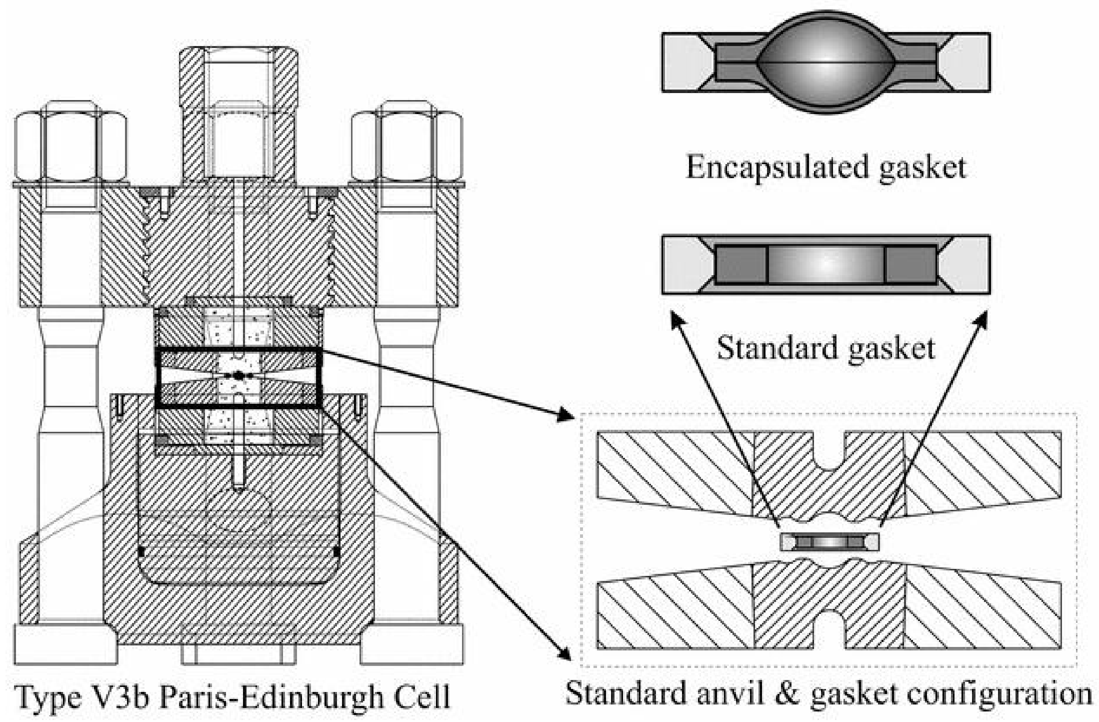

Figure 2.13 (a) Cross-section of the Paris-Edinburgh cell (V3b) and a comparison of the standard and encapsulated gaskets.[43]

2.4.2 Variable-Temperature Insert for the Paris-Edinburgh Cell

The capabilities of the Paris-Edinburgh cell have recently been enhanced by the development of a variable-temperature (v-T) insert, which has been shown to vary sample temperature between 110 and 500 K with excellent control.[44] A liquid nitrogen circuit is used to cool just the sample and the WC anvils, while temperature is increased and controlled by the incorporation of 240 W resistive heaters into the latter, see Figure 2.14. This was in an effort to reduce the volume that is heated or cooled, in order to minimise temperature response times. Cooling to 120 K from room temperature previously required 4 – 5 hours, when the whole of the PE-cell had to be cooled with liquid nitrogen. Commissioning tests on the v-T insert demonstrated its ability to cool to 100 K or warm to 473 K from ambient temperature within 45 minutes.[44] This development has therefore not only opened up the possibility of conducting variable temperature neutron powder diffraction experiments at pressure but also presents a route for rapidly quenching high-pressure or high-pressure/high-temperature polymorphs for their recovery to ambient pressure.

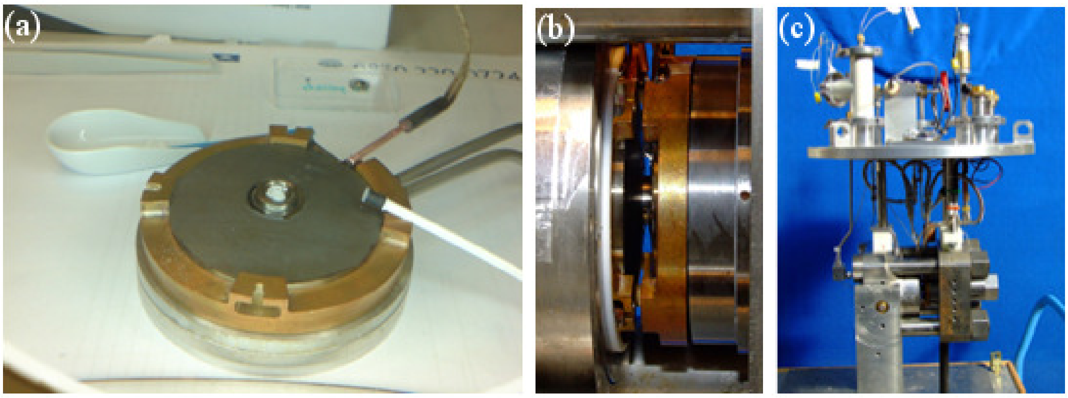

Figure 2.14 The variable-temperature insert for the Paris-Edinburgh cell: (a) the WC anvils, into which both a liquid nitrogen feed and resistive wires have been incorporated to allow rapid heating and cooling; (b) a close-up of the modified anvil within the cell; and, (c) the complete construction of a PE-cell equipped with the vT-insert, underscoring the complexity of such experiments.

2.4.3 Pressure Measurement

Unlike the diamond-anvil cell, the Paris-Edinburgh cell does not allow optical access to the sample chamber and therefore a method for pressure calibration other than the ruby fluorescence method had to be developed. Instead small quantities of internal pressure calibrants are used, typically either NaCl(s) or Pb(s). Both materials have clearly defined equations of state [45, 46], which means that the unit cell volume of the chosen calibrant (as determined by Rietveld refinement of the powder diffraction patterns) is directly related to the pressure within the gasket.

2.5 Experimental Techniques using the Paris-Edinburgh Cell

2.5.1 Neutron Powder Diffraction

While X-ray diffraction if the most widespread technique applied in the determination of crystal structures, a complementary technique using exactly the same principles is neutron diffraction. Neutrons display wave-particle duality and may therefore also be diffracted by a three-dimensional grating. The momentum of a free particle, p, is related to its wavelength, λ, by the de Broglie equation:

$$\lambda = \frac{h}{p} = \frac{h}{mv}$$

where h is Planck's constant, m = mass and v = velocity of the particle. Thus thermal neutrons with average velocities of *ca* 2500 ms^{-1} will have suitable wavelengths for diffraction from atomic planes within a crystal lattice.

In contrast to X-rays, neutrons do not interact significantly with the electron density within a crystal lattice and instead are diffracted by the nuclei of atoms. Since both nuclei and neutrons are small, significant scattering occurs only when a neutron passes close to a nucleus, and thus the total intensity of diffraction of neutrons by a crystal is low compared to that of X-rays – larger sample volumes are required to give comparable diffraction intensities. The point scattering from nuclei imbues this technique with a significant advantage however; the scattering factor does not fall off at higher angles, in stark contrast to X-ray diffraction (see Figure 2.15). This highly penetrating nature of neutrons (in contrast to X-rays) also allows the construction of rather complex sample environments, such as the Paris-Edinburgh cell. Furthermore neutron diffraction locates the atomic nuclei and not the electron density, which may be distorted due to bonding effects, and thus is far more accurate for the determination of atomic positions.

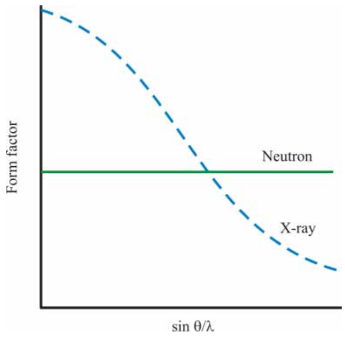

Figure 2.15 Scattering factor of X-rays and neutrons w.r.t. angle of incident.

While the scattering power of an atom with respect to X-ray radiation is directly proportional to its atomic number (Z), there is no direct relationship in neutron diffraction. Indeed neighbouring elements, and even isotopes of the same element, may have considerably different neutron scattering cross-sections – represented in Figure 2.16. This random variation has practical benefits since it is possible to select elements or alloys which display null or very little neutron scattering to construct sample environments. Vanadium (neutron scattering-length, b = -0.4) is regularly used as a sample container for ambient pressure studies; TiZr (null scatterer) is used for sample encapsulation in the Paris-Edinburgh cell. This dramatic effect also means that neutron diffraction is an extremely powerful technique for the structure solution of compounds containing a mixture of light and heavy elements, such as the inorganic azides AgN_3 and $Pb(N_3)_2$ reported in Chapters 5 and 6.

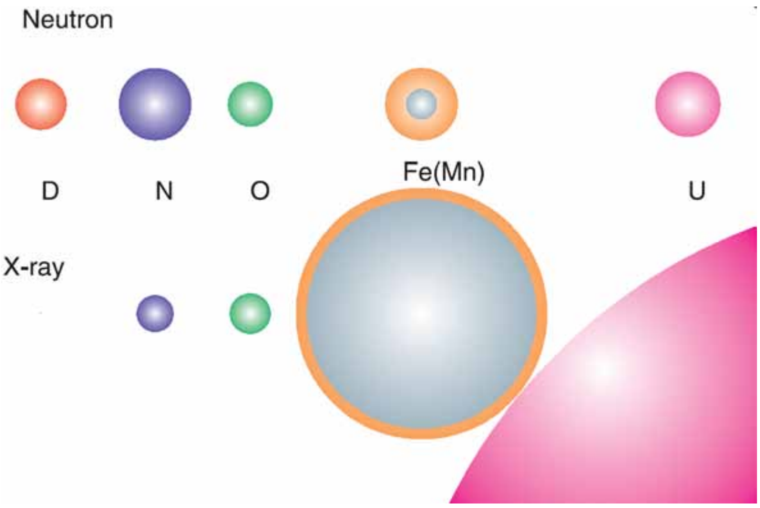

Figure 2.16 Comparison of the scattering powers of different elements with respect to neutrons and X-rays.[34]

The complementarity of X-ray and neutron diffraction is further underlined by studies aimed at the accurate determination of hydrogen positions in a range of molecular and co-ordination solids.[47] X-ray diffraction from hydrogen atoms, having just one electron, is extremely weak. This is not the case, however, in neutron diffraction, although the incoherent scattering from hydrogen normally necessitates sample deuteration.

Finally a significant advantage neutron diffraction displays over X-ray diffraction, although not explored in the present context, is the determination of magnetic structures by the interaction of the magnetic moments of the neutrons with magnetic ions within the crystal lattice. For a detailed account of neutron diffraction of magnetic materials, the reader is directed to Harrison's review.[48]

2.5.2 Neutron Sources

The nature of neutron diffraction experiments is dependent on the source of neutrons. They may be generated by fission (at nuclear reactor sources) or spallation, where short pulses of energetic protons bombard a heavy metal target causing a cascade of high-energy neutrons. At reactor sources the neutron beam is continuous and the wavelength is fixed by means of a crystal monochromator – during the diffraction experiment the detector angle is varied (angle dispersive). In contrast, at spallation sources the energetic neutrons produced must be slowed down (moderated) by collisions with atoms of comparable mass, usually H or D in water or methane, resulting in a distribution of energies impinging on the sample. The pulse of moderated neutrons is very short but stretches out in space as it moves down the flight path, with the higher energy neutrons travelling more quickly. The neutrons travel a known distance, *L*, from the source to the sample and subsequently the detector, which is positioned at a fixed angle. The diffraction pattern is then obtained as a function of the time of flight (ToF) of the arriving neutrons (energy dispersive). Substituting the de Broglie wavelength into Bragg's law then allows the diffraction condition to be expressed in terms of ToF:

$$2d\sin\theta = \lambda = \frac{h}{p} = \frac{h}{m_n v} = \frac{ht}{m_n L}$$

$$t = \frac{2m_n L}{h} d\sin\theta$$

where t is time, m_n is the mass of the neutron, L is the length of the flight path from source to detector, h is Planck's constant, d is the spacing between the atomic planes in the crystal (d-spacing), θ is the scattering angle (fixed) and p is momentum.

It is therefore possible to collect a complete diffraction pattern using a single detector although typical ToF diffractometers utilise banks of detectors to minimise counting times. Outputs from each detector may be summed, provided each diffraction pattern is initially converted into *d*-spacings.

The high-pressure neutron diffraction experiments conducted in this body of work were carried out at ISIS spallation neutron and muon source, STFC Rutherford Appleton Laboratory, UK. The high-flux, medium-resolution instrument PEARL-HiPr is specifically designed for data collections using the Paris-Edinburgh cell, as shown in Figure 2.17. ToF diffraction data were collected in transverse geometry. This arrangement, in which the detectors are fixed at $83° < 2\theta < 97°$, allows access to a range of 0.5 – 4.1 Å in *d*-spacing, with a resolution ($\Delta d/d$) of ~ 0.8%. The individual detector element spectra are electronically summed and normalised to the incident beam monitor and the scattering from a standard vanadium calibration sample. Lastly, the diffraction pattern intensity scale was corrected for the wavelength and scattering-angle dependence of the neutron attenuation by the anvil (WC) and gasket (TiZr) materials. Full-profile Rietveld refinements were carried out using GSAS [37], while any special considerations are highlighted in the pertinent sections.

Figure 2.17 PEARL-HiPr instrument with the Paris-Edinburgh cell, in which the Paris-Edinburgh cell is mounted onto a Tomkinson flange and lowered into a vacuum tank.[49] The red arrow indicates the path of the neutrons through the instrument. Diffracted intensities can be collected by two banks of detectors; transverse geometry was used in this study. Longitudinal mode (detectors situated at $20° < 2\theta < 40°$ and $100° < 2\theta < 120°$) can also be employed to access a wider section of reciprocal space, although resolution is compromised.

2.6 Equations of State

By the structural characterisation of a material throughout its compression, it is possible to obtain a measurement of the variation of the material's density (or volume) with pressure, and sometimes temperature. Generally, static compression studies are conducted at constant temperature, thus the resulting variation of volume with pressure is termed the isothermal 'Equation of State' (EoS). Measured equations of state are usually parameterised in terms of the bulk modulus, $B_0 = -V\partial P/\partial V$, and its pressure derivatives: $B' = \partial B/\partial P$ and $B'' = \partial^2 B/\partial P^2$, which are evaluated at zero pressure. Despite actually being under finite pressure, it is generally accepted that the unit cell volume under ambient conditions may be employed as an approximation to V_0, the zero-pressure volume (which is not measurable).

There is no fundamental thermodynamic derivation of equations of state and therefore a number of approaches have been developed based on a number of assumptions about the behaviour of dense solids, which are addressed in more detail in Anderson's review.[50] The validity of such assumptions may only be assessed on whether the derived EoS accurately reproduces the experimental compression behaviour. The most commonly used formulations, and the only ones used in this study, are the Murnaghan [51], Birch-Murnaghan [52] and Vinet [53] equations.

The Murnaghan EoS is popular due to its simplicity since it can be derived from the assumption that the bulk modulus varies linearly with pressure, such that:

$$P = \frac{B_0}{B'}\left[\left(\frac{V_0}{V}\right)^{B'} - 1\right]$$

The Murnaghan EoS has been found to reproduce both PV data and B_0 for compressions up to about 10% (*i.e.* $V/V_0 = 0.9$) but is not recommended for use beyond this regime.[54]

Other isothermal equations of state, such as the Birch-Murnaghan, employ an assumption that the strain energy applied during compression can be expressed as a Taylor series in the finite strain, f. The 3rd order Birch-Murnaghan EoS is based on the Eulerian strain, $f_E = [(V/V_0)^{2/3}-1]/2$, such that:

$$P = 3B_0 f_E(1+2f_E)^{5/2}\left[1 + \frac{3}{2}(B'-4)f_E + \frac{3}{2}\left(B_0B'' + (B'-4)(B'-3) + \frac{35}{9}\right)f_E^2\right]$$

It may also be appropriate to truncate this expression at second order in the energy term, resulting in the 2nd order Birch-Murnaghan EoS. In this case, the coefficient of f_E must equal zero, thus requiring that B' be fixed at a value of 4.

Finally, the Vinet formalism is often applied for solids under very high compression (*i.e.* $V/V_0 = 0.6$), since it has been observed that finite strain equations of state do not accurately reproduce PV observations in this region.[53] The Vinet EoS is based on a general inter-atomic potential and has been particularly useful in the representation of the compression of simple solids at very high pressures.[54] The Vinet EoS can be calculated according to the following, where $f_V = (V/V_0)^{1/3}$:

$$P = 3B_0\frac{(1-f_V)}{f_V^2}\,exp\left[\frac{3}{2}(B'-1)(1-f_V)\right]$$

In this work, the parameters for the equations of state have been determined by a least-squares fit of the PV data using the program EoSFit v5.2.[55] In this routine it is simpler to consider pressure as the dependent variable [$P_{calc} = EoS(V_{obs})$] and the sum of the squares of the differences between the calculated and observed pressures are minimised during the least-squares solution. It is therefore critical to the success of the fitting procedure that the experimental uncertainties in both the pressure and volume are determined.

The quality of the EoS fitting procedure is also largely dependent upon the number of data points that have been obtained for a particular phase. For example, large errors in B_0 and V_0 may arise in cases where there are very few measurements made close to atmospheric pressure. This is exacerbated in the calculation of these parameters for high-pressure polymorphs, for which it is impossible to determine the unit cell volume at ambient pressure.

It is may therefore be more appropriate to fix V_0 to be the volume determined at the lowest pressure for which structural data have been obtained. It is then necessary to offset all succeeding pressures by this value.

In all of the compression studies reported herein, equations of state have been calculated using all four of the formalisms above. The most appropriate EoS was selected by comparison of the relative uncertainties in the parameters (namely, V_0, B_0 and B') as well as the 'goodness-of-fit' of the least-squares refinement, χ^2. However, the most critical assessment of the quality of the fit is often visual inspection. Where previous EoS data have been published, the same function has been adopted to facilitate comparison between studies, except where this resulted in a considerable reduction in the quality of the fit. A summary of the equations of state derived in this work can be found alongside an assessment of the quality of the fit in each case (by means of R and χ^2) in Appendix 8.2.

2.7 References

1. L. Merrill and W.A. Bassett, *Rev. Sci. Instrum.*, 1974, **45**, 290.
2. J.M. Besson, R.J. Nelmes, G. Hamel, J.S. Loveday, G. Weill, and S. Hull, *Physica B*, 1992, **180-181**, 907.
3. P.W. Bridgman, *Physics of High Pressure*, Dover Publications, New York, 1971.
4. A.W. Lawson and T.Y. Tang, *Rev. Sci. Instrum.*, 1950, **21**, 815.
5. W.A. Bassett, *High Pressure Res.*, 2009, **29**, 163
6. A. Van Valkenburg, *Rev. Sci. Instrum.*, 1962, **33**, 1462.
7. S.A. Moggach, D.R. Allan, S. Parsons, and J.E. Warren, *J. Appl. Crystallogr.*, 2008, **41**, 249.
8. R. Böhler and K. De Hantsetters, *High Pressure Res.*, 2004, **24**, 391
9. R. Böhler, *Rev. Sci. Instrum.*, 2006, **77**, 115103.
10. R.M. Hazen and L.W. Finger, *Rev. Sci. Instrum.*, 1981, **52**, 75.
11. D.J. Dunstan, *Rev. Sci. Instrum.*, 1989, **60**, 3789.
12. R. Miletich, D.R. Allan, and W.F. Kuhs, *High-Pressure Single Crystal Techniques*, in *Reviews in Mineralogy and Geochemistry, 41: High-Temperature and High-Pressure Crystal Chemistry*, R.M. Hazen and R.T. Downs, Editors, 2000, Mineralogical Society of America, Washington, D.C., USA.
13. R.J. Angel, M. Bujak, J. Zhao, G.D. Gatta, and S.D. Jacobsen, *J. Appl. Crystallogr.*, 2007, **40**, 26.
14. S. Klotz, J.C. Chervin, P. Munsch, and G. Le March, *J. Phys. D: Appl. Phys.*, 2009, **42**, 075413.
15. T. Osakabe and K. Kakurai, *Jpn. J. Appl. Phys.*, 2008, **47**, 6544.
16. Y. Shen, R.S. Kumar, M. Pravica, and M.F. Nicol, *Rev. Sci. Instrum.*, 2004, **75**, 4450.
17. G.J. Piermarini, S. Block, J.D. Barnett, and R.A. Forman, *J. Appl. Phys.*, 1975, **46**, 2774.
18. K. Syassen, *High Pressure Res.*, 2008, **28**, 75
19. W.L. Bragg, *Proc. R. Soc. London, Ser. A*, 1913, **89**, 248.
20. W.I.F. David, K. Shankland, J. van de Streek, E. Pidcock, W.D.S. Motherwell, and J.C.Cole, *J. Appl. Crystallogr.*, 2006, **39**, 910.
21. V. Favre-Nicolin and R. Cerny, *J. Appl. Crystallogr.*, 2002, **35**, 734.

22. G. Oszlányi and A. Sütó, Acta Cryst., **A64**, 123.
23. W. Massa, *Crystal Structure Determination, 2nd Edition*, Springer, Berlin-Heidelberg, Germany, 2004.
24. C. Giacovazzo, H.L. Monaco, G. Artioli, D. Viterbo, G. Ferraris, G. Gilli, G. Zanotti, and M. Catti, *Fundamentals of Crystallography, 2nd Edition*, Oxford University Press, Oxford, UK, 2002.
25. A. Dawson, D.R. Allan, S. Parsons, and M. Ruf, *J. Appl. Crystallogr.*, 2004, **37**, 410.
26. Bruker-Nonius, *APEX-II*, Bruker-AXS, Madison, WI, USA, 2000.
27. Bruker-AXS, *SAINT*, Bruker-AXS, Madison, WI, USA, 2003.
28. N. Casati, P. Macchi, and A. Sironi, *J. Appl. Crystallogr.*, 2007, **40**, 628.
29. S. Parsons, *SHADE, Program for Empirical Absorption Corrections to High Pressure Data*, The University of Edinburgh, UK, 2004.
30. G.M. Sheldrick, *SADABS*, University of Göttingen, Germany, 2004.
31. L. Farrugia, *J. Appl. Crystallogr.*, 1999, **32**, 837.
32. A. Altomare, G. Cascarano, C. Giacovazzo, A. Guagliardi, M.C. Burla, G. Polidori, and M. Camalli, *J. Appl. Crystallogr.*, 1994, **27**, 435.
33. P.W. Betteridge, J.R. Carruthers, R.I. Cooper, K. Prout, and D.J. Watkin, *J. Appl. Crystallogr.*, 2003, **36**, 1487.
34. H.E. Maynard-Casely, *personal communication*, 2010.
35. H. Rietveld, *J. Appl. Crystallogr.*, 1969, **2**, 65.
36. A. Le Bail, H. Duroy, and J.L. Fourquet, *Mater. Res. Bull.*, 1988, **23**, 447.
37. R. Von Dreele and A.C. Larson, *General Structure Analysis System (GSAS)*, 1986.
38. A.P. Hammersley, S.O. Svensson, M. Hanfland, A.N. Fitch, and D. Hausermann, *High Press. Res.*, 1996, **14**, 235
39. S.A. Moggach, S. Parsons, and P.A. Wood, *Crystallogr. Rev.*, 2008, **14**, 143.
40. D.R. Allan, S. Parsons, and S.J. Teat, *J. Synchrotron Radiat.*, 2001, **8**, 10.
41. D.R. Allan, W.G. Marshall, D.J. Francis, I.D.H. Oswald, C.R. Pulham, and C. Spanswick, *Dalton Trans.*, 2010, **39**, 3736.
42. F. Datchi, V.M. Giordano, P. Munsch, and A.M. Saitta, *Phys. Rev. Lett.*, 2009, **103**, 185701.
43. W.G. Marshall and D.J. Francis, *J. Appl. Crystallogr.*, 2002, **35**, 122.
44. W.G. Marshall, D.J. Francis, C.J. Barry, O. Kirichek, C.R. Pulham, and M.G. Tucker, *manuscript in preparation*, 2010.
45. D.L. Decker, *J. Appl. Phys.*, 1971, **42**, 3239.
46. A.D. Fortes, PhD Thesis, 2004, Department of Earth Sciences, University College, London, UK.
47. M.T. Weller, P.F. Henry, V.P. Ting, and C.C. Wilson, *Chem. Commun.*, 2009, **45**, 2973.
48. R.J. Harrison, *Neutron Diffraction of Magnetic Materials*, in *Reviews in Mineralogy and Geochemistry, 63: Neutron Scattering in Earth Sciences*, H.R. Wenk, Editor, 2006, Mineralogical Society of America, Chantilly, VA, USA.
49. W.G. Marshall, *personal communication*, 2010.
50. O.L. Anderson, *Equations of State of Solids for Geophysics and Ceramic Science*, Oxford University Press, Oxford, UK, 1995.
51. F.D. Murnaghan, *Am. J. Math.*, 1937, **59**, 235.
52. F. Birch, *Phys. Rev.*, 1947, **71**, 809.
53. P. Vinet, J. Ferrante, J.R. Smith, and J.H. Rose, *J. Phys. C: Solid State Phys.*, 1986, **19**, L467.
54. R.J. Angel, *Equations of State*, in *Reviews in Mineralogy and Geochemistry, 41: High-Temperature and High-Pressure Crystal Chemistry*, R.M. Hazen and R.T. Downs, Editors, 2000, Mineralogical Society of America, Washington, D.C., USA.
55. R.J. Angel, *EOS-FIT V5.2*, Department of Geological Sciences, Virginia Tech., Blacksburg, VA, USA, 2001.

Chapter 3

Structural Studies of RDX

(1,3,5-trinitrohexahydro-1,3,5-triazine)

3 Structural Studies of RDX

3.1 Introduction

RDX (1,3,5-trinitrohexahydro-1,3,5-triazine) was first synthesised by Henning in 1899 [1], although its potential as an explosive was not explored until 1920.[2, 3] War-time impetus meant that the characterisation of RDX and the optimisation of its synthesis were both accelerated until reliable manufacturing processes were implemented in the 1940s. Bachmann's method [4] of obtaining RDX by the nitration of hexamethylenetetramine (hexamine) is still used today, although samples prepared in such a way show typical impurity levels of HMX of around 10%. Despite this, the greater thermal and chemical stability of RDX over explosives of the time led to its more widespread use in munitions during World War II.[5]

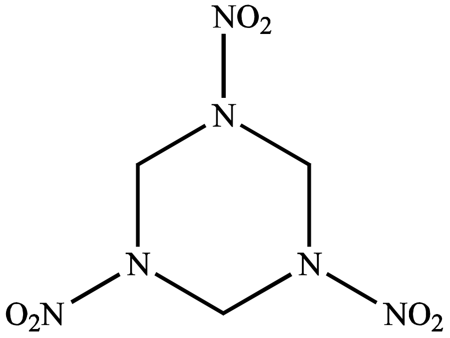

Figure 3.1 Molecular structure of RDX

Due to the sensitivity to detonation by friction or impact of pure RDX, initial efforts were aimed at desensitisation, firstly by coating RDX crystals with wax, oil or grease. The current practice, however, is to obtain 'insensitive munitions' (IMs) by embedding crystals of energetic materials in synthetic rubbers or polymer matrices (polymer bonded explosives, PBXs). RDX is the energetic component of the well-known plastic explosives C4 and Semtex, although numerous examples of PBXs have been reported.[5] The most recent development in RDX-based formulations, however, has focussed on reducing the sensitivity of PBXs to accidental detonation. Various manufacturers have promoted samples of RDX that have been observed to be less sensitive to shock initiation than neat RDX, particularly upon their inclusion in plastic explosives.[6-9] An international inter-laboratory comparison (the Reduced Sensitivity RDX Round Robin) program was therefore initiated to assess the physical properties, such as melting point and purity, as well as the impact sensitivity of seven different RDX formulations, produced by different synthetic procedures or crystallisation methods.[10] It was found that samples containing very little HMX impurity displayed the greatest insensitivity to initiation.[11] It should be noted that synthetic and crystallisation methods are often proprietary information and are not available in the open literature. It is difficult therefore to draw conclusions on the effects these procedures have on sample quality.

The amount of research on RDX over the last 70 years is a reflection of the importance of this material. It has been the subject of a vast range of experimental and theoretical studies that include, for example, its vibrational spectroscopic properties [12-14], its molecular geometry in the gas phase [15], its decomposition mechanism [16-18], and its toxicological and environmental effects.[19-21] Despite this there is a relative paucity of detailed structural information on RDX. In fact, until 2008 only the crystal structure of the ambient polymorph had been determined, even though spectroscopic studies have presented evidence of at least three more forms depending on pressure/temperature/crystallisation conditions.

3.2 Polymorphism of RDX

The crystal structure of the stable polymorph of RDX at ambient conditions has been determined by single-crystal neutron [22] and single-crystal X-ray diffraction.[23] The α-form was found to crystallise in the orthorhombic crystal system (*Pbca*) with one molecule in the asymmetric unit. The conformation of the RDX molecule in this form (Figure 3.2) has been termed the AAE conformation based on the orientations of the three nitro groups relative to the six-membered ring: two nitro groups adopt pseudo-axial positions (A), while the third is in a pseudo-equatorial position (E). A more rigorous description of these orientations can be made by reference to the angle (δ) between the plane of the nitro group and the plane of the corresponding C-N-C ring atoms (Figure 3.3).[15]

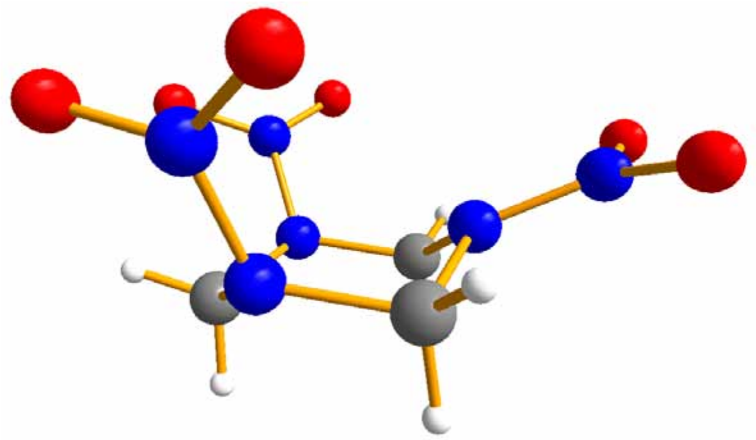

Figure 3.2 AAE molecular conformation of α-RDX

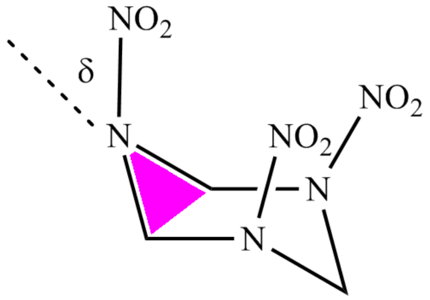

Figure 3.3 Schematic showing parameter δ used to describe orientation of the nitro groups in RDX.

In addition to the α-form, McCrone identified a highly metastable β-form obtained at ambient conditions by crystallisation from non-volatile solvents such as nitrobenzene, thymol (2-isopropyl-5-methylphenol) and even molten TNT (trinitrotoluene).[24] This form could only be isolated in small quantities and it was suggested by McCrone that "*because of its physical instability, there is no possibility of obtaining (this form) even in laboratory crystallisations… it should never be obtained on a laboratory scale*." A subsequent study by Karpowicz *et al.* [25] showed that small dendritic crystals of β-RDX could survive for several days in the absence of 'undue handling'. The β-form was also observed to transform to α-RDX upon contact with the more stable α-form or upon agitation. It was therefore asserted that the β-form is 'unlikely to survive routine handling' and is 'primarily a research curiosity'.[25]

Further spectroscopic studies have suggested that the RDX molecules in the β-form adopt essentially C_{3v} symmetry based on fewer vibrational bands being observed for β-RDX than for the α-form.[25-27] Each of these studies concluded that all of the nitro groups are equivalent and similar to the AAA conformation adopted in the solution and vapour phases. The most recent spectroscopic study on β-RDX by Infante-Castillo *et al.* has provided evidence for an α → β solid-solid phase transition at 477 K (at ambient pressure).[28] Samples of β-RDX produced in this way were not observed to undergo a reverse transition to the α-form, although no comment was made pertaining to the stability of these samples in the presence of the more stable α-form. A further aspect of this study, however, was the close agreement of the vibrational spectra and solid-state ^{15}N NMR spectrum with those calculated for the AAA conformer by DFT methods, thus providing further support for this hypothesis.[14] Unfortunately the instability of β-RDX at ambient conditions has precluded the possibility of obtaining good quality single crystals and therefore structure determination has so far proved impossible.

Various groups have examined the behaviour of RDX under variable temperature and pressure using spectroscopic and diffraction techniques.[29-35] All studies have shown that the α-form remains stable up to a pressure of ~3.9 GPa, at which point a reversible, first-order transition to a high-pressure γ-form occurs. The studies that investigated the tandem effects of pressure and temperature [31, 32, 34] found that the α → γ transition pressure did not vary with temperature, although Miller did observe that the rate of transformation did increase with temperature.

Olinger *et al.* observed that the volume decreased by approximately 1.6% over the α → γ transition with a sudden increase in the crystallographic *b*-axis but the metric symmetry remained orthorhombic. In 2006, a study by Goto *et al.* used a combination of X-ray powder diffraction and IR spectroscopy to characterise the γ-form above 4.0 GPa.[36] They proposed a structural model in which the space group (*Pbca*) is retained and the only conformational change of the molecule is a 'marginal' change in the torsion angles of the $N-NO_2$ groups. Nevertheless, the observation that the crystal packing is different from that in α-RDX led the authors to conclude the α- and γ-forms are indeed distinct. This structure was initially employed in the Rietveld refinements in Davidson's combined X-ray and neutron diffraction study of RDX up to ~8.0 GPa. Numerous intensity misfits, however, led the authors to conclude that this structure was incorrect and instead to propose their own structural model for γ-RDX.[37]

In accordance with previous observations, the orthorhombic crystal system was retained over this transition, although the space group symmetry was reduced from *Pbca* to $Pca2_1$. This reduction in symmetry is due to two molecules, which were formerly arranged over an inversion centre in the α-form, becoming inequivalent in order to maximise packing efficiency and to minimise unfavourable short O…O and N…O interactions. The molecular conformations of the two independent molecules in γ-RDX are shown in Figure 3.4; their respective δ angles are presented in Table 3.1 alongside those for the α-form and for isolated molecules in a range of conformations as calculated by DFT methods.[38] It is clear that one molecule adopts a conformation in which all of the nitro groups are in pseudo-axial positions (AAA). In the second molecule however, one nitro group lies in an intermediate position between axial and equatorial; this conformation has thus been termed the AAI conformation.

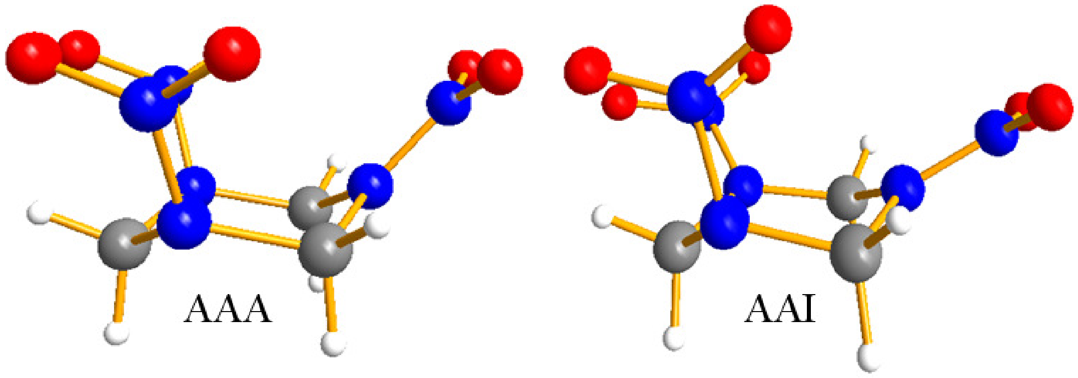

Figure 3.4 Molecular conformations of the two independent molecules in γ-RDX.

α-form	γ-form molecule 1	γ-form molecule 2	AAA*	AAE*	AAA-AAE (TS-1)*
33.4(1)	39.6(7)	36.4(9)	30.3	34.0	34.1
33.9(1)	17.3(8)	35.5(9)	30.1	34.0	33.8
-19.8(1)	-2.4(12)	9.5(11)	29.9	-37.9	1.5

Table 3.1 Values of δ (°) for different conformations of RDX. Note that values marked (*) have been calculated from ref. [38].

Figure 3.5 shows the packing arrangements in both α- and γ-RDX. This highlights that the change in molecular conformation in the γ-form allows two neighbouring molecules to effectively ‘cup’ one another to form dimers over a pseudo-inversion centre. This interlocking arrangement results in a *ca* 3% decrease in unit cell volume over the α → γ transition. Furthermore the high quality of data obtained for both polymorphs allowed the fitting of equations of state. The variation in volume with pressure over the stability range of the α-form was expressed as a 3rd order Birch-Murnaghan EoS with V_0 = 1640(2) Å^3, B_0 = 10.0(5) GPa, and B’ = 11.3(7). The compression of the γ-form from 3.90 GPa to the highest pressure studied (7.99 GPa) was fitted using V_0 = 1632(4) Å^3, B_0 = 8.73(16) GPa, and B’ = 11.26 (fixed) thus demonstrating that γ-RDX is significantly less compressible than α-RDX.[39] In the case of γ-RDX, B’ was not treated as a free parameter due to the lack of low-pressure data and the relatively limited pressure range for which structural data was collected. The authors therefore used the value derived for the α-form as an appropriate approximation.

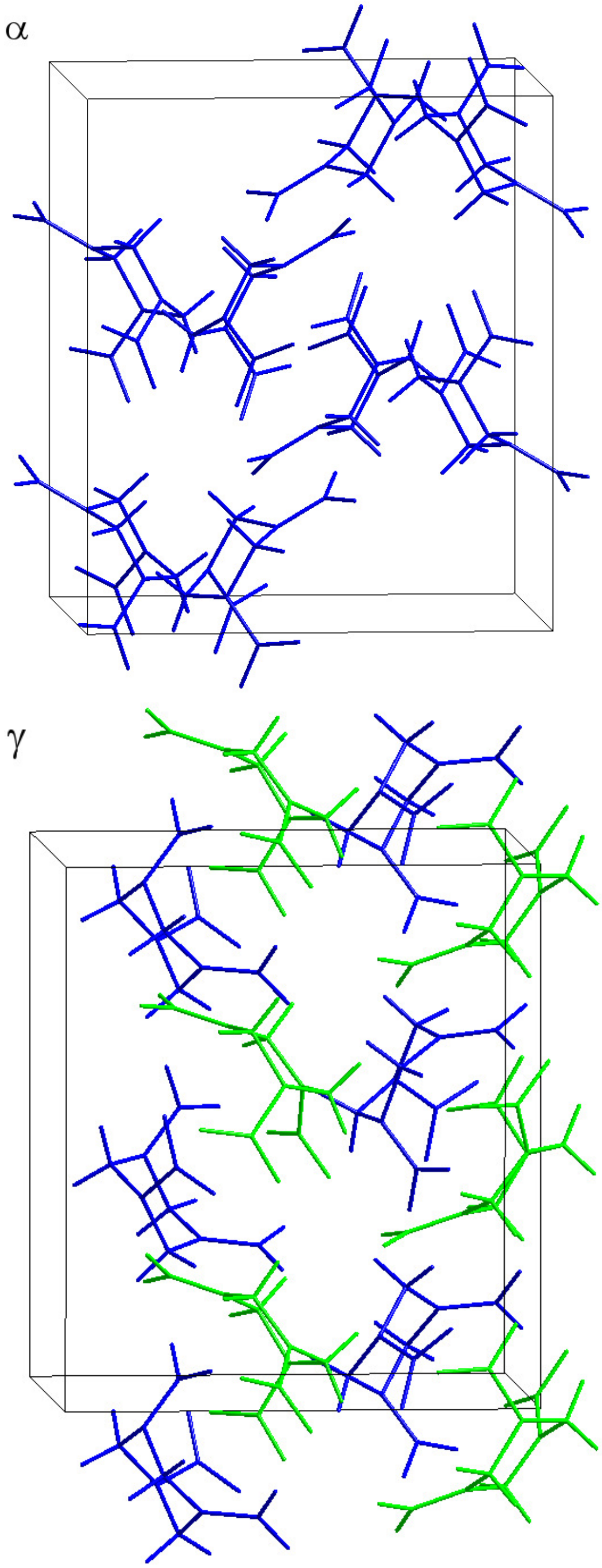

Figure 3.5 Crystal packing of α-RDX and γ-RDX, coloured by symmetry equivalence.

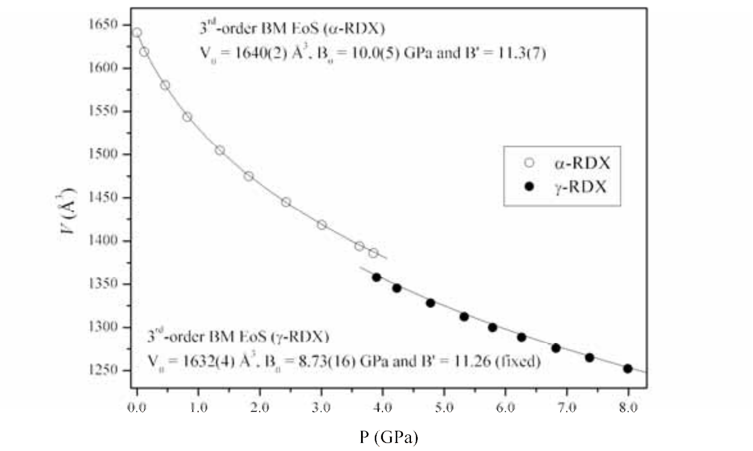

Figure 3.6 *PV* plots for the α- and γ-forms of RDX. The smooth compression of the unit cell volume with pressure has, in each case, been fitted to a 3rd-order Birch-Murnaghan EoS.[39]

Computational studies on the hydrostatic compression of RDX [40-46] have, until recently, been limited to the stability region of the α-form (i.e. $P < 3.9$ GPa). In the most recent computational study by Sorescu and Rice, however, semi-empirical atom-pairwise dispersion corrections were applied to conventional density functional theory (DFT) calculations to account for the van der Waals interactions in these molecular crystals.[47] Such calculations (termed DFT-D) were developed by Grimme [48] and have been particularly successful in reproducing experimental structures of molecular solids.[49] In their theoretical study, Sorescu and Rice were able to predict unit cell parameters within 2% of experimental data at ambient pressure. Furthermore, they investigated the evolution of the unit cell parameters upon hydrostatic compression and, in the case of RDX, were able not only to re-create the compression of α-RDX to 3.9 GPa but also to obtain excellent agreement with the experimental compression of the γ-form conducted by Davidson *et al.*[37]

By using helium as pressure-transmitting medium for their Raman measurements, Ciezak *et al.* [33, 34] have extended the pressure range for sprectroscopic studies of RDX to ~ 30 GPa. These studies confirmed the stability of γ-RDX up to ~ 18 GPa but the appearance of new vibrational bands and discontinuities in the vibrational spectra above 17.8 GPa led the authors to conclude that there was a reversible phase transition to a further high-pressure polymorph of RDX, subsequently referred to as δ-RDX. It is interesting to note that compression of single crystals to 22 GPa under non-hydrostatic conditions (resulting from the pressure-induced freezing of the mineral oil pressure-transmitting medium) does not give rise to any irreversible changes in the Raman spectrum.[35] Due to the increased overlap of peaks under non-hydrostatic conditions, the focus of this study was monitoring the spatial variation in one selected Raman mode across the crystal in order to estimate the pressure gradient over the crystal. The mode selected in this study however (885 cm^{-1} at ambient pressure) has been shown to retain its peak-profile and intensity over the purported $\gamma \rightarrow \delta$ transition and this should therefore not be considered contradictory to the full spectroscopic analysis of RDX under very high pressures.[33]

Finally, investigations into the behaviour of RDX at elevated temperatures *and* pressures have provided evidence for another polymorph. The study by Baer *et al.* [31] using liquid nitrogen as pressure-transmitting medium observed a phase transition at $P > 3.8$ GPa and a temperature of 375 K. Miller's study [32] using Fluorinert as a pressure-transmitting medium also found this high-pressure/high-temperature polymorph at similar pressures but at a higher temperature (488 K).

Despite the differences in the conditions required to produce this form, both authors observed a simplification of the vibrational spectra, indicating a higher molecular symmetry with respect to both the α- and γ-forms. Furthermore they report that once this polymorph is formed at elevated temperatures and pressures, it can be cooled to ambient temperature and it persists on decompression 'almost to ambient pressure'. These observations led both authors to conclude that this form was the same as the metastable polymorph at ambient conditions and it has thus denoted β-RDX.

In addition to the static compression studies and the computational studies summarised above, shock compression experiments have provided complementary information on the real-time response of RDX to shock-waves at the molecular level. Patterson *et al.* were able to present Raman spectroscopic evidence for the occurrence of the $\alpha \rightarrow \gamma$ transition on the timescale of a shock compression experiment.[50, 51] This is a significant observation since it clearly demonstrates that this phase transition occurs prior to initiation, thus complicating the decomposition mechanism. These studies have since been extended to the investigation of products formed immediately after shock-wave induced decomposition by Raman and emission spectroscopy and quantum chemical calculations. Although no definitive decomposition mechanism has been determined, Patterson *et al.* propose that '*NO_2 is an important species in the initial decomposition of RDX*' and that this mechanism may, in fact, change above a threshold shock-wave pressure of *ca* 10 GPa.[52] In this higher pressure regime they suggest a more complex bimolecular decomposition mechanism between RDX and radical decomposition products.[53]

The voluminous, and at times confusing, information on the polymorphism of RDX has been summarised in Figure 3.7 that shows the regions of pressure/temperature space in which each polymorph is the stable form.

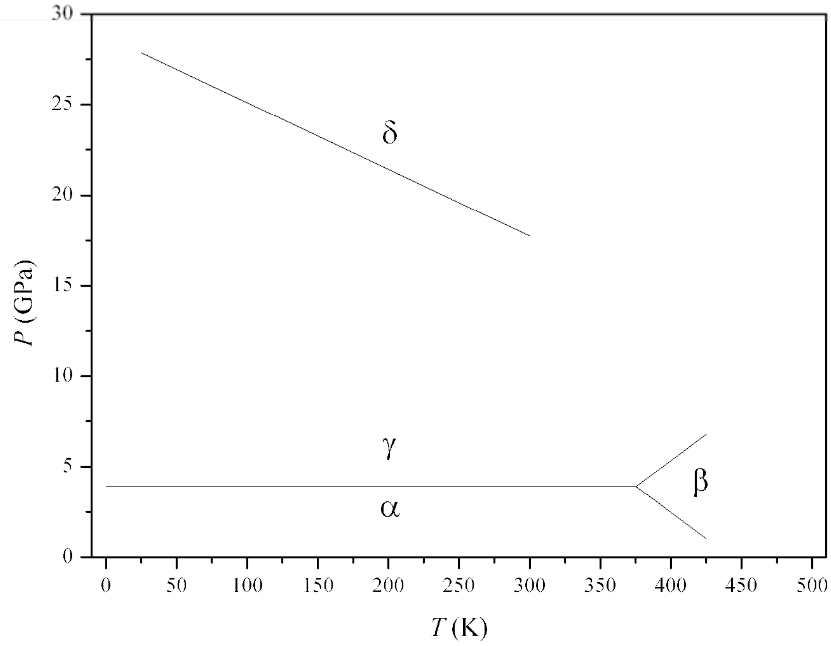

Figure 3.7 Phase diagram of RDX, taken from Ciezak *et al.* [34], with the inclusion of data from Baer *et al.* [31]

3.3 Aims

Given the confusion over the polymorphism of RDX and the paucity of detailed structural information the aims of this work were:

- to determine the structure of β-RDX at ambient conditions;
- to investigate the high-pressure/high-temperature form to determine if this was indeed the same as the β-form obtained at ambient conditions *and* to investigate the recovery of this form to ambient conditions;
- to extend the pressure range of diffraction studies to ~ 20 GPa to obtain an equation of state for RDX to this pressure and to characterise δ-RDX.

3.4 Experimental

3.4.1 *Materials*

Crystalline samples of RDX (SME type II; 100–300 μm) were kindly provided by W.G. Proud (Cavendish Laboratory, University of Cambridge). For neutron powder diffraction experiments, a mixture of deuterated RDX and its tetrameric oligomer HMX was prepared from deuterated paraformaldehyde and deuterated ammonia in a two-step synthesis following Bulusu's synthetic procedure [54] displayed in Reaction Scheme 2. The initial combination of paraformaldehyde and ammonia yielded the nitramine hexamethylenetetramine (hexamine), which was subsequently nitrated by concentrated nitric acid and ammonium nitrate in a complex multi-step mechanism.

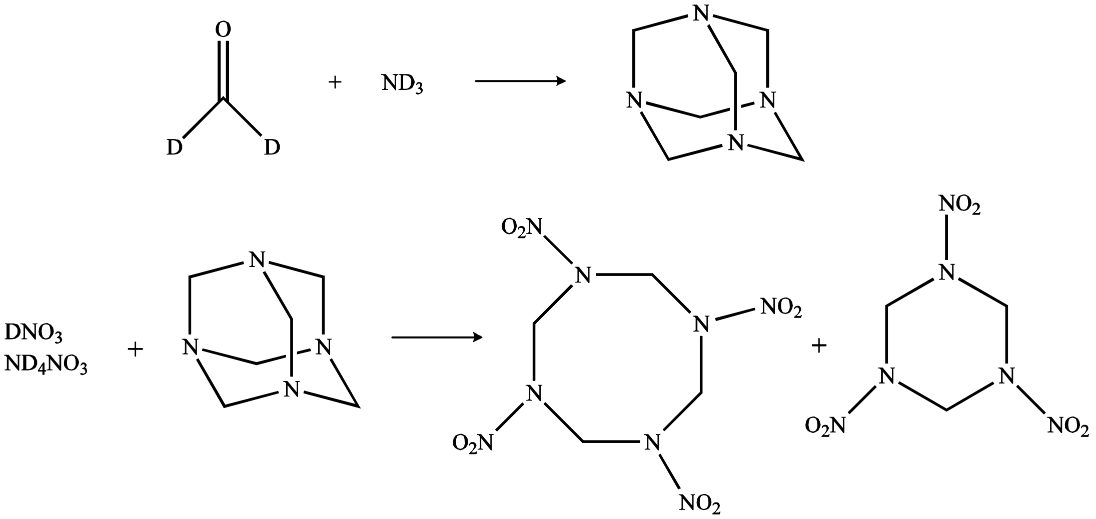

Reaction Scheme 2: The two-step synthesis of HMX and RDX. The formation of hexamethylenetetramine-d_{12} from paraformaldehyde and ammonia is followed by its nitration with nitric acid (98 – 100%) and ammonium nitrate. This resulted in an 85:15 mixture of HMX:RDX in the Bulusu synthesis.

Formation of hexamine-d_{12}: Initially, the recrystallisation of hexamine from D_2O was investigated to see if this would provide a cheaper and more facile route to hexamine-d_{12}. Infrared studies showed no evidence for hydrogen-deuterium exchange however.

Under an inert atmosphere, deuterated ammonia, ND_3, was bubbled into a solution of paraformaldehyde-d_2 ($(CD_2O)_n$, 3.28 g) in D_2O until the solution was saturated. The solvent was removed by heating and evaporation at ambient pressure; recrystallisation by azeotropic distillation with benzene gave pure hexamine in 73 % yield (2.0 g; m.p. 535 K decomp., lit. m.p. 536 K decomp.).

Nitrolysis of hexamine-d_{12}: A mixture of glacial acetic acid (CH_3CO_2D, 15 cm^3), acetic anhydride (0.25 cm^3) and paraformaldehyde-d_2 (0.35 g) was maintained at 317 K in a vessel fitted with three glass syringes. The following solutions were then added to this mixture simultaneously and uniformly over a period of 15 mins: (a) hexamine (2.0 g) in CH_3COOD (3.35 cm^3); (b) $(CH_3CO)_2O$ (5.5 cm^3); and (c) the nitrating mixture of DNO_3 (98 – 100 %, 1.89 g) and ND_4NO_3 (99 %, 1.65 g). After stirring for 15 mins, additional portions of $(CD_3CO)_2O$ (9.0 cm^3) and the nitrating mixture (DNO_3, 2.85 g; ND_4NO_3 2.63 g) were subsequently added uniformly, as before.

The reaction mixture was stirred at 317 K for an hour before dilution with D_2O and subsequent heating under reflux for 30 mins. Addition of 50 g frozen D_2O precipitated the crude product which was then collected, washed with cold H_2O and allowed to dry. This yielded 3.5g (85 %) of a mixture of HMX and RDX.

The crude mixture was stirred in 1,1-dichloroethane (300 cm^3) in order to dissolve the more soluble RDX. After filtration, the white solid was recrystallised from acetone to give the colourless crystals (3.2 g, m.p. 548 K, lit. m.p. 549 – 550 K). The RDX was then recovered from the dichloroethane extract before recrystallisation from 50 % aqueous acetone yielded the fraction in pure form (0.03 g, m.p. 468 K, lit. m.p. 478 K).

In order to increase the yield of RDX-d_6 for the structural studies outlined below it was necessary to undertake a second preparation. In this case hexamine-d_{12} was added to concentrated DNO_3 at 298 K before warming to 328 K. The RDX fraction was then precipitated with cold water before recrystallisation with acetone gave the pure solid.

Although both RDX and HMX are relatively insensitive to initiation, these are nevertheless potentially explosive materials and various safety precautions were taken to prevent initiation and explosive decomposition. Both materials were kept away from sources of ignition and care was taken to avoid the risk of detonation by friction or spark, e.g. metal spatulas. In addition appropriate safety equipment was used to minimise any risk of serious harm: all work during the nitration of hexamine was carried out behind a blast screen; Kevlar gloves and sleeves were worn to protect the hands when dealing with these materials; a reinforced face-mask was worn when close-handling of the samples was necessary. It should also be noted that all vessels which were exposed to the energetic materials were bathed in concentrated NaOH to destroy the HMX and RDX. Samples were stored in a police-licensed explosives locker.

3.4.2 High-Pressure Neutron Powder Diffraction

Neutron powder diffraction data were collected using the high flux, medium-resolution time-of-flight diffractometer PEARL-HiPr at the ISIS Neutron Facility, Rutherford Appleton Laboratory. High pressures and high temperatures were attained using a Paris-Edinburgh cell [55] with a newly commissioned variable temperature insert.[56] A lightly ground sample of RDX-d_6 (*ca* 100 mg) was loaded into an encapsulated TiZr gasket [57] with perdeuterated 4:1 methanol-ethanol as pressure-transmitting medium and a lead pellet as an internal pressure calibrant.[58] The P-E press ram pressure was monitored and varied by means of a computer-controlled hydraulic system. Time-of-flight (ToF) neutron powder diffraction data were collected using the $2\theta = 90°$ detectors with a transverse (through-anvil) scattering geometry. The resulting summed pattern was then normalised with respect to the incident beam monitor and the scattering from a standard vanadium calibration sample. Finally, the diffraction pattern intensity scale was corrected for the wavelength and scattering-angle dependence of the neutron attenuation by the anvil (tungsten carbide, WC) and gasket (titanium-zirconium alloy, TiZr) materials. Data analysis was performed by Rietveld refinement using the General Structure Analysis System (GSAS) suite of programs, in which a convolution of Gaussian (with coefficient σ_1) and Lorentzian (γ_1) functions was used to describe peak profiles (GSAS ToF profile 3).[59]

3.4.3 Ambient-Pressure Single-Crystal X-Ray Diffraction

X-ray diffraction intensities were collected using Mo-Kα radiation on a Bruker SMART APEX CCD diffractometer [60] equipped with an Oxford Cryostream-*Plus* low-temperature device.[61] Structures were solved [62] and refined by full-matrix least squares against F^2 using all data.[63] All non-hydrogen atoms were refined anisotropically. The hydrogen atoms were geometrically placed on the parent carbon.

3.4.4 High-Pressure Single-Crystal X-Ray Diffraction

High pressures were attained using the Merrill-Bassett diamond-anvil cell (DAC) [64] equipped with 600 μm culet diamonds and a 250 μm thick tungsten gasket (indented to ~100 μm) with a 300 μm diameter hole. In order to maximise the volume of reciprocal space that could be sampled it was necessary to use Böhler-Almax type diamonds and WC backing plates [65] that provide a wider opening angle than the typical beryllium-backed DACs. Initial studies focussed on the compression and subsequent heating of single crystals of α-RDX loaded in a DAC. Unfortunately, the high temperatures involved in this study led to the dissolution of the crystals in the pressure-transmitting medium (4:1 methanol:ethanol mixture). As an alternative, a high-pressure re-crystallisation route to *in situ* crystal growth was performed. In this case, polycrystalline RDX was loaded into a DAC with MeOH:EtOH and was subsequently compressed to *ca* 5.0 GPa and heated to 500 K. Upon cooling, a crystal large enough for single-crystal X-ray diffraction was obtained at 5.7 GPa (see Section 3.5.2 for more details). Accurate determination of sample pressure was made by the ruby fluorescence method [66] using a 632.8 nm excitation line from a He-Ne laser. The fluorescence was detected by a Jobin-Yvon LabRam 300. High-pressure data sets were collected using ω-scans in 12 settings of 2θ and φ with 0.3° step-size for 60 s.[67] X-ray diffraction intensities were collected using Mo-Kα radiation on a Bruker SMART APEX II CCD diffractometer.[60] Single-crystal data were processed according to the procedure described by Dawson *et al*.[67] Integration of data sets and global cell refinement was carried out using the program SAINT [68], in which 'dynamic masks' were employed to prevent integration of areas of the detector shaded by the body of the DAC. SHADE [69] was used to reject reflections partly shaded by the DAC and absorption corrections were applied by SADABS [70] to allow for different path-lenghts of the X-rays through the crystal, depending on its orientation during the scan. Structures were solved by direct methods using SIR92 [62] and full-matrix least-squares-refinement against F^2 was carried out using CRYSTALS.[63]

3.4.5 High-Pressure X-Ray Powder Diffraction

High-pressure X-ray powder diffraction experiments were carried out using a Merrill-Bassett diamond-anvil cell (DAC) [64] equipped with 400 μm culet diamonds and a 150 μm thick tungsten gasket (pre-indented to ~20 GPa) with a 100 μm hole. Due to the cut of the diamond anvils it was necessary to use DACs fitted with Be backing plates but the high degree of collimation of the synchrotron X-ray beam (typically 30 – 50 μm) meant that this did not have a detrimental effect on data collections. Pressure measurement was made by monitoring the R_1 fluorescence line of ruby spheres.[66] Data were collected at the Extreme Conditions beamline (I15) and the High Resolution Powder Diffraction beamline (I11) at Diamond Light Source.

I15: Two experiments were carried out at beamline I15. In the first a polycrystalline sample of RDX was loaded into a DAC with methanol:ethanol (4:1) as pressure-transmitting medium. The X-ray beam (λ = 0.484693 Å) was collimated to a diameter of 50 μm and samples were exposed for 300 s. Similarly, a polycrystalline sample of RDX was loaded into a DAC with MeOH:EtOH as pressure medium in the second I15 experiment but the beam diameter was reduced to 20 μm. The wavelength for this experiment was 0.47686 Å and it was necessary to lengthen exposure times to 1800 s due to the overall reduction in X-ray intensity.

I11: Polycrystalline RDX was loaded, with no pressure transmitting medium, into a DAC. Diffraction data were recorded using a beam of wavelength 0.485947 Å, which was slitted to 50 x 50 μm. Exposure times of 1800 s were required.

In all cases 2D diffraction patterns were collected using a Mar345 image plate and integrated using Fit2D.[71] The sample to detector distance was calibrated using either Si (I15) or CeO_2 (I11) standards. Data analysis was performed by Le Bail refinement using GSAS, in which a convolution of Gaussian (GU, GV), Lorentzian (LX, LY) and asymmetry (asym) coefficients was implemented to fit peak profiles (GSAS CW profile 2).[59]

3.4.6 DFT-MD calculations

A plane-wave density-functional theory molecular-dynamics simulation of β-RDX was carried out by Dr. A. M. Reilly using the CPMD program [72] and the PBE functional [73] augmented by a van der Waals dispersion-correction term.[74] The simulation was performed on a single unit cell, using periodic boundary conditions, at 150 K with data being collected for a total of 20 ps. The positions adopted by the atoms in the course of the simulation were analysed to produce time-averaged positions and variances that approximately correspond to the atomic positions and anisotropic displacement parameters (ADPs) determined experimentally. Further details of the analysis procedure and typical MD simulation parameters can be found elsewhere.[75]

3.5 Results and Discussion

3.5.1 β-RDX: a highly metastable polymorph at ambient conditions

Due to its observed instability, initial experiments focussed on crystallisation of RDX from nitrobenzene solution in sealed glass capillaries (o.d. ~2 mm). By thorough warming of this sealed system such that *all* of the solid was dissolved, it was possible to reduce the likelihood of seeding by residual traces of the α-form. In this way, reproducible crystallisation conditions were achieved and on cooling of a very concentrated hot solution to 298 K small crystallites were obtained which exhibited a very different morphology from α-RDX. Raman spectroscopy identified these as the β-form by comparison with previously reported spectra.[27, 28] Representative Raman spectra for the α- and β-forms are presented in Figure 3.8.

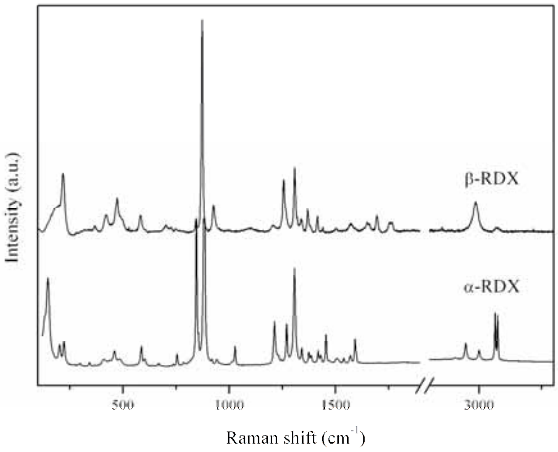

Figure 3.8 Comparison of the Raman spectra collected for α-RDX and β-RDX at ambient conditions. The spectral range between 1900 and 2800 cm^{-1} is omitted due to low spectral intensity of the vibrational modes within this region.

A single crystal was successfully grown using this same technique in a smaller diameter capillary (~0.3 mm) and single-crystal X-ray diffraction data were recorded at 273 K (see Appendix 8.1 for full structural information). The reflections were indexed to an orthorhombic unit cell ($Pca2_1$), implying 8 molecules in the unit cell and 2 independent molecules in the asymmetric unit. Structure solution and refinement showed that this was an unsolvated form of RDX. Attempts to cool the capillary resulted in freezing of the nitrobenzene and destruction of the crystal.

Subsequent crystallisation trials therefore focussed on growing single crystals that could be separated from the solvent so that low-temperature data could be collected. The most successful route proved to be when a concentrated solution of RDX in nitrobenzene on a hot glass slide was covered with an upturned glass vial to reduce the evaporation rate (see Figure 3.9). In the cases where the drop contacted the side of the upturned vial, small dendritic crystals of β-RDX were observed to form at the meniscus during evaporation. This method is very similar to the phenomenon of “contact-line crystallisation” described by Capes *et al.* for the growth of a metastable polymorph of paracetamol.[76] In this case, it has been proposed that the increased evaporation rate at the meniscus caused an increase in concentration in this region, thus permitting the nucleation of the metastable form. This form was then unable to transform to the more stable polymorph *via* a solvent-mediated transition as the solvent level dropped and the crystals were removed from solution.

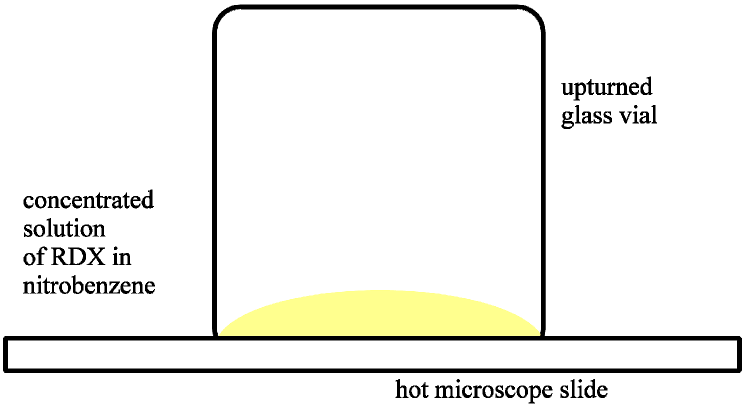

Figure 3.9 Experimental set-up for ‘Contact-line Crystallisation’ of β-RDX from nitrobenzene

Crystals grown in this way proved to be sufficiently metastable with respect to the α-form such that they could be manipulated and transferred to a fibre, which was subsequently mounted on the diffractometer. In this way, single-crystal X-ray diffraction data were recorded at 150 K and were consistent with the data collected at 273 K (structural information presented in Table 3.2). In the crystal structure of the β-form, both independent molecules adopt the chair conformation with all nitro groups in axial positions, resulting in approximate C_{3v} molecular symmetry (see Figure 3.10), thus supporting earlier suggestions based on vibrational spectra.[25-27] It is interesting to note that the unit cell *a*-axis actually shortens upon warming. The exact reasons for this remain unclear but a variable temperature X-ray diffraction study would be instructive.

	150 K	273 K
Space Group	$Pca2_1$	$Pca2_1$
a (Å)	15.1267(11)	15.0972(7)
b (Å)	7.4563(6)	7.5463(4)
c (Å)	14.3719(11)	14.4316(6)
V (Å^3)	1621.0(2)	1644.16(13)
D_c (Mg m^{-3})	1.820	1.795

Table 3.2 Structural information for β-RDX at 273 and 150 K.

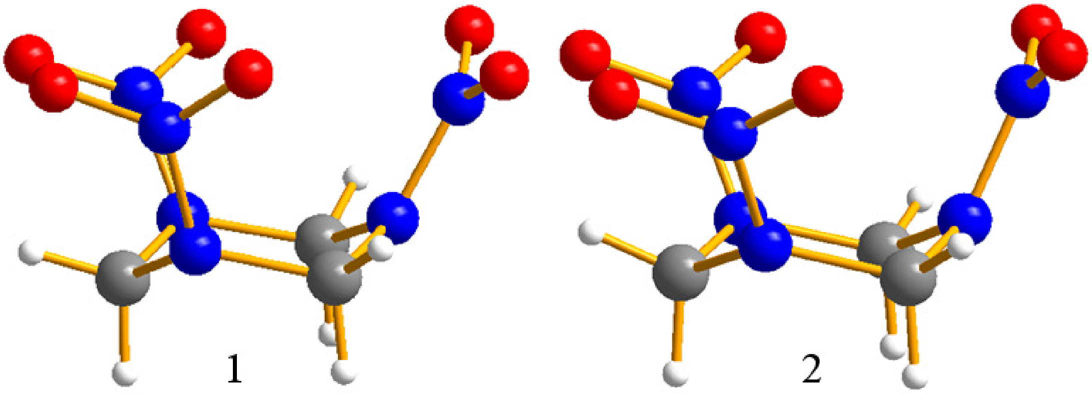

Figure 3.10 Molecular conformations of the two independent molecules in β-RDX.

The orientations of the nitro-groups can conveniently be compared by reference to the angle δ, the angle between the plane of the C-N-C ring atoms and the corresponding N-N bond.[15] The δ-values for both molecules in β-RDX are presented in Table 3.3 alongside those for α-RDX and for the *isolated* molecule in the AAA conformation as calculated using DFT methods.[38] For both molecules 1 and 2 the δ-values are very close to the calculated AAA geometry.

α-form	β-form molecule 1	β-form molecule 2	AAA*
33.4(1)	39.3(3)	33.4(3)	30.3
33.9(1)	32.4(4)	29.9(3)	30.1
-19.8(1)	28.5(4)	28.7(3)	29.9

Table 3.3 Values of δ (°) for the independent molecules in β-RDX, presented alongside those for the α-form and the AAA conformation as calculated by Vladimiroff and Rice.[38]

The packing of the molecules in β-RDX may be described as two interpenetrating lattices, one of which is composed solely of type 1 molecules and the other composed solely of type 2 molecules. Molecules within these lattices are linked by weak intermolecular C-H…O interactions. When the two independent lattices are overlayed to represent the full crystal packing (Figure 3.11) one can see similar weak C-H…O interactions occur between molecules 1 and 2 in the full lattice. This arrangement results in a slightly less dense crystal structure (1.795 Mg m^{-3} at 273 K) compared to α-RDX (1.806 Mg m^{-3} at 293 K) [22], which displays a more efficient packing of zig-zagging planes (Figure 3.5). Comparison of the α- and β-forms shows that there is no direct relationship between the two structures and that there are fewer C-H…O intermolecular interactions in β-RDX.

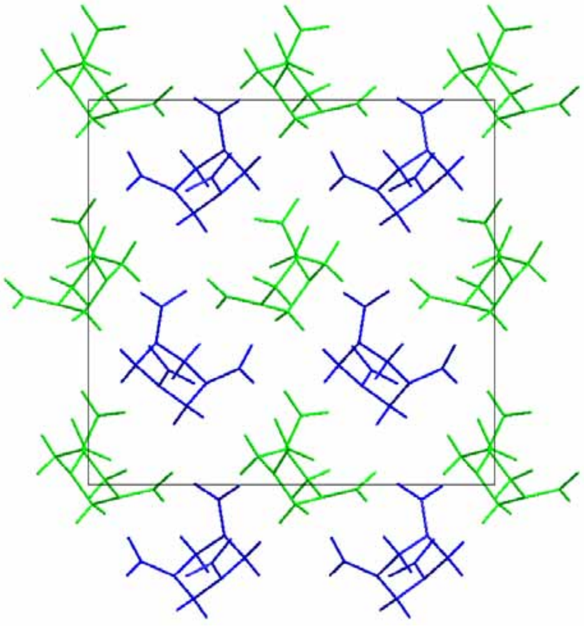

Figure 3.11 Full crystal packing in β-RDX, viewed down the *b*-axis, displaying the two interpenetrating lattices of molecules of types 1 and 2 (green and blue, respectively).

A particularly striking feature of the structure of the metastable β-form is the unusually large anisotropic displacement parameters (illustrated in Figure 3.12) associated with the nitro groups and even the ring atoms of molecule 1. These large amplitude motions (observed even at 150 K) suggest that this molecule is librating significantly about its position in the lattice and it is perhaps this that is the reason for the instability of this form with respect to the α-form. This observation prompted further investigation in order to establish the true nature of these unusual thermal ellipsoids. Initially it was suspected that a subtle static disorder may exist within the crystal structure, in which the long range order of the type 1 molecules displays a periodicity that is not commensurate with the translation symmetry defined by the crystallographic unit cell. In high-resolution single-crystal X-ray diffraction experiments, this incommensurate behaviour would be expected to result in the splitting of any single-crystal reflections dominated by scattering from type 1 molecules. Unfortunately the resolution of the data collected during the current experiment was not sufficient to identify any splitting, although slight broadening of the reflections can be seen in Figure 3.13. It would therefore be extremely useful to conduct analogous single-crystal studies exploiting the longer wavelength of, for example, a Cu-Kα source to determine conclusively whether the broadening observed in the present study was a result of the crystal quality or the occurrence of poorly-resolved satellite peaks. Furthermore, the high resolution and high incident flux of synchrotron radiation may provide additional experimental evidence for either a static or dynamic disorder model.

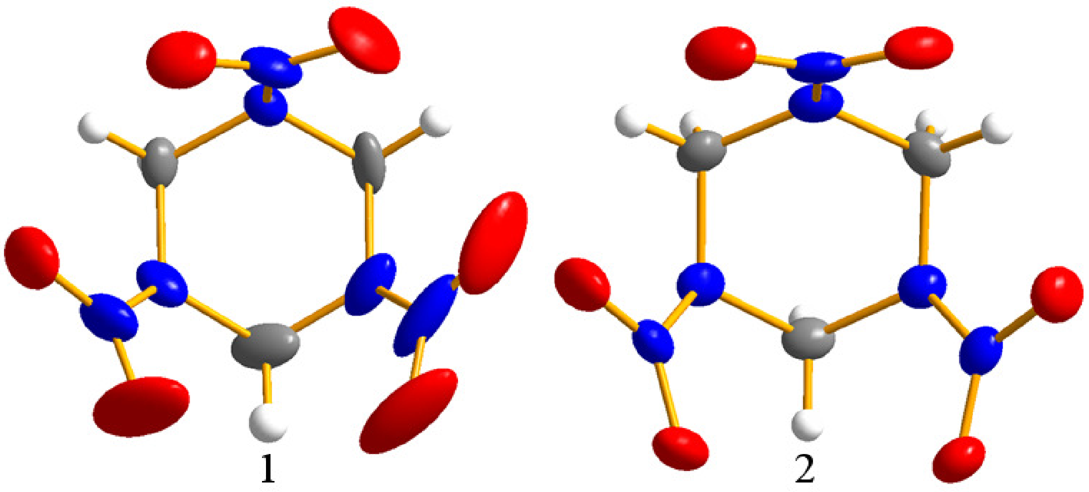

Figure 3.12 Anisotropic displacement parameters for β-RDX at 150 K.

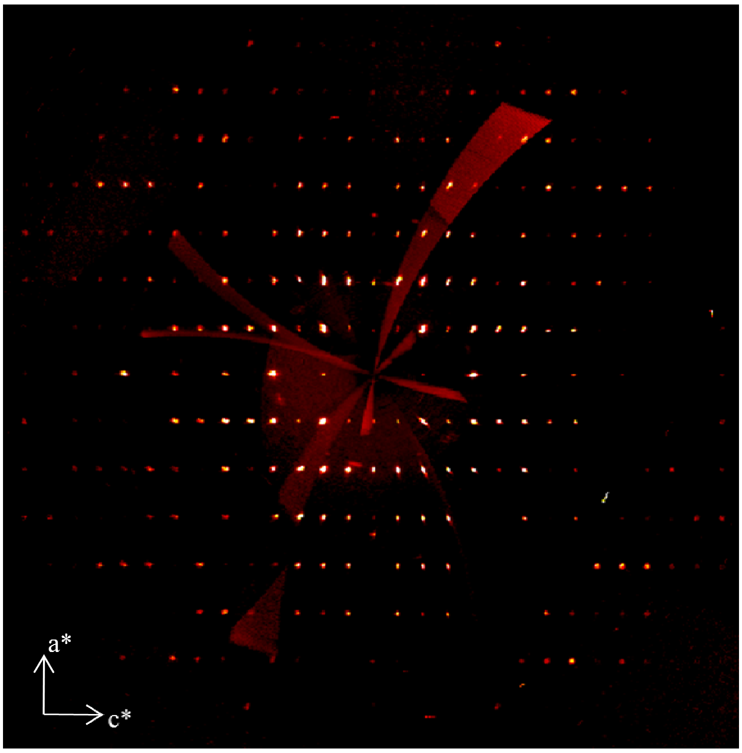

Figure 3.13 Calculated precession image of the *h*0*l* zone (produced using Bruker APEX-II software package) representing the single-crystal X-ray diffraction data collected for β-RDX at 150 K. Despite broadening of some of the reflections, it is not clear whether this is indicative of incommensurate modulation within the structure or is an experimental artefact.

In order to clarify further the disorder within β-RDX, a molecular dynamics (MD) simulation of β-RDX was carried out by Dr. A. M. Reilly (School of Chemistry, University of Edinburgh). Analysis of the motions of the molecules during the course of the simulation can be used to determine a number of 'experimental' quantities including thermal ellipsoids. The MD-derived thermal ellipsoids (plotted in Figure 3.14) have the same relative shape and orientations as the experimental ellipsoids. The theoretically determined ADPs are smaller than the experimental values, possibly due to the inability of the MD simulation to model dispersive phonon modes and zero-point energy contributions.[77, 78] Nevertheless, the similarity of the theoretical ellipsoids with the elongated ellipsoids observed in the experimental structure suggests that this feature is not due to experimental error or static structural effects such as static disorder or incommensurate modulation as neither of these can be modelled by the MD simulation. On this basis, it is more likely that the elongation is due to some dynamic process within the unit cell.

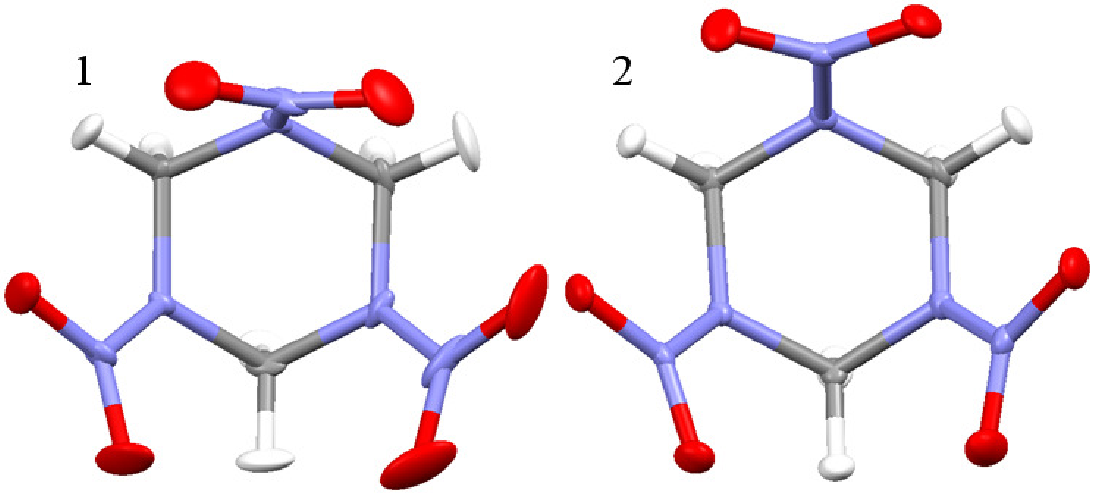

Figure 3.14 Representation of the anisotropic displacement parameters calculated for β-RDX by Molecular Dynamics Simulation.

Finally the results of this study indicate that β-RDX is rather less prone to transform to the α-form than has been previously suggested.[24] Crystals of the β-form survived gentle handling at room temperature and survived cooling to 150 K with no discernible deterioration in crystal quality (although this does not rule out a phase transition below this temperature for example). Furthermore the crystals could be manipulated in solution provided that there were no traces of the α-form present to initiate a rapid solvent-mediated transformation. Similarly, an isolated crystal of the β-form immediately transformed upon contact with a fibre or needle contaminated with residual traces of α-RDX. On this occasion a wavefront was observed to pass through the crystal leading to a marked reduction in crystal quality, indicating that this transition is reconstructive. Raman measurements conducted on these deposits confirmed that only the α-form was present after this transition was observed.

In accordance with previous conclusions [25] this instability would exclude the possibility of the presence of the β-form in RDX-containing munitions. This would therefore rule out any direct effects attributable to β-RDX on the performance of these compositions (e.g.

sensitivity to shock) although it is certainly reasonable to suggest that the reconstructive nature of this transition may adversely affect crystal quality by the introduction of shear stresses and/or crystal defects. This would have significant implications for the creation of ‘hot spots’ [79, 80], thereby potentially affecting performance.

It would therefore be extremely desirable to explore fully the effect of phase history on the properties of RDX, particularly sensitivity. Full-profile refinements of the powder diffraction patterns collected for samples that have undergone the β → α transition may facilitate the characterisation of shear stresses, micro strain and defect content.[81, 82] Furthermore, comparison of these powder diffraction patterns with those collected for samples of Reduced-Sensitivity (RS-RDX) will perhaps allow the direct evaluation of sensitivity based solely on diffraction data.

3.5.2 Investigation of the high-pressure/high-temperature form of RDX

Having determined the structure of β-RDX under ambient conditions, this study was extended to identify and structurally characterise the high-pressure/high-temperature form, which some authors have suggested is the same as this metastable polymorph.[31, 32] We therefore investigated this form by neutron powder diffraction using a Paris-Edinburgh cell with a newly-commissioned variable temperature insert.[56] A sample of RDX-d_6 was initially compressed in MeOD/EtOD (4:1) to obtain the γ-form at a pressure of 4.1 GPa (293 K). The sample was then heated incrementally to 423 K but no changes in the diffraction pattern were evident; only on brief warming to 448 K (30 mins) was a new pattern observed (see Figure 3.15). In order to avoid potential decomposition at these elevated temperatures, the sample was cooled initially to 323 K and then to 293 K – the new pattern persisted on cooling to ambient temperature. Subsequent decompression at 293 K showed that this form also persisted to 0.99 GPa (Figure 3.16). At the next pressure point (0.85 GPa) the characteristic diffraction pattern of α-RDX was observed. Raman spectroscopic and powder X-ray diffraction analysis on the recovered material confirmed that the sample had not undergone decomposition.

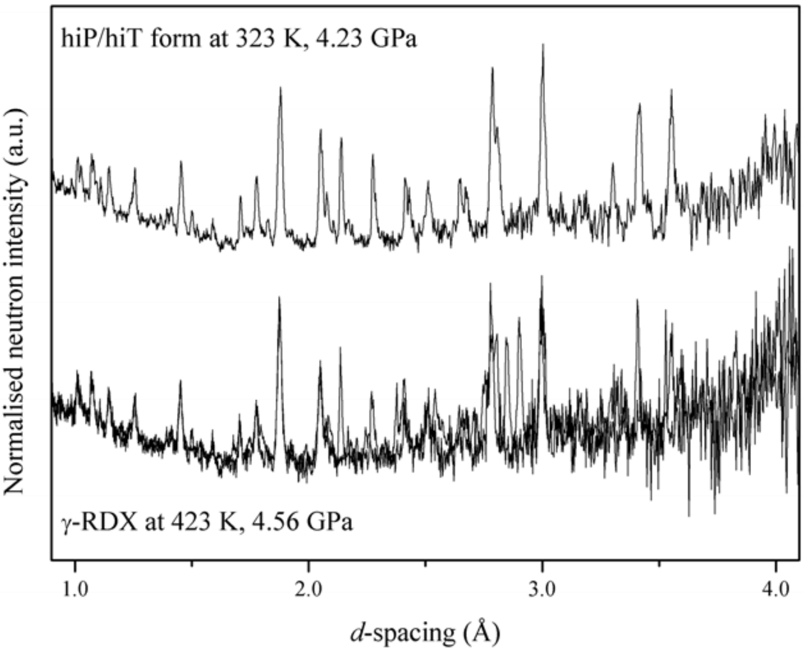

Figure 3.15 Comparison of the neutron powder diffraction patterns collected for γ-RDX-d_6 and the pattern observed for the high-pressure, high-temperature form.

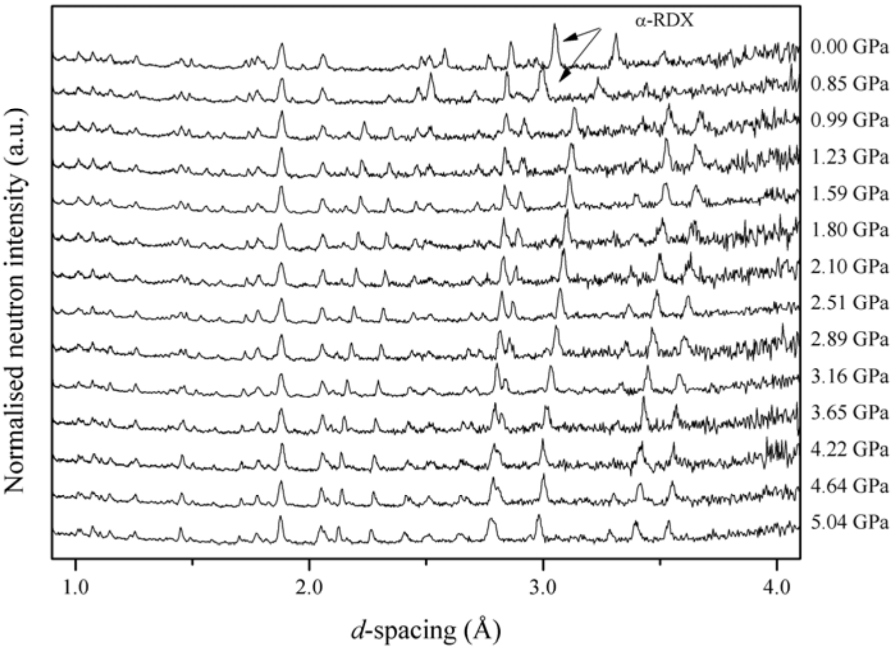

Figure 3.16 Neutron powder diffraction patterns collected during the decompression of the high-pressure/high-temperature polymorph of RDX-d_6 at ambient temperature.

Comparison of the patterns collected for this form with the calculated pattern from the crystal structure of β-RDX (Figure 3.17) allowed us to prove conclusively that the high-pressure/high-temperature polymorph of RDX is *not* the same as the metastable form at ambient conditions. Instead this represents a fifth polymorph of RDX and should therefore be re-named ε-RDX. Unfortunately indexing (and hence structure solution) was not possible on the basis of the neutron diffraction patterns collected.

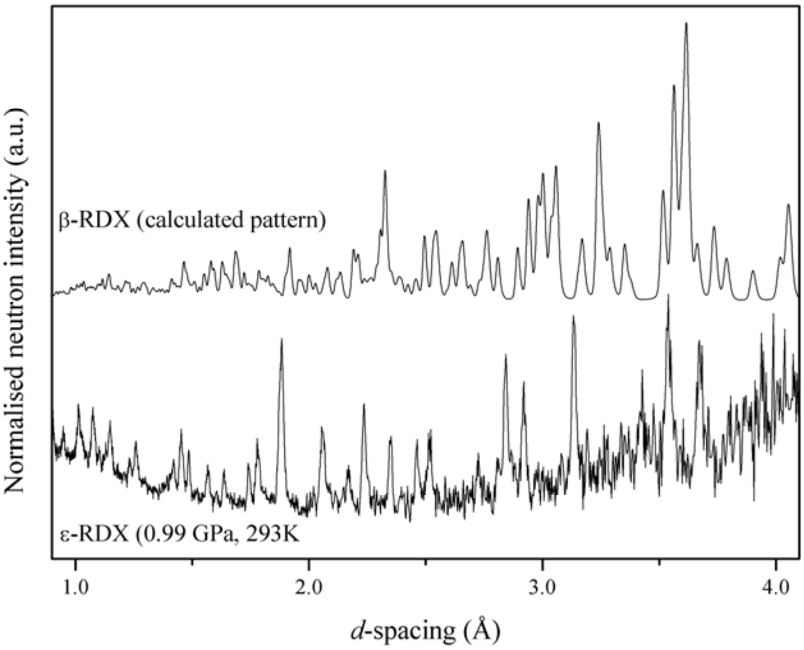

Figure 3.17 Comparison of the neutron powder diffraction pattern obtained for a sample of RDX-d_6 subjected to elevated temperatures and pressure (at 0.99 GPa and 293 K) with the simulated pattern for perdeuterated β-RDX (ambient pressure and 150 K)

These findings were mirrored in the results of a Raman spectroscopic study of RDX-h_6 contained in a diamond-anvil cell (DAC) subjected to similar temperature and pressure conditions. The Raman spectra collected for this sample were in excellent agreement with those reported by Baer *et al.*[31] Furthermore this study confirmed that, once formed, the ε-form persisted on cooling to ambient temperature and on decompression to ~ 1.0 GPa. At this pressure ε-RDX transformed to the α-form; at no point during the decompression was the γ-form observed (see Figure 3.18). In addition, the re-naming of the high-pressure/high-temperature form of RDX has been substantiated by the comparison of the Raman spectra (Figure 3.19) obtained for ε-RDX and the β-form, with which it has previously been confused. It is interesting to note that the Raman spectrum observed for β-RDX is consistent with those published by Torres *et al.*[27], suggesting that the confusion over these distinct forms could perhaps have been remedied sooner.

In their very recent spectroscopic investigation of this form, Dreger and Gupta concur with the re-naming of this form (ε-RDX).[83] Several noticeable differences were observed between Raman spectra collected for the β- and ε-forms, particularly in the low frequencey lattice modes. It was also possible to perform compression and decompression studies of the ε-form in order to assess its structural stability. Below 0.6 GPa ε-RDX readily converted to the α-form; upon compression, however, the ε-form remained stable to 20.0 GPa, the highest pressure studied. Furthermore, the same authors conducted a parallel study on the high-pressure/high-temperature behaviour of the three forms that have been identified under these conditions (*i.e.* the α-, γ- and ε-forms).[84] Careful spectroscopic and optical measurements allowed the identification of the phase boundaries, as well as a triple point at 3.7 GPa and 466 K.

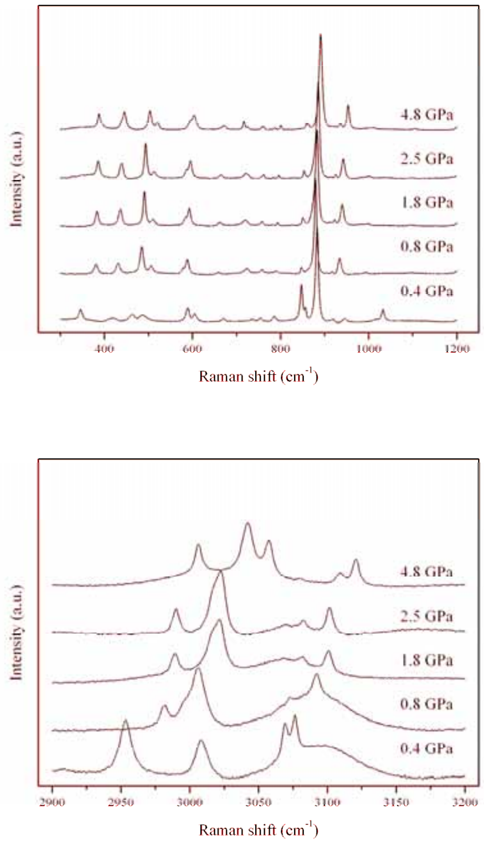

Figure 3.18 Raman decompression study of ε-RDX showing clear evidence of phase transition to the α-form between 0.8 and 0.4 GPa. The spectral intensities have been scaled for clarity and the ranges between 1200 - 1500 and 1500 - 2900 cm^{-1} have been omitted due to masking from the strong diamond signal and low sample spectral intensity, respectively.

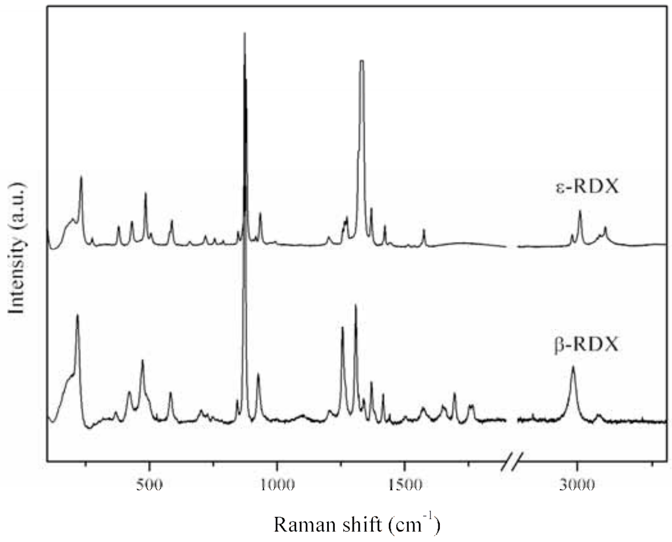

Figure 3.19 Comparison of the Raman spectra collected for β-RDX at ambient conditions and ε-RDX at 1.0 GPa and 293 K.

An important result of the complementary neutron diffraction studies on RDX-d_6 and the Raman analysis of the hydrogenous material is that the transition pressures concur within experimental error. It is therefore reasonable to conclude that the effect of deuteration on the α → γ, γ → ε, and ε → α phase transitions is negligible.

Having demonstrated that the ε-form could be obtained reproducibly, the focus of this study turned to obtaining crystals suitable for single-crystal X-ray diffraction (SXD). A single crystal of α-RDX was compressed (in a DAC) through the α → γ transition to a pressure of ~ 5.0 GPa before heating to 500 K. Unfortunately this resulted in the dissolution of the crystal in the pressure-transmitting medium (4:1 MeOH/EtOH) at these elevated temperatures.[4] For this reason, we opted to attempt the recrystallisation of RDX from solution at ~ 5.0 GPa. Whilst recrystallisation at lower pressures (i.e. up to 1.0 GPa) has been shown to be successful,[85, 86] this technique has not been used at these much higher pressures on account of pressure-induced freezing of the solvent and the low intrinsic solubilities of molecular compounds under these conditions.

Polycrystalline α-RDX was loaded into a DAC with a small quantity of MeOH:EtOH (4:1) and the pressure increased to ~ 5.0 GPa before heating to 500 K for 1 hr. At these elevated

---

[4] The dissolution of the crystal in MeOH:EtOH has also been reported by Dreger and Gupta (ref. [83]), who observed shattering in cases where nitrogen was employed as the pressure-transmitting medium. In contrast, crystal quality was maintained when these studies were conducted in argon. The authors do not comment on crystal quality after the ε → α transition.

temperatures the enhanced solubility of RDX in the pressure-transmitting medium and the reduced viscosity of the medium resulted, in many cases, in complete dissolution of the sample. This was overcome by loading an excess of the solute in the diamond-anvil cell. After numerous crystallisation trials, recrystallisation at 5.7 GPa produced a single crystal large enough for single-crystal X-ray diffraction.

Structure solution and refinement showed that ε-RDX crystallises in the orthorhombic crystal system (*Pca*2_1) with only one molecule in the asymmetric unit. With this structure as a starting point it was then possible to refine all of the neutron powder diffraction patterns extremely well (χ^2 values of 1.26 were typical) thus providing additional support that the structural model was correct. An illustrative example of the Rietveld refinement can be seen in Figure 3.20.

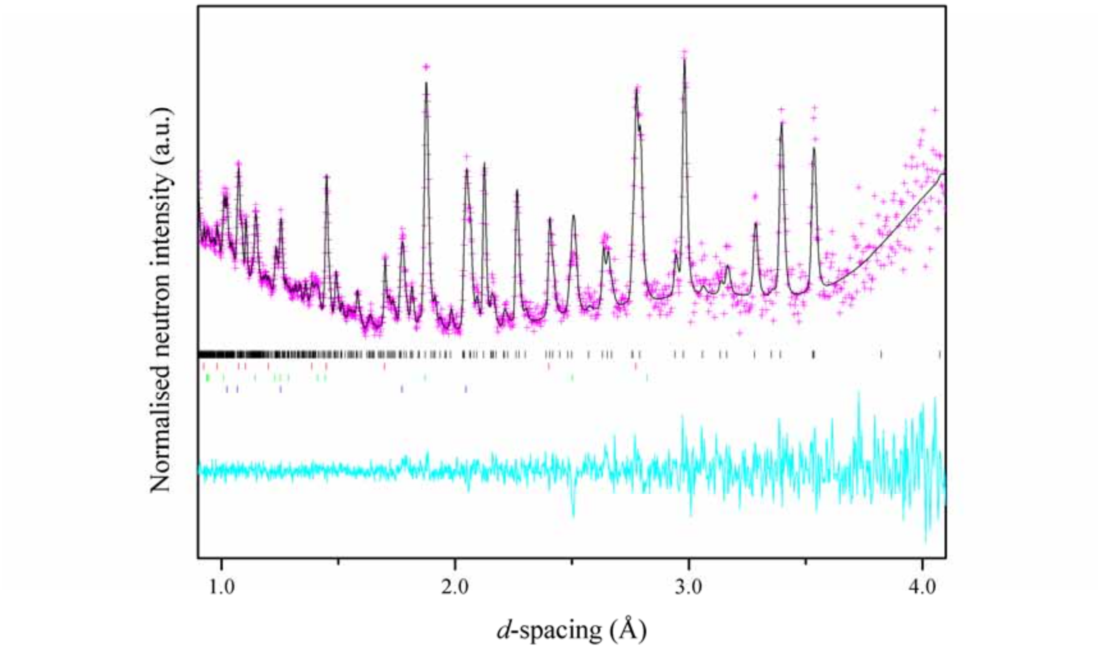

Figure 3.20 Example of the Rietveld refinement of neutron powder diffraction pattern (at 5.04 GPa and 293 K) using the structure determined for ε-RDX. The experimental data (I_{obs}) are shown in pink; the calculated pattern (I_{calc}) meanwhile is represented as a black line. The difference curve ($I_{obs} - I_{calc}$) is shown in cyan. Tick-marks for each phase are also shown for clarity: ε-RDX (black), Pb (red), WC (green) and Ni (blue).

Although there is only a small decrease in molecular volume over the $\gamma \rightarrow \varepsilon$ transition, and the space group is retained, comparison of the structures shows that there must be a significant rerrangement of the molecules over this transition. At a molecular level this involves a change in molecular conformation: the molecules in ε-RDX adopt the AAA conformation shown in Figure 3.21, while the molecules in the γ-form adopt either the AAA or AAI conformation. The variation in molecular conformation amongst the different forms of RDX is highlighted by reference to the δ-angle between the plane created by the C-N-C ring atoms and that of the respective nitro groups. These values are presented in Table 3.4 alongside those for the isolated molecule calculated by DFT methods.[38]

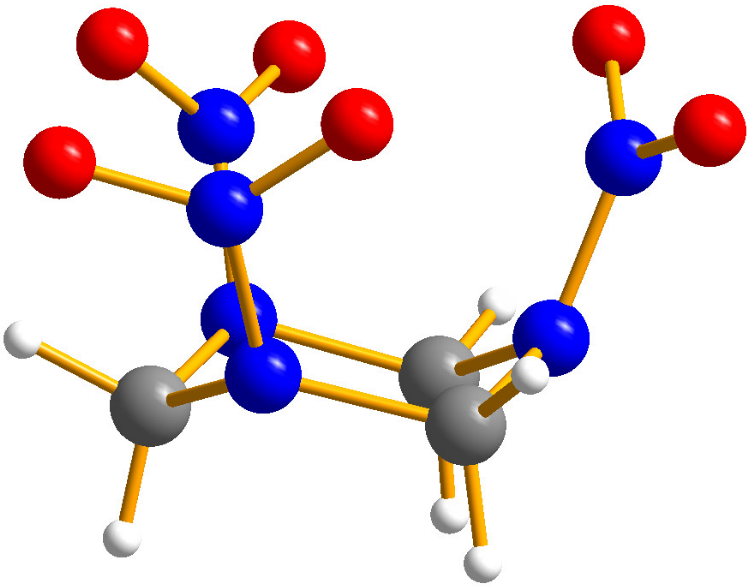

Figure 3.21 AAA molecular conformation observed in ε-RDX.

α-form	β-form molecule 1	β-form molecule 2	γ-form molecule 1	γ-form molecule 2	ε-form	AAA
33.4(1)	39.3(3)	33.4(3)	39.6(7)	36.4(9)	35.5(8)	30.3
33.9(1)	32.4(4)	29.9(3)	17.3(8)	35.5(9)	36.3(9)	30.1
-19.8(1)	28.5(4)	28.7(3)	-2.4(12)	9.5(11)	42.7(9)	29.9

Table 3.4 Values of the angle δ (°) for the molecular conformations observed in α-, β-, γ-, and ε-RDX along with the calculated values for the AAA conformation.[38]

Moreover a major reorientation of at least one of the molecules in γ-RDX must also occur in order to achieve the packing observed in the ε-form (see Figure 3.22). While the two inequivalent molecules in γ-RDX are arranged over a pseudo-inversion centre, the molecules in the ε-form (Z’ = 1) adopt a head-to-tail packing arrangement.

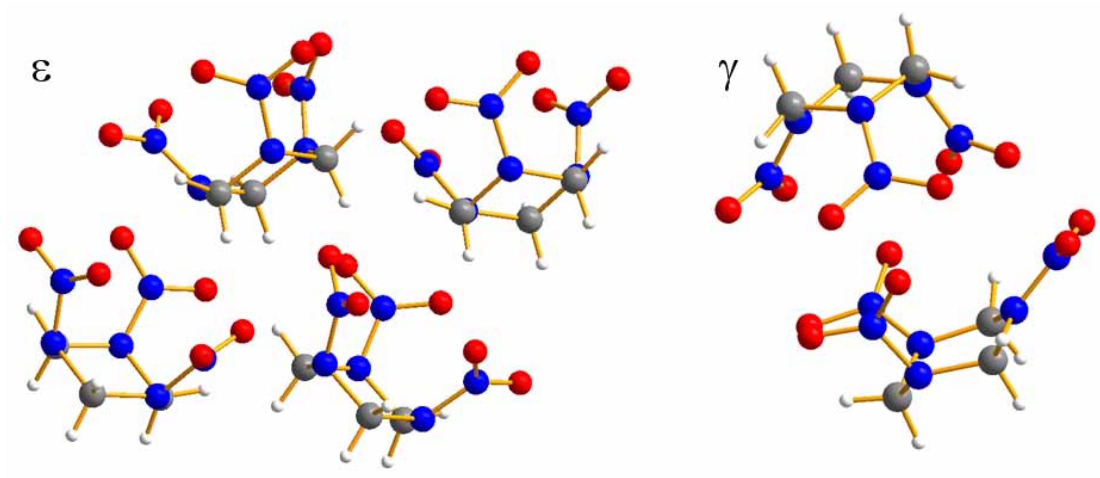

Figure 3.22 (a) 'Head-to-tail' molecular packing in ε-RDX; (b) packing of γ-RDX 'dimers' that are arranged over a pseudo-inversion centre.

The unit cell parameters obtained for ε-RDX from the neutron powder diffraction experiment are presented in Table 3.5 and in Figure 3.23(a). The smooth variation in volume with pressure is also shown in Figure 3.23(b). In order to provide an estimate of the unit cell volume, and hence crystal density, of ε-RDX at atmospheric pressure, these data have been fit to a Murnaghan[5] equation of state (EoS) with V_0 = 808(4) Å^3, B_0 = 10.3(8) GPa and B' = 7.8(3). The most exciting observation, however, is that at every pressure studied ε-RDX is denser than the α-form – this is highlighted by a plot of the molecular volumes with pressure for each polymorph (see Figure 3.24). At 3.65 GPa, the ε-form is 2.2% denser than the α-form (at 3.62 GPa) and even the extrapolated density of the ε-form at ambient pressure indicates that it has a higher density than α-RDX under the same conditions. This result has significant implications: should it be possible to recover ε-RDX to ambient pressures, one would expect this denser form to have a greater detonation velocity.

---

[5] Although Murnaghan EoS are generally not reliable for compression of greater than 10%, in this case it was necessary to estimate V_0 at zero pressure. Refinement of other formulations gave larger uncertainties in the EoS parameters. Meanwhile, extrapolating V_0 from a 'pressure-normalised' EoS, as outlined in Section 2.6, also introduces greater uncertainties.

P (GPa)	a (Å)	b (Å)	c (Å)	V (Å^3)	wR_p
5.04	7.0655(12)	10.6043(12)	8.8223(12)	661.00(10)	0.0295
4.64	7.0849(17)	10.6373(18)	8.8455(17)	666.64(15)	0.0521
4.33	7.1062(9)	10.6810(9)	8.8608(9)	672.55(8)	0.0239
3.65	7.1355(18)	10.7355(18)	8.8947(17)	681.37(15)	0.0545
3.16	7.1702(12)	10.8038(12)	8.9269(11)	691.53(10)	0.0287
2.89	7.1875(16)	10.8383(17)	8.9471(16)	696.99(14)	0.0459
2.51	7.2164(18)	10.8977(19)	8.9737(17)	705.72(16)	0.0468
2.10	7.2458(12)	10.9616(13)	9.0056(11)	715.27(10)	0.0296
1.80	7.2759(18)	11.0159(20)	9.0294(17)	723.71(16)	0.0522
1.59	7.2975(20)	11.0659(20)	9.0552(19)	731.24(18)	0.0604
1.32	7.3213(12)	11.1235(13)	9.0786(12)	739.35(11)	0.0290
1.23	7.3404(20)	11.1501(20)	9.0891(19)	743.91(18)	0.0490
0.99	7.3589(20)	11.2064(20)	9.1107(20)	751.33(20)	0.0492
0.85	*13.001(3)*	*11.357(3)*	*10.465(2)*	*1546.2(4)*	0.0560
0.00	*13.195(3)*	*11.597(3)*	*10.719(2)*	*1640.2(4)*	0.0422

Table 3.5 Unit cell parameters obtained during the decompression of ε-RDX at ambient temperature, as determined by neutron powder diffraction. Patterns refined using the structure of the α-form have been italicised.

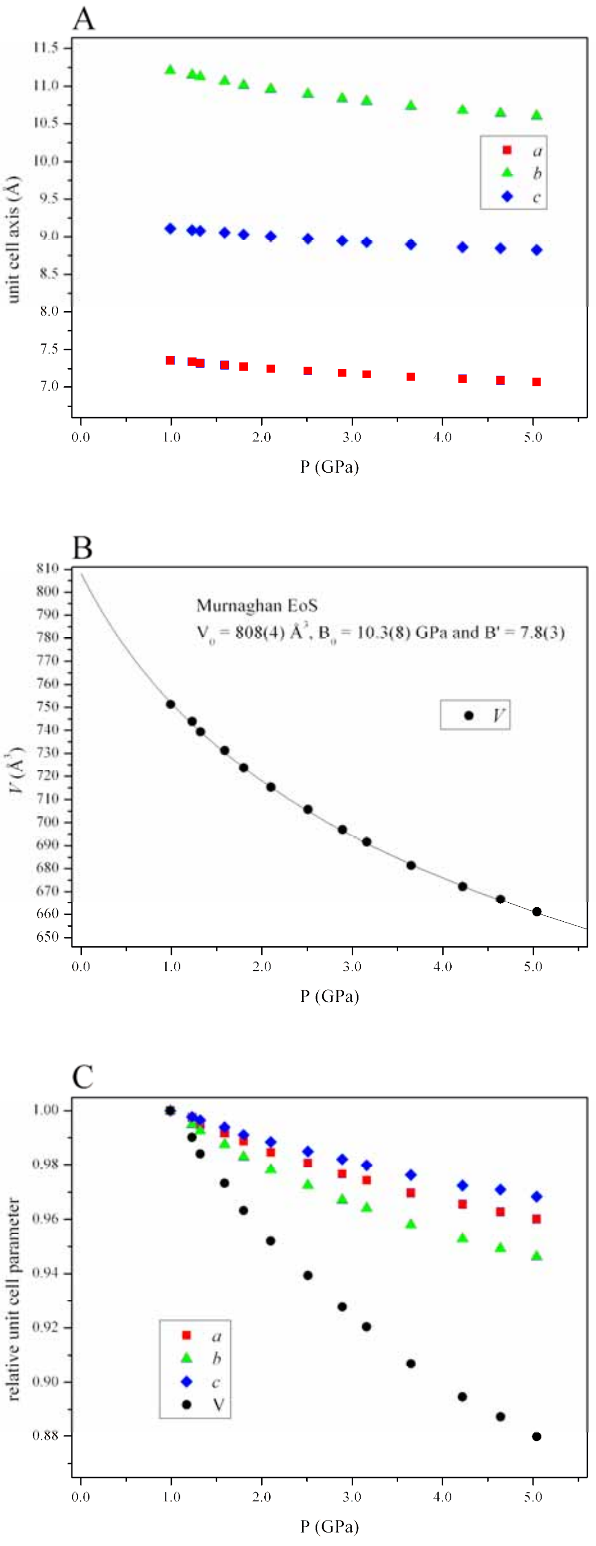

Figure 3.23 Graphical illustration of the decompression of ε-RDX: (a) plot of the unit cell axes, as determined by neutron powder diffraction; (b) the Murnaghan EoS that has been fit to the *PV*-plot; and, (c) the relative contraction of the unit cell parameters, normalised to the lowest pressure dataset (0.99 GPa).

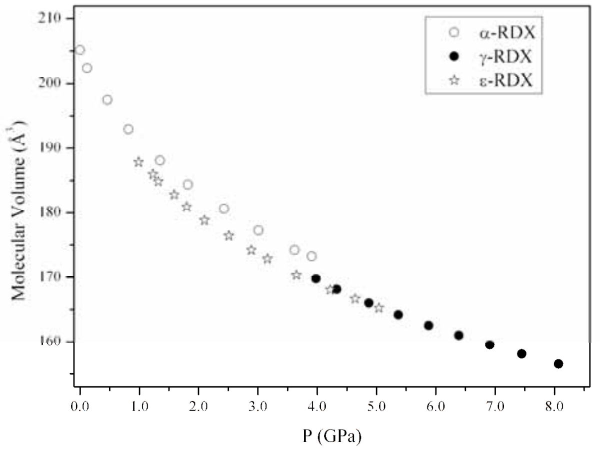

Figure 3.24 Comparison of the variation of the molecular volumes of α-, γ- and ε-RDX-d_6 with pressure.

The observation that the ε-form can be recovered almost to ambient pressure, coupled with Miller's observation that the α → ε transition is reversible at high temperatures, suggests that the ε-form is thermodynamically unstable with respect to the α-form, but may persist due to a significant kinetic barrier. If this interpretation is correct, it is reasonable to suggest that ε-RDX may be recovered to ambient pressure if the decompression were carried out at sub-ambient temperatures. Using the Paris-Edinburgh cell fitted with a variable temperature insert, a sample of ε-RDX-d_6 was formed at elevated temperatures and pressures (as described above) before the sample was gradually decompressed to ambient pressure at 150 K. Diffraction patterns were collected on warming (in 10 K intervals, Figure 3.25) and ε-RDX was observed to persist at ambient pressure up to 230 K, at which point it slowly transformed into the α-form over a period of 2 hours.

Moreover, in order to prove unequivocally that the ε-form is the denser form, the sample of α-RDX was then cooled to 220 K in order to compare the molecular volumes under exactly the same conditions. These results are shown in Table 3.6 and show clearly that the ε-form is 0.86% denser than the α-form. Furthermore it was possible to determine an expression for the volumetric thermal expansion of the ε-form over the temperature range 150 – 220 K ($\alpha_v = \partial (\ln V)/\partial T = [1.99(5) + 0.010(5)*(T-185)] \times 10^{-4}\ K^{-1}$). Using this expression, it was possible to obtain another estimation of the unit cell volume of ε-RDX at room temperature and ambient pressure: V_0 (293 K) = 819(2) Å^3 which is slightly larger than the value calculated from the Birch-Murnaghan EoS (808(4) Å^3). This result does, however, further substantiate the expectation that the ε-form would be the denser form at ambient temperature *and* pressure: V_0 = 1641.10 Å^3 for α-RDX-d_6 at 293 K.